Balancing fluorescence and singlet oxygen formation in push-pull type near-infrared BODIPY photosensitizers

Peer-reviewed author version

DECKERS, Jasper; CARDEYNAELS, Tom; Doria, Sandra; Tumanov, Nikolay; Lapini, Andrea; ETHIRAJAN, Anitha; AMELOOT, Marcel; Wouters, Johan; Di Donato, Mariangela; Champagne, Benoit & MAES, Wouter (2022) Balancing fluorescence and singlet oxygen formation in push-pull type near-infrared BODIPY photosensitizers. In: Journal of Materials Chemistry C, 10 (24) , p. 9344 -9355.

DOI: 10.1039/d2tc01526a
Handle: http://hdl.handle.net/1942/37598

Table of contents

1. Materials and methods

General

All commercially available reagents were obtained from Abcr, Acros Organics, Alfa Aesar, Fluorochem, J&K Scientific, Sigma-Aldrich, TCI Europe, or VWR Chemicals and these were used without further purification. Solvents were obtained from Fisher Scientific, Sigma-Aldrich, or VWR Chemicals and also used without further purification. Dry solvents were obtained from a MBraun solvent purification system (MB SPS-800) equipped with alumina columns. Microwave syntheses were performed using a CEM Discover SP equipped with a Gas Addition accessory for reactions under argon atmosphere. The temperature inside the vessel was monitored *via* fiber optic temperature control. Preparative (recycling) size exclusion chromatography (prep-SEC) was performed on a JAI LC-9110 NEXT system equipped with JAIGEL 1H and 2H columns (eluent: chloroform, flow rate: 3.5 mL min^{-1}).

Proton and carbon nuclear magnetic resonance (^{1}H and ^{13}C NMR) spectra were obtained at room temperature on a Varian or Jeol spectrometer operating at a frequency of 400 MHz for ^{1}H (100 MHz for ^{13}C). Measurements were performed in deuterated chloroform ($CDCl_3$) and chemical shifts (δ) are given in ppm relative to $CDCl_3$ (δ = 7.26 ppm for ^{1}H NMR, δ = 77.16 ppm for ^{13}C NMR). Coupling constants (*J*) are given in Hz. Due to the typical small coupling constants for pyrrolic dyes, the multiplicity of the signals is often unclear. In these cases, NMR signals appear as singlets.

Matrix-assisted laser desorption/ionization - time-of-flight (MALDI-ToF) mass spectra were recorded on a Bruker Daltonics Ultraflex II ToF/ToF. Approximately 1 µL of the matrix solution (16 mg mL^{-1} *trans*-2-[3-(4-*tert*-butylphenyl)-2-methyl-2-propenylidene]malononitrile (DTCB) in chloroform) was spotted onto an MTP Anchorchip 600/384 MALDI plate. The spot was allowed to dry and 1 µL of the analyte solution (0.5 mg mL^{-1} in chloroform) was spotted on top of the matrix.

Density functional theory calculations

The ground-state geometries of all compounds were optimized at the M06-2X/6-311G(d) level using density functional theory (DFT). All compounds were optimized in chloroform using the polarizable continuum solvation model (PCM). Time-dependent DFT (TDDFT) calculations were carried out at the M06-2X/6-311G(d) level using the PCM model for chloroform. Excited state geometries were optimized using TDDFT with the M06-2X/6-311G(d) method and the PCM (chloroform). All calculations were performed using Gaussian16.[1]

TDDFT calculations were used to evaluate the difference of electronic density between the excited states and the ground states, $\Delta\rho(\vec{r}) = \rho_e(\vec{r}) - \rho_g(\vec{r})$. Following the procedure described by Le Bahers *et al.*,[2] the barycenters of the positive $[\Delta\rho^{+}(\vec{r})]$ and negative $[\Delta\rho^{-}(\vec{r})]$ electronic density variations were evaluated. The distance between these barycenters defines the charge-transfer distance (d_{CT}), while their integration over the whole space gives the amount of charge transferred (q_{CT}). The product of these two quantities gives $\Delta\mu_{ge} = q_{CT} \times d_{CT}$.

Photophysical characterization

All electronic absorption spectra were recorded on a Varian Cary 5000 UV-Vis-NIR spectrophotometer from Agilent Technologies. Corrected steady-state emission spectra were recorded on a Horiba-Jobin Yvon Fluorolog-3 spectrofluorometer equipped with a 450 W Xe lamp as light source, with an excitation wavelength (λ_{exc}) of 605 nm and a slit width of 2 nm (which was adjusted to 5 nm for the somewhat less fluorescent species **5b-d** in the dilution experiments). Freshly prepared samples in 1 cm quartz cells were used to perform all UV-Vis-NIR absorption and fluorescence measurements. Fluorescence

measurements were performed under a right-angle arrangement. Three independent experiments were used to determine the spectral maxima ($\lambda_{abs}(max)$ and $\lambda_{em}(max)$), the full-width-at-half-maximum of the absorption ($fwhm_{abs}$) and the fluorescence emission ($fwhm_{em}$) bands, and the Stokes shifts ($\Delta\bar{\nu} = 1/\lambda_{abs}(max) - 1/\lambda_{em}(max)$) in each solvent. The standard uncertainty (square root of variance) on the absorption and emission maxima, obtained from at least three independent measurements in each solvent, is approximately 1 nm. All spectroscopic measurements were done in non-degassed, spectroscopic grade solvents at 20 °C.

Fluorescence quantum yields

For the determination of the relative fluorescence quantum yields (Φ_f) in solution, dilute solutions with an absorbance around 0.1 at the excitation wavelength were used. Nile blue (λ_{exc} = 605 nm, Φ_f = 0.27 in ethanol) was used as a standard to determine the fluorescence quantum yields.[3] The average Φ_f was calculated from three independent measurements in each solvent. The fluorescence quantum yield of the tested compound ($\Phi_{f,x}$) was calculated using Equation (1), in which Φ_{st} is the fluorescence quantum yield of the standard, F_x and F_{st} are the integrated fluorescence of the test compound and the standard, A_x and A_{st} are the absorbance of the test compound and the standard at the excitation wavelength, and n_x and n_{st} are the refractive indices of the solvents in which the test compound and standard were dissolved, respectively.

$$\Phi_{f,x} = \Phi_{f,st} \frac{F_x\left(1-10^{-A_{st}}\right){n_x}^2}{F_{st}\left(1-10^{-A_x}\right){n_{st}}^2} \quad (1)$$

Singlet oxygen quantum yields

1,3-Diphenylisobenzofuran (1,3-DPBF) was used as a singlet oxygen ($^1O_2$) scavenger to determine the singlet oxygen quantum yields (Φ_Δ). The $^1O_2$ production was monitored by following the absorbance of 1,3-DPBF at 414 nm upon excitation of the respective BODIPY dye at 639 nm using a single LED630E from Thorlabs (λ_{exc} = 639±10 nm, *fwhm* = 17 nm, *P* = 7.2 mW).[4] The average Φ_Δ was calculated from three independent measurements in each solvent. To determine Φ_Δ, a relative method was used according to Equation (2). Here, *x* and *st* represent the sample and the standard. Φ_Δ, *A*, *m*, and *n* represent the singlet oxygen quantum yield, the absorbance at the excitation wavelength (λ_{exc} = 639 nm), the slope of the decrease in absorbance of 1,3-DPBF over time, and the refractive index of the solvent used for the measurement, respectively. Optically matched solutions with an absorbance around 0.6 at 414 nm and 0.3 at 639 nm were used. Methylene blue was used as the standard for these experiments (Φ_Δ = 0.52 in spectrograde ethanol).[5, 6] All solutions were continuously stirred during all measurements using a Cimarec i magnetic stirrer.

$$\Phi_{\Delta,x} = \Phi_{\Delta,st}\left(\frac{1-10^{-A_{st}}}{1-10^{-A_x}}\right)\left(\frac{m_x}{m_{st}}\right)\left(\frac{n_x}{n_{st}}\right)^2 \quad (2)$$

Attenuation coefficient, brightness, and phototoxic power

Molar attenuation coefficients were obtained by dissolving ca. 2 mg of the photosensitizer in chloroform (~5 mL). This stock solution was serially diluted to yield different dye concentrations from which absorption spectra were obtained in quartz cells with 1 cm optical path length (*l*). Minimal three solutions with an absorbance between 0.01 and 0.1 at $\lambda_{abs}(max)$ were used to plot the absorbance (*A*) versus molar concentration (*c*). The molar attenuation coefficient (ε) was then determined using the Beer-Lambert law as given in Equation (3).

$$A = \varepsilon\, l\, c \quad (3)$$

The brightness (*BT*) and phototoxic power (*PP*) were obtained by combining the attenuation coefficient and the fluorescence or singlet oxygen quantum yield, respectively. In this way, the brightness of a compound is defined as $BT = \varepsilon \Phi_f$ and the phototoxicity as $PP = \varepsilon \Phi_\Delta$.

Femtosecond transient absorption spectroscopy

Pump-probe experiments were performed on a setup based on a regenerative amplifier Ti:sapphire laser (Legend, Coherent), pumped by a Ti:sapphire oscillator (Micra, Coherent), able to deliver 3.2 W, 40 fs pulses at 800 nm, at 1 KHz repetition rate. The pump and probe beams for transient absorption spectroscopy (TAS) experiments are generated by two independent home-made Non-Collinear Optical Amplifiers (NOPA). Both pump and probe pulses are compressed through a pair of chirped mirrors to a ca. 25 fs time duration. The probe beam is split in two parts through a beam splitter in order to generate a reference beam. The pump, probe, and reference beams are focused on the sample using a 250 mm spherical mirror. Pump-probe delay times are introduced by sending the pump pulse through a motorized delay stage, allowing to record spectra with a maximum pump-probe delay of about 250 ps. After passing through the sample, the probe and reference beams are dispersed with a monochromator and sent to a double array home-made detector.

In case of samples **5b** and **5e**, additional TAS measurements were performed, covering a pump-probe delay up to 1.5 ns. The employed setup was based on the same laser source. Pump pulses are generated using a home-made NOPA. The broadband NOPA output is spectrally narrowed using an interference filter centered at 620 nm. The probe beam is obtained by focusing a portion of the fundamental laser output on a 3 mm thick calcium fluoride window, generating a white light continuum covering the 380–750 nm spectral window, which is subsequently split in a probe and reference beam using a 50% beam splitter. The pulse fraction used to generate the white light probe has been sent to a motorized delay stage before white light generation, allowing to record transient spectra with a maximum pump probe delay of 1.5 ns. Both pump and probe are spectrally overlapped at the sample position. The probe and reference beams are sent through a spectrograph coupled to a home-made detector.

All samples were contained in 1 mm quartz cuvettes, mounted on a movable stage in case of photosensitive samples. Sample concentrations were in the range of 2.5 to 5 x 10^{-5} M. The data were analyzed by means of singular value decomposition and global analysis, employing the software Glotaran.[7] All the spectral and time-resolved data were simultaneously analyzed according to a catenary compartmental model (linear, unbranched kinetic scheme) with the kinetic rate constants between the compartments as global fitting parameters. The analysis software allows to take into account the instrument response function, which is fitted in terms of a Gaussian function convoluted to the kinetic traces and to correct for the spectral dispersion of the probe beam.

2. Photosensitizer synthesis

Synthesis of the BODIPY core

1,3,5,7-Tetramethyl-8-mesityl-BODIPY **2** was synthesized from 2,4-dimethylpyrrole (**1**) according to a literature procedure.[8]

Synthesis of the donor moieties

Carbazole (**3e**, Acros Organics, 96%) was alkylated to obtain 3,6-di-*tert*-butylcarbazole (**3f**) as described in a published procedure.[9]

Aldehydes **4a-f** were synthesized according to the following general procedure for Buchwald-Hartwig amination starting from amines **3a-f** and 4-bromobenzaldehyde. 4-Bromobenzaldehyde (1 equiv), amine **3a-f** (1.1 equiv), tris(dibenzylideneacetone)dipalladium(0) (0.05 equiv), cesium carbonate (3 equiv), and 1,1'-bis(diphenylphosphino)ferrocene (0.1 equiv) were combined under inert atmosphere and dissolved in dry toluene (6 mL/mmol 4-bromobenzaldehyde). After stirring for 16 h at 100 °C, the reaction mixture was cooled down to room temperature and quenched with water. The toluene fraction was separated and the water phase was extracted with chloroform. The combined organic phases were dried over anhydrous Na_2SO_4, filtered, and evaporated to dryness. The crude product was purified by column chromatography (silica) to obtain pure aldehyde **4a-f**.

4-(9,9-Dimethyl-9,10-dihydroacridin-10-yl)benzaldehyde (**4a**)[10]: Obtained according to the general Buchwald-Hartwig procedure using 4-bromobenzaldehyde (1.00 g, 5.40 mmol), 9,9-dimethyl-9,10-dihydroacridine (**3a**, Fluorochem, 95%) (1.25 g, 5.95 mmol), tris(dibenzylideneacetone)dipalladium(0) (247 mg, 0.27 mmol), cesium carbonate (5.3 g, 16.2 mmol), and 1,1'-bis(diphenylphosphino)ferrocene (299 mg, 0.54 mmol). The crude product was purified by column chromatography (chloroform:hexanes, 50:50) to give 4-(9,9-dimethyl-9,10-dihydroacridin-10-yl)benzaldehyde (**4a**) as a pale yellow solid (1.54 g, 91%). ^{1}H NMR ($CDCl_3$, 400 MHz): δ(ppm) = 10.13 (s, 1H), 8.17-8.10 (m, 2H), 7.57-7.52 (m, 2H), 7.51-7.46 (m, 2H), 7.04-6.96 (m, 4H), 6.36-6.31 (m, 2H), 1.69 (s, 6H). ^{13}C NMR ($CDCl_3$, 100 MHz): δ(ppm) = 191.3, 147.5, 140.4, 135.4, 132.3, 131.4, 130.9, 126.5, 125.5, 121.6, 114.9, 36.3, 31.0.

4-(Phenoxazin-10-yl)benzaldehyde (**4b**): Obtained according to the general Buchwald-Hartwig procedure using 4-bromobenzaldehyde (1.00 g, 5.40 mmol), phenoxazine (**3b**, Fluorochem, 98%) (1.09 g, 5.95 mmol), tris(dibenzylideneacetone)dipalladium(0) (247 mg, 0.27 mmol), cesium carbonate (5.28 g, 16.2 mmol), and 1,1'-bis(diphenylphosphino)ferrocene (299 mg, 0.54 mmol). The crude product was purified by column chromatography (ethyl acetate:hexanes, 2:98→5:95) to give 4-(phenoxazin-10-yl)benzaldehyde (**4b**) as an orange solid (1.30 g, 85%). ^{1}H NMR ($CDCl_3$, 400 MHz): δ(ppm) = 10.11 (s, 1H), 8.16-8.07 (m, 2H), 7.59-7.52 (m, 2H), 6.76-6.66 (m, 4H), 6.65-6.56 (m, 2H), 5.96 (dd, J = 7.9, 1.4 Hz, 2H). ^{13}C NMR ($CDCl_3$, 100 MHz): δ(ppm) = 191.1, 145.0, 144.1, 135.9, 133.5, 132.4, 131.5, 123.4, 122.1, 115.9, 113.5.

4-(Phenothiazin-10-yl)benzaldehyde (**4c**): Obtained according to the general Buchwald-Hartwig procedure using 4-bromobenzaldehyde (1.00 g, 5.40 mmol), phenothiazine (**3c**, Abcr, 98%) (1.18 g, 5.95 mmol), tris(dibenzylideneacetone)dipalladium(0) (247 mg, 0.27 mmol), cesium carbonate (5.28 g, 16.2 mmol), and 1,1'-bis(diphenylphosphino)ferrocene (299 mg, 0.54 mmol). The crude product was

purified by column chromatography (toluene) to give 4-(phenothiazin-10-yl)benzaldehyde (**4c**) as a yellow glass (1.30 g, 79%). ^{1}H NMR ($CDCl_3$, 400 MHz): δ(ppm) = 9.85 (s, 1H), 7.75 (d, J = 8.8 Hz, 2H), 7.43 (d, J = 8.0 Hz, 2H), 7.33-7.26 (m, 4H), 7.22-7.13 (m, 4H). ^{13}C NMR ($CDCl_3$, 100 MHz): δ(ppm) = 190.6, 150.3, 141.2, 132.5, 131.7, 130.5, 128.8, 127.4, 126.0, 125.5, 117.0.

4-(Diphenylamino)benzaldehyde (**4d**): Obtained according to the general Buchwald-Hartwig procedure using 4-bromobenzaldehyde (1.00 g, 5.40 mmol), diphenylamine (**3d**, Alfa Aesar, 98%) (1.01 g, 5.95 mmol), tris(dibenzylideneacetone)dipalladium(0) (247 mg, 0.27 mmol), cesium carbonate (5.28 g, 16.2 mmol), and 1,1'-bis(diphenylphosphino)ferrocene (299 mg, 0.54 mmol). The crude product was purified by column chromatography (ethyl acetate:hexanes, 2:98→5:95) to give 4-(diphenylamino)benzaldehyde (**4d**) as a beige solid (877 mg, 59%). ^{1}H NMR ($CDCl_3$, 400 MHz): δ(ppm) = 9.81 (s, 1H), 7.71-7.65 (m, 2H), 7.38-7.31 (m, 4H), 7.20-7.14 (m, 6H), 7.04-6.99 (m, 2H). ^{13}C NMR ($CDCl_3$, 100 MHz): δ(ppm) = 190.5, 153.4, 146.2, 131.4, 129.8, 129.1, 126.4, 125.2, 119.4.

4-(Carbazol-9-yl)benzaldehyde (**4e**): Obtained according to the general Buchwald-Hartwig procedure using 4-bromobenzaldehyde (1.00 g, 5.40 mmol), carbazole (**3e**, Acros Organics, 96%) (995 mg, 5.95 mmol), tris(dibenzylideneacetone)dipalladium(0) (247 mg, 0.27 mmol), cesium carbonate (5.28 g, 16.2 mmol), and 1,1'-bis(diphenylphosphino)ferrocene (299 mg, 0.54 mmol). The crude product was purified by column chromatography (chloroform:hexanes, 40:60→60:40) to give 4-(carbazol-9-yl)benzaldehyde (**4e**) as an off-white solid (1.09 g, 74%). ^{1}H NMR ($CDCl_3$, 400 MHz): δ(ppm) = 10.12 (s, 1H), 8.18-8.11 (m, 4H), 7.83-7.78 (m, 2H), 7.51 (d, J = 8.2 Hz, 2H), 7.47-7.41 (m, 2H), 7.36-7.31 (m, 2H). ^{13}C NMR ($CDCl_3$, 100 MHz): δ(ppm) = 191.0, 143.3, 140.0, 134.6, 131.4, 126.8, 126.3, 124.0, 120.9, 120.6, 109.8.

4-(3,6-Di-*tert*-butylcarbazol-9-yl)benzaldehyde (**4f**): Obtained according to the general Buchwald-Hartwig procedure using 4-bromobenzaldehyde (601 mg, 3.25 mmol), 3,6-di-*tert*-butylcarbazole (**3f**) (1.00 g, 3.58 mmol), tris(dibenzylideneacetone)dipalladium(0) (147 mg, 0.16 mmol), cesium carbonate (3.18 g, 9.76 mmol), and 1,1'-bis(diphenylphosphino)ferrocene (183 mg, 0.33 mmol). The crude product was purified by column chromatography (chloroform:hexanes, 40:60→60:40) to give 4-(3,6-di-*tert*-butylcarbazol-9-yl)benzaldehyde (**4f**) as a white solid (1.14 g, 92%). ^{1}H NMR ($CDCl_3$, 400 MHz): δ(ppm) = 10.10 (s, 1H), 8.16-8.09 (m, 4H), 7.81-7.77 (m, 2H), 7.51-7.44 (m, 4H), 1.48 (s, 18H). ^{13}C NMR ($CDCl_3$, 100 MHz): δ(ppm) = 191.1, 144.0, 138.5, 134.2, 131.4, 126.3, 124.2, 124.1, 116.6, 109.4, 34.9, 32.1.

Synthesis of the BODIPY dyads[10]

Photosensitizers **5a-f** (and BODIPY **5H**) were synthesized according to the following Knoevenagel-type procedure: 1,3,5,7-Tetramethyl-BODIPY **2** (1 equiv) and aldehyde **4a-f** (or benzaldehyde) (4 equiv) were put under inert atmosphere and dissolved in dry *N*,*N*-dimethylformamide (60 mL/mmol BODIPY). Glacial acetic acid (1 mL/mmol BODIPY) and piperidine (1 mL/mmol BODIPY) were added to the reaction mixture. The vessel was heated for 5 min at 150 °C under microwave irradiation (1 min pre-stirring). After evaporating the solvent, the crude product was purified by column chromatography (silica) to obtain BODIPY dyads **5a-f** (and BODIPY **5H**). Because of the small differences in R_f values of the mono-, di-, tri-, and tetra-substituted compounds, further purification was performed *via* preparative (recycling) size exclusion chromatography (prep-SEC) to obtain BODIPYs **5a-f** (and **5H**) in pure form.

1,7-Dimethyl-3,5-di(4-(9,9-dimethyl-9,10-dihydroacridin-10-yl)styryl)-8-mesityl-4,4-difluoro-4-bora-3a,4a-diaza-*s*-indacene (**5a**)[10]: Obtained according to the general Knoevenagel-type procedure using 1,3,5,7-tetramethyl-8-mesityl-BODIPY **2** (36.6 mg, 0.1 mmol) and 4-(9,9-dimethyl-9,10-dihydroacridin-10-yl)benzaldehyde (**4a**) (125.4 mg, 0.4 mmol). The crude product was purified by column chromatography (dichloromethane:hexanes, 30:70), followed by prep-SEC, affording **5a** as a dark blue solid with red metallic luster (63.4 mg, 66%). ^{1}H NMR ($CDCl_3$, 400 MHz): δ(ppm) = 7.89-7.81 (m, 6H), 7.45 (dd, *J* = 7.7, 1.6 Hz, 4H), 7.40-7.33 (m, 6H), 7.03-6.89 (m, 10H), 6.71 (s, 2H), 6.34 (dd, *J* = 8.1, 1.4 Hz, 4H), 2.38 (s, 3H), 2.18 (s, 6H), 1.69 (s, 12H), 1.51 (s, 6H). ^{13}C NMR ($CDCl_3$, 100 MHz): δ(ppm) = 152.4, 141.9, 141.7, 140.9, 139.7, 139.0, 136.7, 135.4, 135.1, 133.0, 131.8, 131.2, 130.2, 129.9, 129.2, 126.6, 125.4, 120.8, 120.5, 117.8, 114.2, 36.1, 31.4, 21.4, 19.9, 13.9. MS (MALDI-ToF): calculated for $C_{66}H_{59}BF_2N_4$: 956.480; found: 956.481.

1,7-Dimethyl-3,5-di(4-(phenoxazin-10-yl)styryl)-8-mesityl-4,4-difluoro-4-bora-3a,4a-diaza-*s*-indacene (**5b**): Obtained according to the general Knoevenagel-type procedure using 1,3,5,7-tetramethyl-8-mesityl-BODIPY **2** (36.6 mg, 0.1 mmol) and 4-(phenoxazin-10-yl)benzaldehyde (**4b**) (115 mg, 0.4 mmol). The crude product was purified by column chromatography (chloroform:hexanes, 40:60→60:40), followed by prep-SEC, affording **5b** as a purple solid with copper metallic luster (48.5 mg, 54%). ^{1}H NMR ($CDCl_3$, 400 MHz): δ(ppm) = 7.86-7.76 (m, 6H), 7.39-7.28 (m, 6H), 7.00 (s, 2H), 6.72-6.57 (m, 14H), 6.00 (dd, *J* = 7.7, 1.7 Hz, 4H), 2.37 (s, 3H), 2.16 (s, 6H), 1.50 (s, 6H). ^{13}C NMR ($CDCl_3$, 100 MHz): δ(ppm) = 152.3, 144.0, 142.0, 139.8, 139.3, 139.0, 136.9, 135.3, 134.8, 134.3, 133.0, 131.3, 131.1, 130.0, 129.2, 123.4, 121.5, 120.7, 117.8, 115.6, 113.4, 21.4, 19.8, 13.9. MS (MALDI-ToF): calculated for $C_{60}H_{47}BF_2N_4O_2$: 904.376; found: 904.370

1,7-Dimethyl-3,5-di(4-(phenothiazin-10-yl)styryl)-8-mesityl-4,4-difluoro-4-bora-3a,4a-diaza-*s*-indacene (**5c**): Obtained according to the general Knoevenagel-type procedure using 1,3,5,7-tetramethyl-8-mesityl-BODIPY **2** (36.6 mg, 0.1 mmol) and 4-(phenothiazin-10-yl)benzaldehyde (**4c**) (121 mg, 0.4 mmol). The crude product was purified by column chromatography (chloroform:hexanes, 40:60→60:40), followed by prep-SEC, affording **5c** as a cyan solid with blue metallic luster (85.3 mg, 91%). ^{1}H NMR ($CDCl_3$, 400 MHz): δ(ppm) = 7.82-7.74 (m, 6H), 7.40-7.31 (m, 4H), 7.30 (d, *J* = 16.3 Hz, 2H), 7.08 (dd, *J* = 7.5, 1.6 Hz, 4H), 6.99 (s, 2H), 6.97-6.83 (m, 8H), 6.68 (s, 2H), 6.43 (dd, *J* = 8.1, 1.3 Hz, 4H), 2.37 (s, 3H), 2.15 (s, 6H), 1.49 (s, 6H). ^{13}C NMR ($CDCl_3$, 100 MHz): δ(ppm) = 152.3, 143.9, 142.1, 141.8, 139.3, 138.9, 135.8, 135.4, 134.9, 132.9, 131.2, 129.6, 129.1, 127.1, 127.1, 123.2, 122.2, 120.1, 117.7, 21.4, 19.8, 13.8. MS (MALDI-ToF): calculated for $C_{60}H_{47}BF_2N_4S_2$: 936.330; found: 936.330.

1,7-Dimethyl-3,5-di(4-(diphenylamino)styryl)-8-mesityl-4,4-difluoro-4-bora-3a,4a-diaza-*s*-indacene (**5d**): Obtained according to the general Knoevenagel-type procedure using 1,3,5,7-tetramethyl-8-mesityl-BODIPY **2** (36.6 mg, 0.1 mmol) and 4-(diphenylamino)benzaldehyde (**4d**) (109 mg, 0.4 mmol). The crude product was purified by column chromatography (chloroform:hexanes, 40:60→60:40), followed by prep-SEC, affording **5d** as a dark green solid (77.4 mg, 86%). ^{1}H NMR ($CDCl_3$, 400 MHz): δ(ppm) = 7.61 (d, *J* = 16.2 Hz, 2H), 7.47 (d, *J* = 8.7 Hz, 4H), 7.31-7.26 (m, 8H), 7.18 (d, *J* = 16.3 Hz, 2H), 7.15-7.11 (m, 8H), 7.09-7.01 (m, 8H), 6.96 (s, 2H), 6.60 (s, 2H), 2.35 (s, 3H), 2.13 (s, 6H), 1.44 (s, 6H). ^{13}C NMR ($CDCl_3$, 100 MHz): δ(ppm) = 152.5, 148.6, 147.3, 141.0, 138.6, 137.5, 135.6, 135.4, 132.6, 131.5, 130.6, 129.5, 129.0, 128.6, 125.1, 123.7, 122.6, 117.6, 117.3, 21.4, 19.8, 13.8. MS (MALDI-ToF): calculated for $C_{60}H_{51}BF_2N_4$: 876.417; found: 876.415.

1,7-Dimethyl-3,5-di(4-(carbazol-9-yl)styryl)-8-mesityl-4,4-difluoro-4-bora-3a,4a-diaza-*s*-indacene (**5e**): Obtained according to the general Knoevenagel-type procedure using 1,3,5,7-tetramethyl-8-mesityl-BODIPY **2** (36.6 mg, 0.1 mmol) and 4-(carbazol-9-yl)benzaldehyde (**4e**) (109 mg, 0.4 mmol). The crude product was purified by column chromatography (chloroform:hexanes, 40:60→60:40), followed by prep-SEC, affording **5e** as a green solid (48.8 mg, 56%). ^{1}H NMR ($CDCl_3$, 400 MHz): δ(ppm) = 8.15 (d, *J* = 7.7 Hz, 4H), 7.91-7.81 (m, 6H), 7.62 (d, *J* = 8.4 Hz, 4H), 7.51-7.27 (m, 14H), 7.01 (s, 2H), 6.72 (s, 2H), 2.38 (s, 3H), 2.17 (s, 6H), 1.51 (s, 6H). ^{13}C NMR ($CDCl_3$, 100 MHz): δ(ppm) = 152.3, 141.8, 140.7, 139.4, 138.9, 138.1, 135.7, 135.4, 134.9, 133.0, 131.2, 129.2, 128.9, 127.2, 126.2, 123.6, 120.5, 120.3, 120.1, 117.8, 110.0, 21.4, 19.8, 13.9. MS (MALDI-ToF): calculated for $C_{60}H_{47}BF_2N_4$: 872.386; found: 872.384.

1,7-Dimethyl-3,5-di(4-(3,6-di-*tert*-butylcarbazol-9-yl)styryl)-8-mesityl-4,4-difluoro-4-bora-3a,4a-diaza-*s*-indacene (**5f**): Obtained according to the general Knoevenagel-type procedure using 1,3,5,7-tetramethyl-8-mesityl-BODIPY **2** (36.6 mg, 0.1 mmol) and 4-(3,6-di-*tert*-butylcarbazol-9-yl)benzaldehyde (**4f**) (153 mg, 0.4 mmol). The crude product was purified by column chromatography (chloroform:hexanes, 30:70→50:50), followed by prep-SEC, affording **5f** as a green solid (65.5 mg, 60%). ^{1}H NMR ($CDCl_3$, 400 MHz): δ(ppm) = 8.14 (d, *J* = 1.3 Hz, 4H), 7.89-7.81 (m, 6H), 7.62 (d, *J* = 8.5 Hz, 4H), 7.50-7.42 (m, 8H), 7.36 (d, *J* = 16.3 Hz, 2H), 7.01 (s, 2H), 6.71 (s, 2H), 2.38 (s, 3H), 2.18 (s, 6H), 1.51 (s, 6H), 1.47 (s, 36H). ^{13}C NMR ($CDCl_3$, 100 MHz): δ(ppm) = 152.4, 143.2, 141.8, 139.2, 139.0, 138.9, 138.7, 135.5, 135.2, 135.1, 132.9, 131.3, 129.2, 128.9, 126.7, 123.8, 123.7, 119.9, 117.8, 116.4, 109.5, 34.9, 32.1, 21.4, 19.8, 13.8. MS (MALDI-ToF): calculated for $C_{76}H_{79}BF_2N_4$: 1096.637; found: 1096.637.

1,7-Dimethyl-3,5-distyryl-8-mesityl-4,4-difluoro-4-bora-3a,4a-diaza-*s*-indacene (**5H**): Obtained according to the general Knoevenagel-type procedure using 1,3,5,7-tetramethyl-8-mesityl-BODIPY **2** (36.6 mg, 0.1 mmol) and benzaldehyde (0.04 mL, 0.4 mmol). The crude product was purified by column chromatography (chloroform:hexanes, 40:60→60:40), followed by prep-SEC, affording **5H** as a dark blue solid with red metallic luster (45.0 mg, 83%). ^{1}H NMR ($CDCl_3$, 400 MHz): δ(ppm) = 7.75 (d, *J* = 16.4 Hz, 2H), 7.64 (d, *J* = 7.2 Hz, 4H), 7.40 (t, *J* = 7.4 Hz, 4H), 7.35-7.22 (m, 4H), 6.97 (s, 2H), 6.64 (s, 2H), 2.35 (s, 3H), 2.13 (s, 6H), 1.46 (s, 6H). ^{13}C NMR ($CDCl_3$, 100 MHz): δ(ppm) = 152.5, 141.6, 139.2, 138.8, 136.8, 136.1, 135.4, 132.7, 131.3, 129.1, 129.0, 128.9, 127.7, 119.5, 117.6, 21.4, 19.8, 13.8.

3. DFT orbital topologies and energies

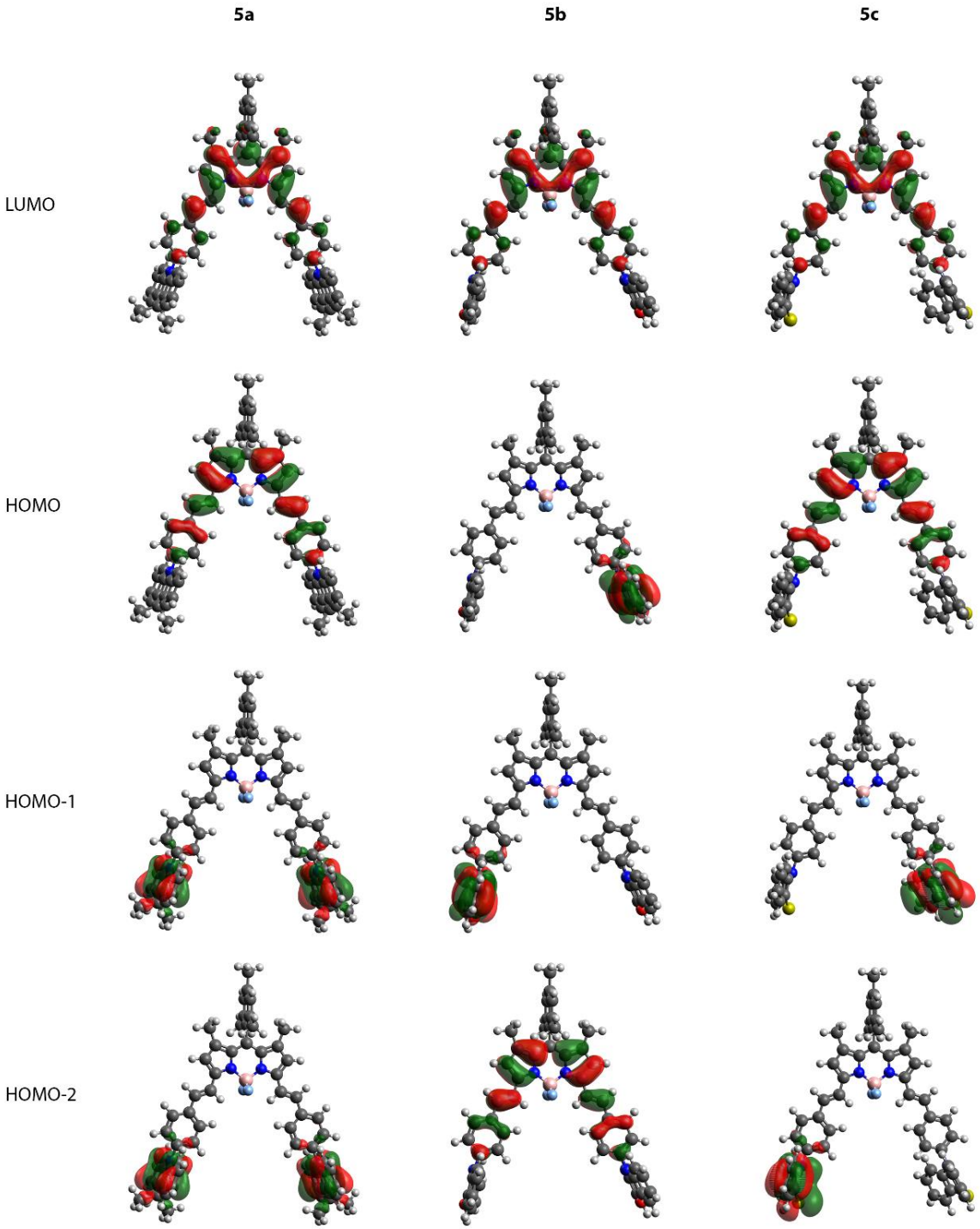

Figure S1: Orbital topologies for BODIPYs **5a-c** in chloroform solution as obtained using density functional theory calculations with M06-2X/6-311G(d) and the polarizable continuum solvation model. Isosurface values of 0.02 (a.u.) were used for all orbitals.

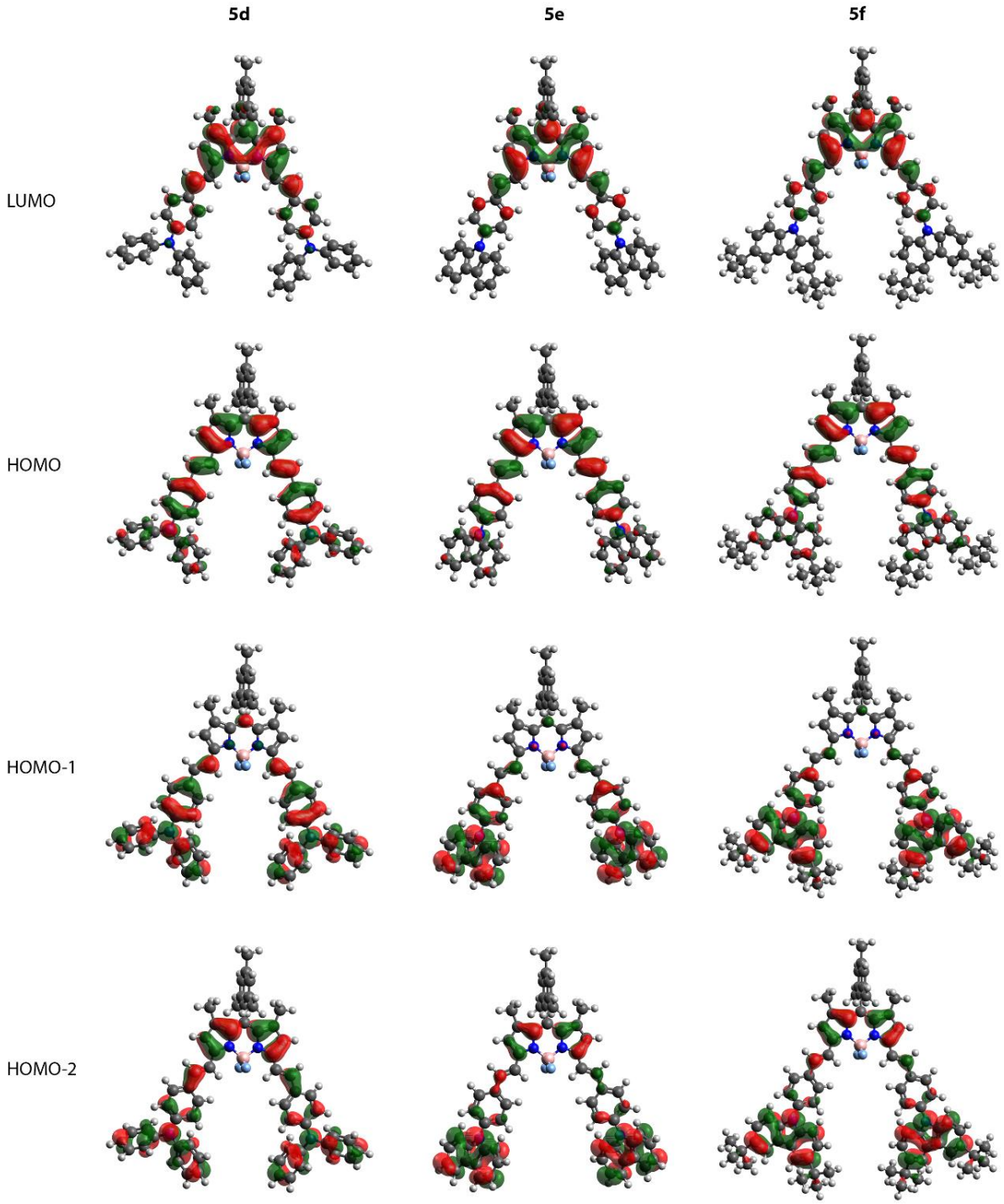

Figure S2: Orbital topologies for BODIPYs **5d-f** in chloroform solution as obtained using density functional theory calculations with M06-2X/6-311G(d) and the polarizable continuum solvation model. Isosurface values of 0.02 (a.u.) were used for all orbitals.

Table S1: Orbital energies (in eV) for the LUMO, HOMO, HOMO-1, and HOMO-2 of BODIPYs **5a-f** as obtained by density functional theory calculations using M062X/6-311G(d).

BODIPY	HOMO-2	HOMO-1	HOMO	LUMO
5a	-6.469	-6.469	-6.427	-2.489
5b	-6.462	-6.422	-6.415	-2.518
5c	-6.635	-6.632	-6.455	-2.513
5d	-6.910	-6.469	-5.975	-2.330
5e	-7.066	-6.893	-6.323	-2.475
5f	-6.883	-6.688	-6.263	-2.457

4. Single-crystal X-ray diffraction

Single crystals of BODIPYs **5a**, **5c**, and **5e** were obtained by slow evaporation from tetrahydrofuran (THF). Metallic dark blue plate-like single crystals of each compound were selected and mounted on a MiTeGen MicroMounts sample holder. Single-crystal X-ray diffraction data were collected using an Oxford Diffraction Gemini R Ultra diffractometer (Mo *Kα* with graphite monochromator for **5a**, Cu *Kα* with multilayer mirror for **5c** and **5e**, Ruby CCD area detector) at 295(2) K. Data collection, unit cell determination, and data reduction were carried out using the CrysAlis PRO software package[11]. Using Olex2[12] and shelXle[13], the structure was solved with the SHELXT 2015[14] structure solution program by Intrinsic Phasing methods and refined by full-matrix least squares on $|F|^2$ using SHELXL-2018/3[15]. Non-hydrogen atoms were refined anisotropically. Most of the hydrogen atoms were localized from the electron density map. All hydrogen atoms were placed on calculated positions in riding mode with temperature factors fixed at 1.2 times U_{eq} of the parent carbon atoms (1.5 times for methyl groups).

- The structure of BODIPY **5a** contains five molecules of disordered THF per two main molecules (Figure S3). The tetrahydrofuran molecules were localized and refined.
- The structure of BODIPY **5c** contains two molecules of highly disordered THF per one main molecule (Figure S4). These solvent molecules were taken into account using the SQUEEZE[16] procedure.
- We observed and refined displacement disorder of a 9*H*-carbazole fragment with 60:40 occupancy ratio in the structure of BODIPY **5e** (Figure S5).

Additional crystallographic details are given in Table S2.

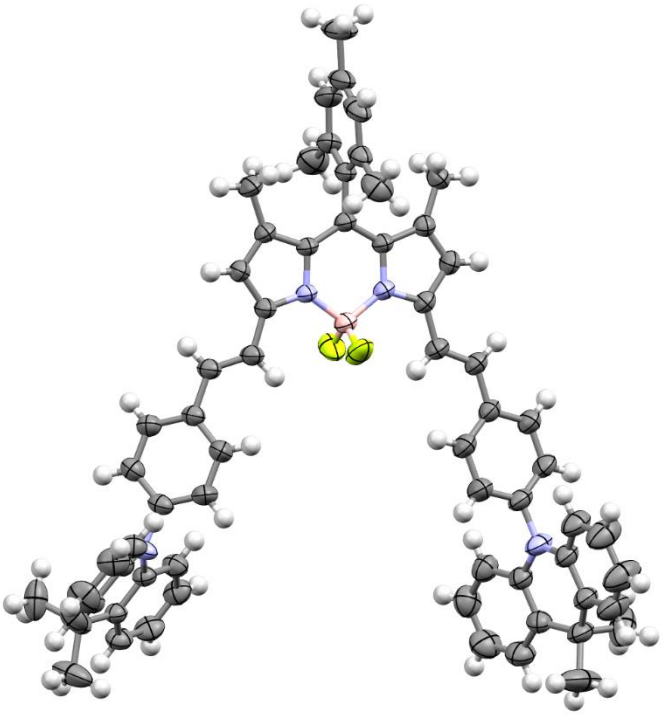

Figure S3: Molecular structure of BODIPY **5a**, obtained from single-crystal X-ray diffraction analysis. THF solvent molecules are omitted for clarity.

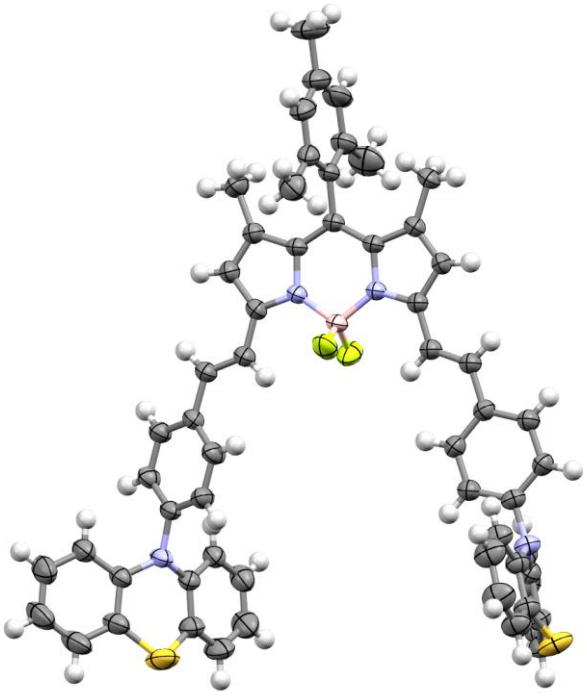

Figure S4: Molecular structure of BODIPY **5c**, obtained from single-crystal X-ray diffraction analysis.

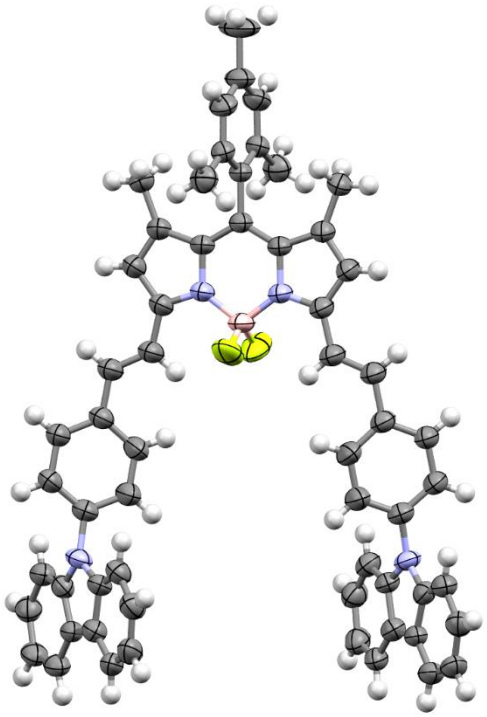

Figure S5: Molecular structure of BODIPY **5e**, obtained from single-crystal X-ray diffraction analysis. The second component of the disorder is omitted for clarity.

Table S2: Crystallographic details for BODIPYs **5a**, **5c**, and **5e**.

	5a	**5c**	**5e**
Chemical formula	$2(C_{66}H_{59}BF_2N_4)\cdot5(C_4H_8O)$	$C_{60}H_{47}BF_2N_4S_2\cdot2(C_4H_8O)$	$C_{60}H_{47}BF_2N_4$
M_r[a]	2274.47	1081.15	872.82
Crystal system	Triclinic	Monoclinic	Monoclinic
Space group	*P*$^{-}$*1*	*P2₁/c*	C2/c
a, *b*, *c* (Å)[b]	9.2327 (4), 18.5957 (8), 20.4172 (9)	18.46202 (13), 33.0260 (2), 8.81015 (6)	15.9492 (2), 18.5820 (2), 15.84353 (19)
α, *β*, *γ* (°)[c]	72.149 (4), 79.347 (4), 76.492 (4)	90, 96.2948 (7), 90	90, 99.2982 (12), 90
V (Å^3)[d]	3220.0 (3)	5339.40 (7)	4633.84 (10)
Z[e]	1	4	4
Radiation type	Mo *Kα*	Cu *Kα*	Cu *Kα*
μ (mm^{-1})[f]	0.07	1.38	0.62
Crystal size (mm)	0.71 × 0.21 × 0.08	0.41 × 0.17 × 0.02	0.34 × 0.15 × 0.02
Absorption correction	Analytical *CrysAlis PRO*	Gaussian *CrysAlis PRO*	Analytical *CrysAlis PRO*
T_{min}, T_{max}[g]	0.958, 0.995	0.600, 1.000	0.882, 0.986
No. of measured, independent, and observed [$I > 2\sigma(I)$] reflections	25118, 11355, 7964	28841, 9453, 8159	12050, 4102, 3464
R_{int}[h]	0.025	0.022	0.013
$(\sin\theta/\lambda)_{max}$ (Å^{-1})	0.595	0.598	0.597
$R[F^2 > 2\sigma(F^2)]$, $wR(F^2)$, S[i]	0.062, 0.195, 1.02	0.041, 0.116, 1.04	0.037, 0.107, 1.02
No. of reflections	11355	9453	4102
No. of parameters	848	627	426
No. of restraints	563	0	144
$\Delta\rho_{max}$, $\Delta\rho_{min}$ (e·Å^{-3})[j]	0.40, -0.25	0.25, -0.37	0.11, -0.16
CCDC deposition number[k]	2122792	2122793	2122794

[a] Formula mass. [b] Unit cell vector lengths. [c] Unit cell inner-vector angles. [d] Unit cell volume. [e] Number of formula units in the unit cell. [f] Absorption coefficient. [g] Transmission limits. [h] Residual/reliability factor. [i] Framework parameters. [j] Residual density. [k] CCDC = Cambridge Crystallographic Data Centre.

5. Excited state – ground state electron density differences

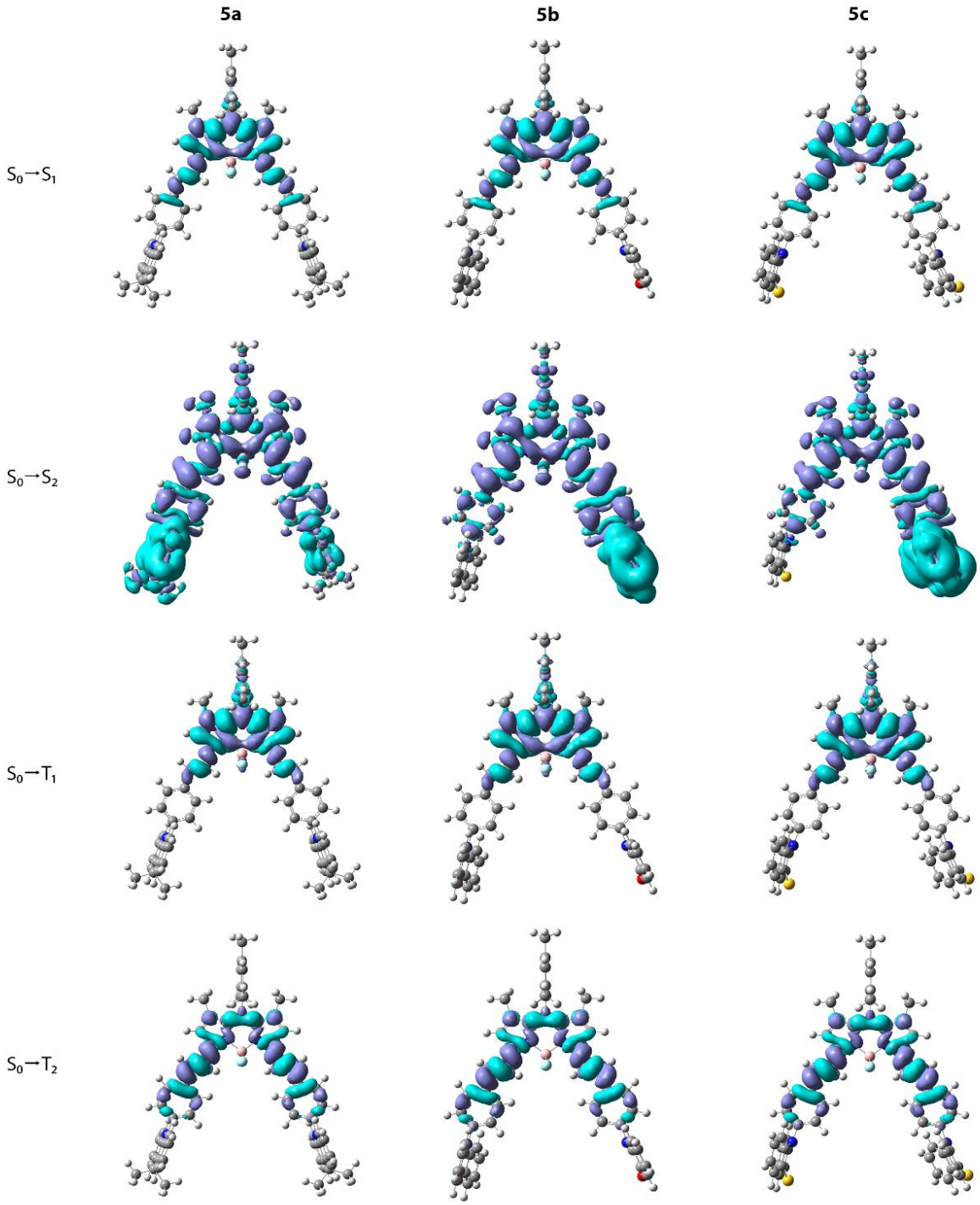

Figure S6: Excited state – ground state electron density differences for BODIPYs **5a-c** as obtained using M06-2X/6-311G(d) and the polarizable continuum solvation model (chloroform). Purple indicates areas of increased electron density, while cyan indicates areas of decreased electron density (isosurface value = 0.0004 a.u. for all densities).

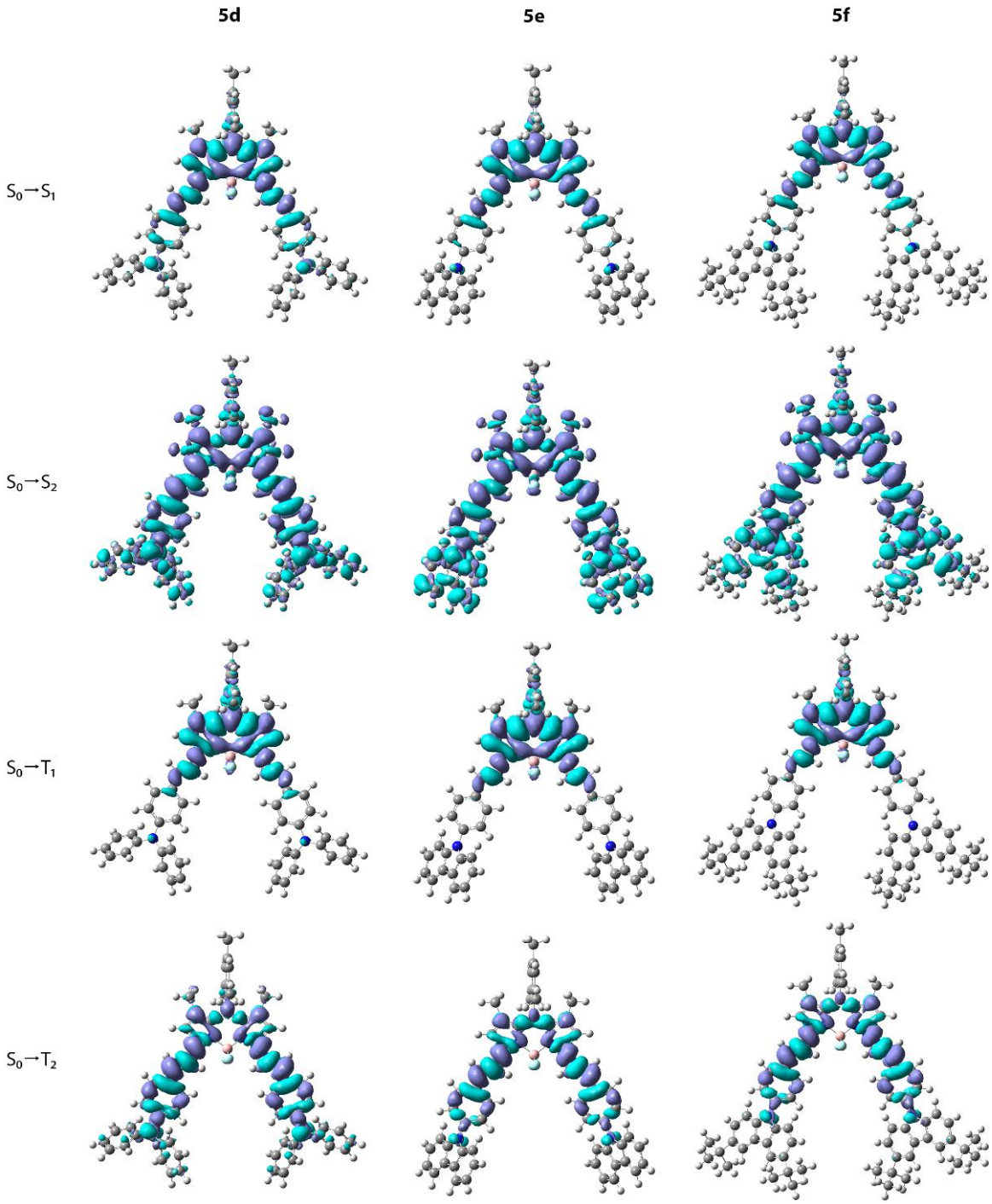

Figure S7: Excited state – ground state electron density differences for BODIPYs **5d-f** as obtained using M06-2X/6-311G(d) and the polarizable continuum solvation model (chloroform). Purple indicates areas of increased electron density, while cyan indicates areas of decreased electron density (isosurface value = 0.0004 a.u. for all densities).

6. Singlet oxygen generation plots

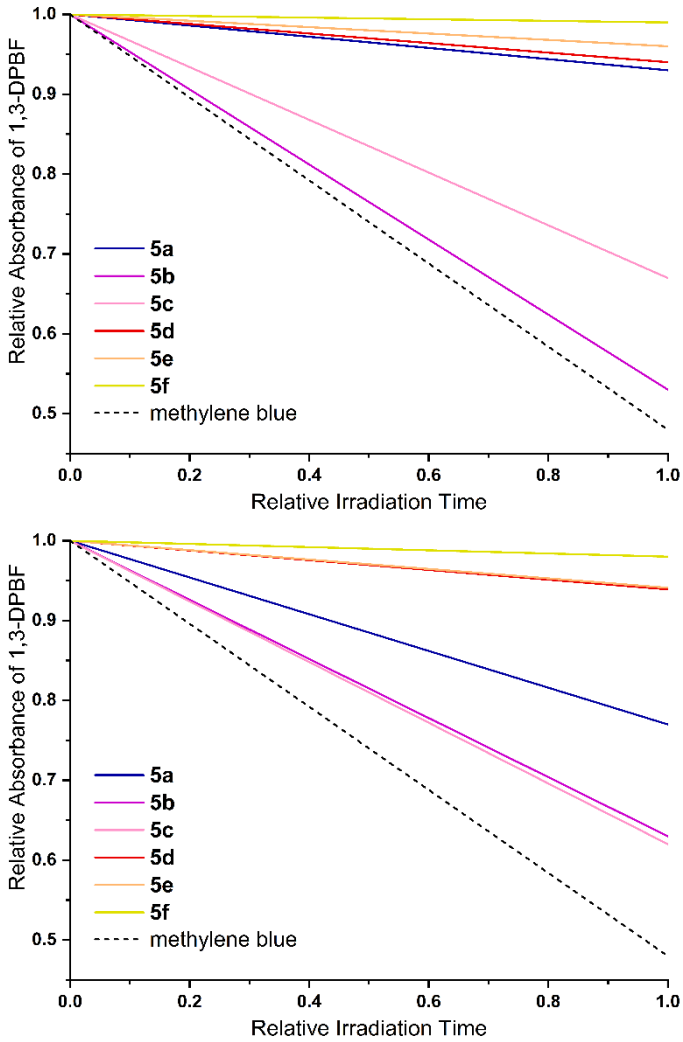

Figure S8: Relative decrease in absorbance of 1,3-diphenylisobenzofuran (1,3-DPBF) at 414 nm under continuous irradiation using a single 639 nm LED in the presence of BODIPY dyads **5a-f** in toluene (top) and chloroform (bottom). Methylene blue was used as a standard (Φ_Δ = 0.52 in ethanol).

7. Full absorption spectra and data

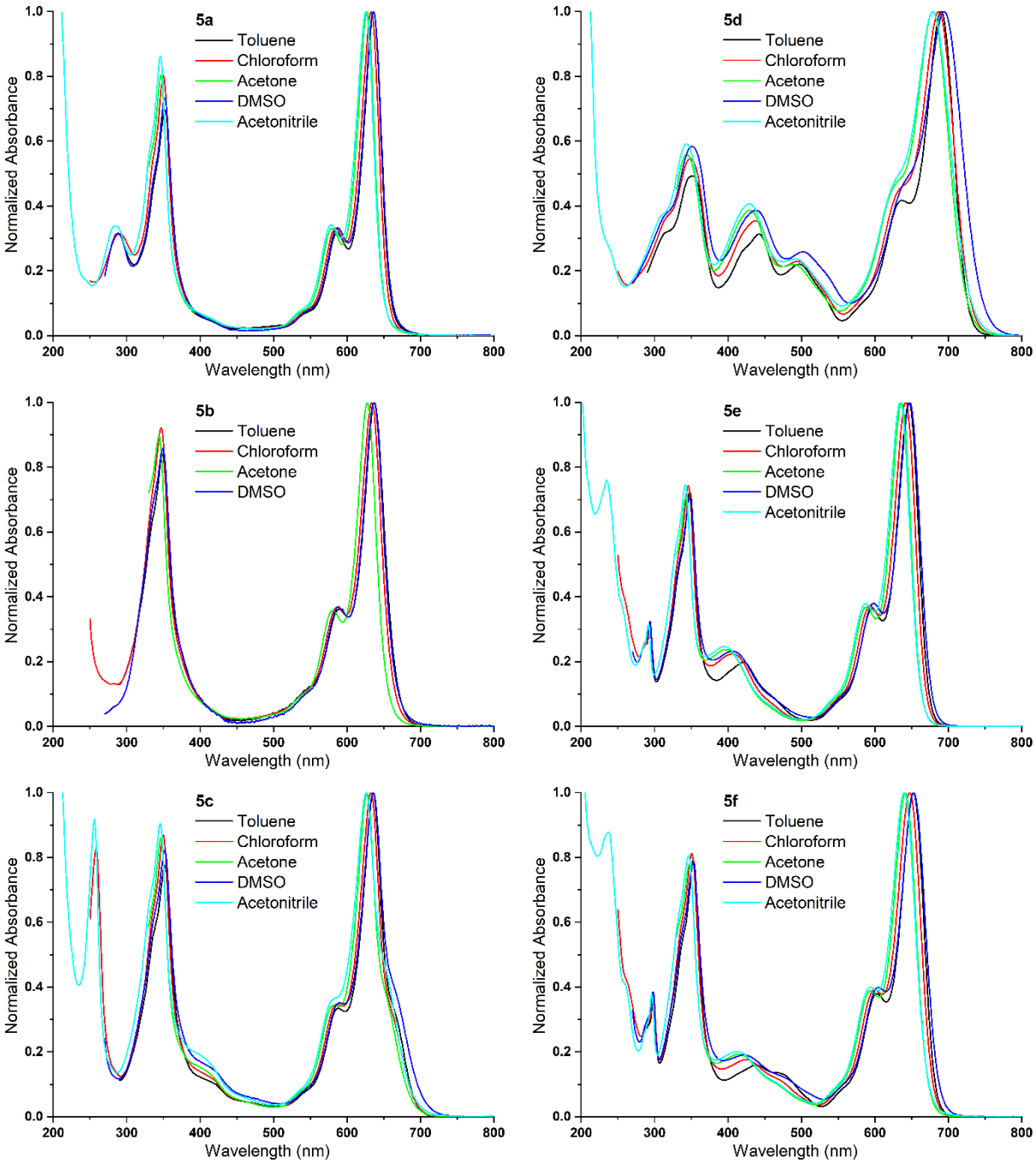

Figure S9: Normalized absorption spectra of BODIPYs **5a-f** in toluene, chloroform, acetone, dimethyl sulfoxide, and acetonitrile solution. Compound **5b** is not soluble in acetonitrile.

Table S3: Additional spectroscopic absorption data (*i.e.* UV absorption bands) for BODIPY dyads **5a-f** in toluene, chloroform, acetone, dimethyl sulfoxide, and acetonitrile solution.[a]

BODIPY	Solvent	λ_{abs} (nm)[b]	$fwhm_{abs}$ (cm^{-1})[c]
5a	Toluene	352	2852
	Chloroform	350	2674
	Acetone	347	2710
	DMSO	352	2676
	Acetonitrile	346	2684
5b	Toluene	349	3353
	Chloroform	347	3099
	Acetone	344	3688
	DMSO	349	3483
	Acetonitrile	-[d]	-[d]
5c	Toluene	352	3263
	Chloroform	350	3016
	Acetone	346	2820
	DMSO	352	3431
	Acetonitrile	346	3190
5d	Toluene	351	6563
	Chloroform	348	6567
	Acetone	344	6964
	DMSO	351	7012
	Acetonitrile	344	6747
5e	Toluene	348	2810
	Chloroform	346	2820
	Acetone	343	2852
	DMSO	348	3309
	Acetonitrile	342	2948
5f	Toluene	353	2892
	Chloroform	351	3006
	Acetone	347	3051
	DMSO	352	4577
	Acetonitrile	346	3209

[a] Spectrograde solvents were used for all measurements. [b] Absorption maximum of the main UV band. [c] Full-width-at-half-maximum of the main UV absorption band. [d] Not soluble.

8. Phenothiazine coplanar conformer – relaxed potential energy surface scan, geometry, orbital topologies, and electron density differences

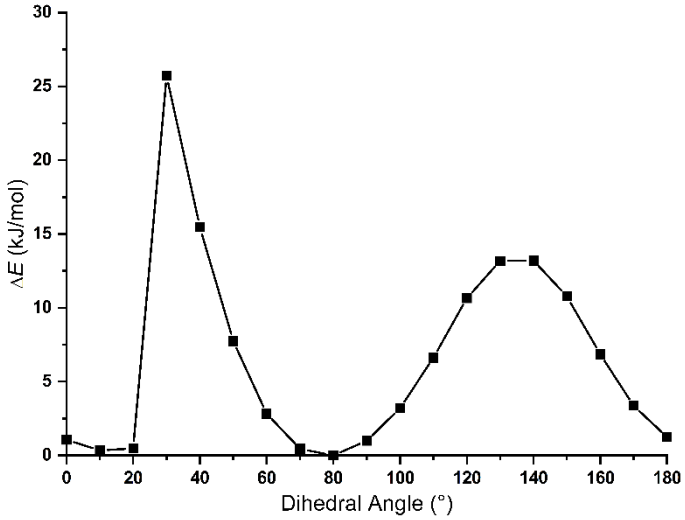

Figure S10: Relaxed potential energy surface scan for BODIPY **5c** in chloroform solution, wherein one donor is rotated with respect to the distyryl substituent. Calculations were performed using M06-2X/6-311G(d) and the polarizable continuum solvent model.

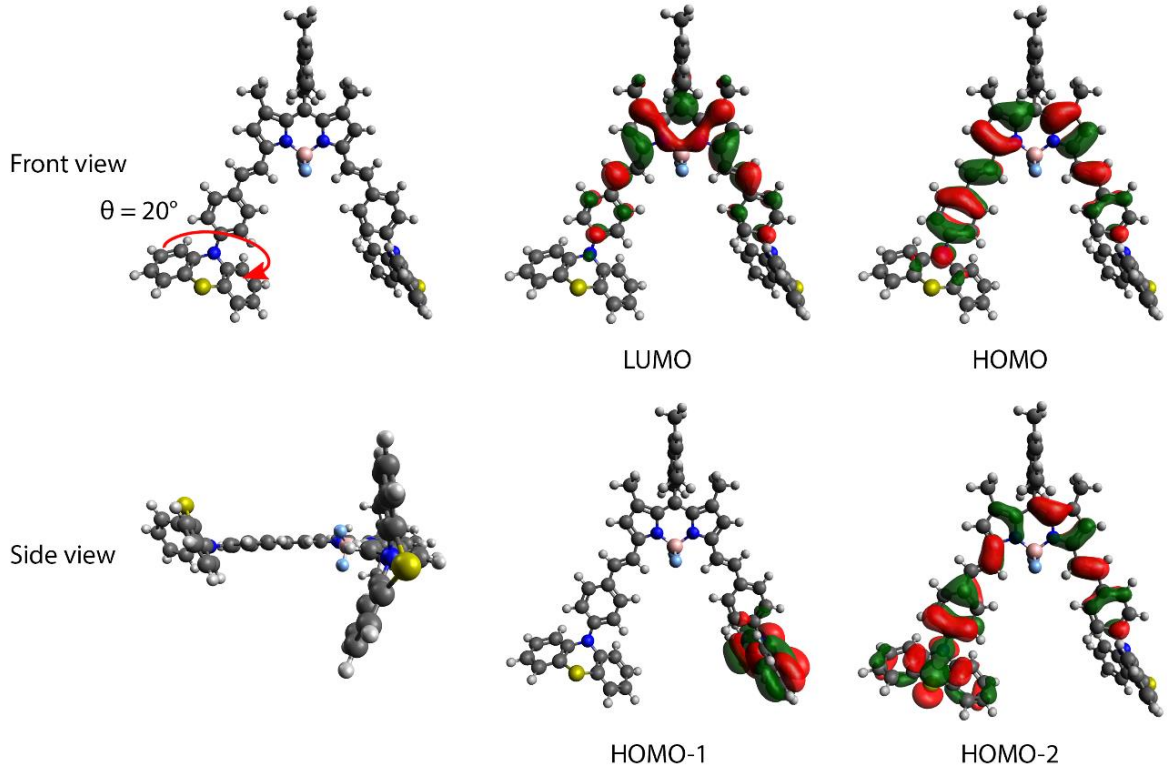

Figure S11: Optimized ground-state geometry and orbital topologies for the coplanar conformer of BODIPY **5c** in chloroform solution as obtained using density functional theory calculations with M06-2X/6-311G(d) and the polarizable continuum solvation model. Isosurface values of 0.02 (a.u.) were used for all orbitals.

Table S4: Calculated vertical singlet (S_1 and S_2) excitation energies and their corresponding oscillator strengths for the coplanar conformer of BODIPY **5c**. The dominant nature of the one-particle excitations is also given.

BODIPY	$S_0 \rightarrow S_1$			$S_0 \rightarrow S_2$		
	ΔE (eV)[a]	Osc. Str.[b]	Nature[c]	ΔE (eV)[a]	Osc. Str.[b]	Nature[c]
5c conformer	2.06 (603 nm)	1.28	H→L (94%)	3.27	1.50	H-2→L (81%)

[a] Vertical excitation energy/wavelength. [b] Oscillator strength. [c] H = HOMO, L = LUMO.

Table S5: Amount of charge-transfer character (d_{CT}) and change in dipole moment ($\Delta\mu$, excited state dipole – ground state dipole) accompanying the $S_0 \rightarrow S_n$ (n = 1,2) transitions in chloroform.

BODIPY	$S_0 \rightarrow S_1$		$S_0 \rightarrow S_2$	
	d_{CT} (Å)[a]	$\Delta\mu$ (D)[b]	d_{CT} (Å)[a]	$\Delta\mu$ (D)[b]
5c conformer	1.64	3.8	4.29	15.8

[a] Distance over which charge is transferred between the indicated states upon excitation. [b] Change in dipole moment upon excitation.

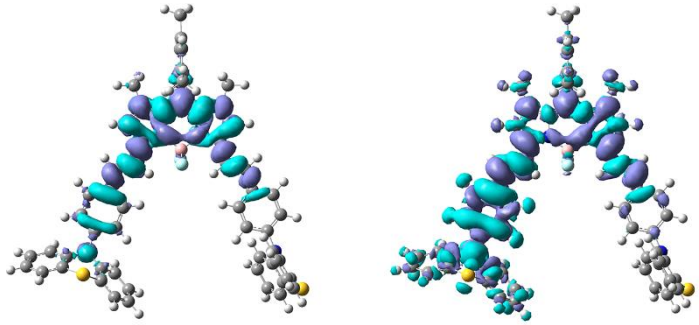

Figure S12: Excited state – ground state electron density differences for the coplanar conformer of BODIPY **5c** as obtained using M06-2X/6-311G(d) and the polarizable continuum solvation model (chloroform). Purple indicates areas of increased electron density, while cyan indicates areas of decreased electron density (isosurface value = 0.0004 a.u. for all densities).

9. Additional absorption and emission spectra and data

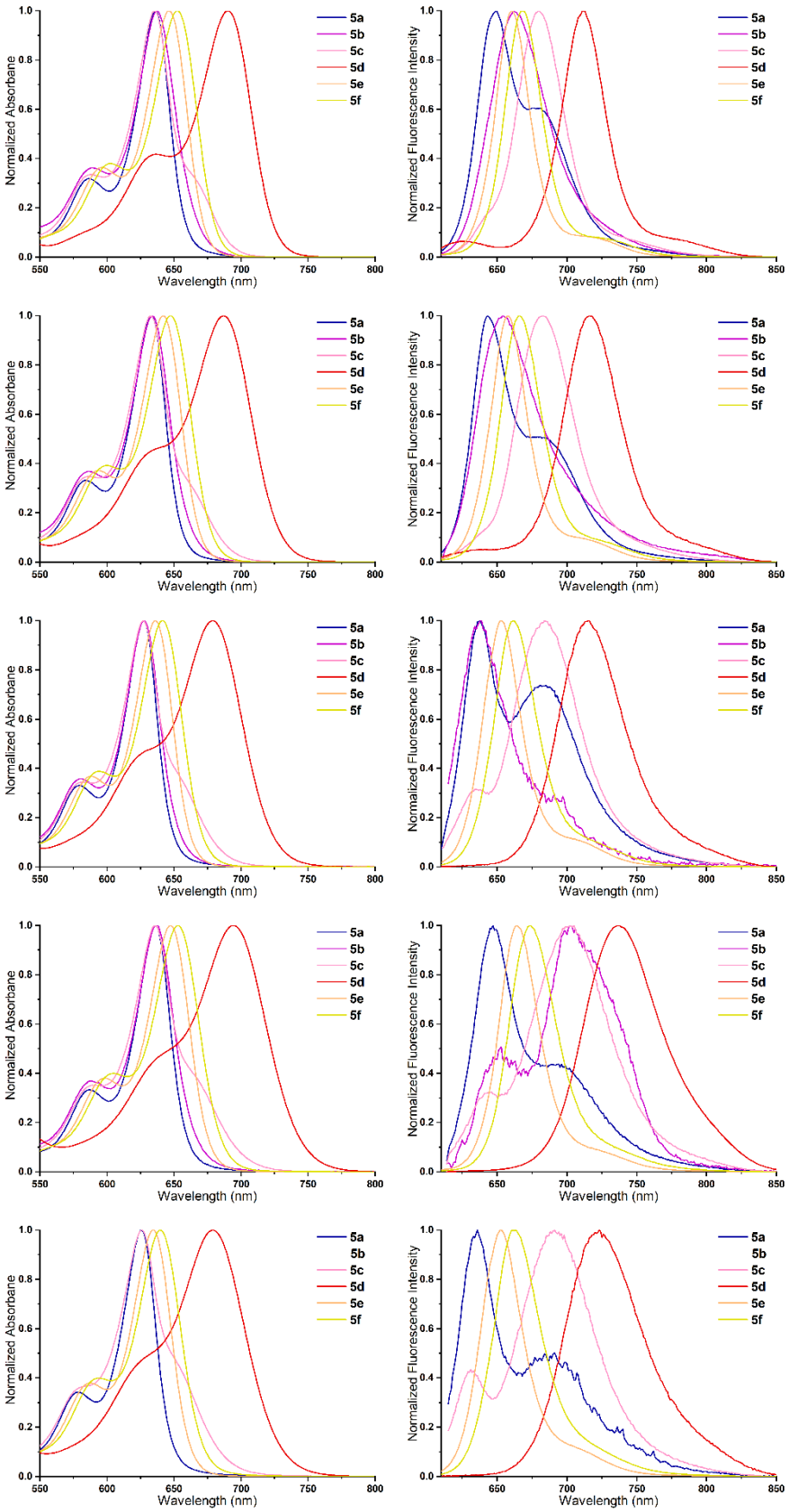

Figure S13: Normalized absorption (left) and fluorescence emission (right; λ_{exc} = 605 nm) spectra of BODIPYs **5a-f** in – from top to bottom – toluene, chloroform, acetone, dimethyl sulfoxide, and acetonitrile solution.

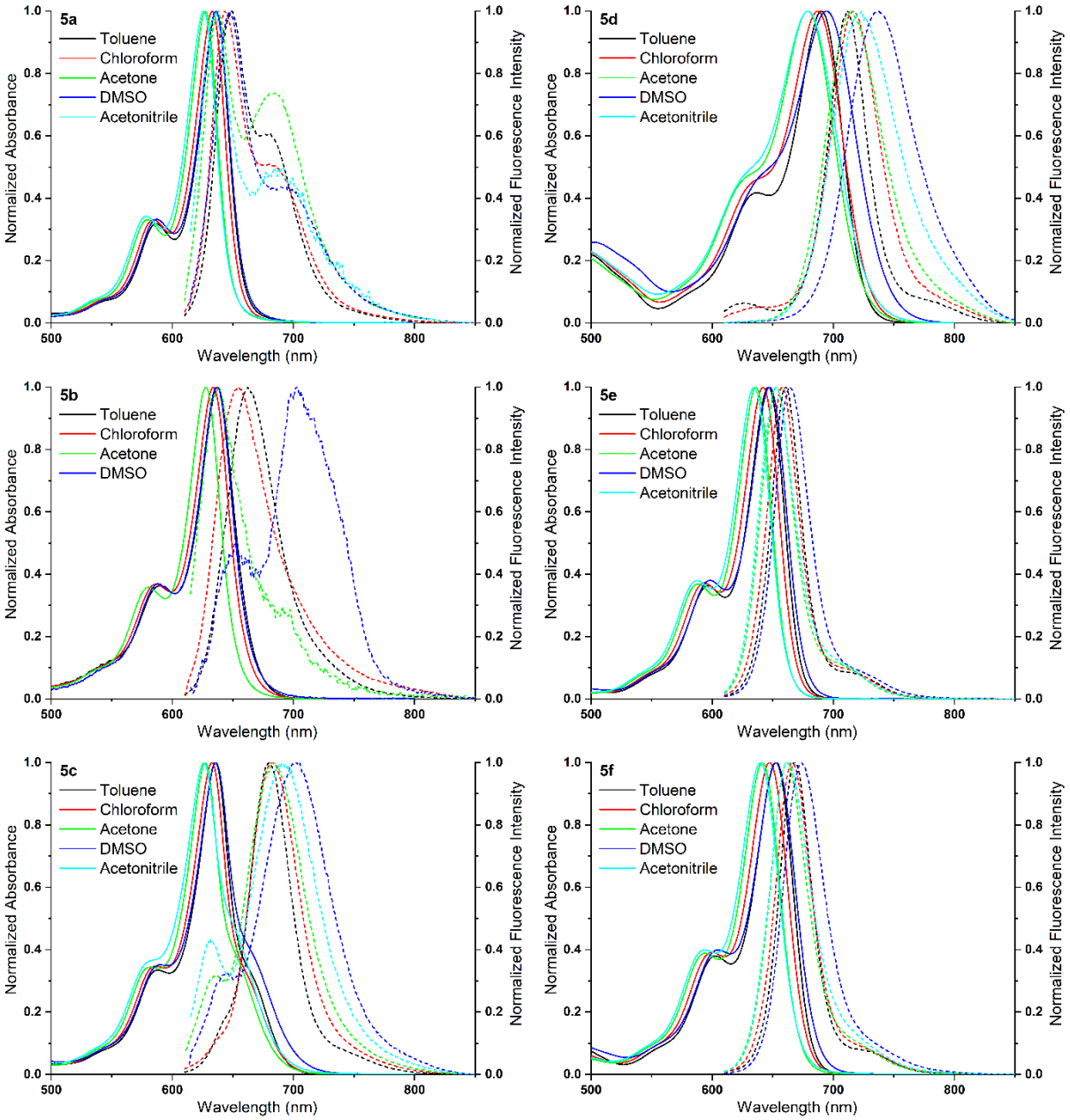

Figure S14: Normalized absorption spectra (solid lines) for BODIPYs **5a-f** and their corresponding normalized fluorescence emission spectra (dashed lines; λ_{exc} = 605 nm) in toluene, chloroform, acetone, dimethyl sulfoxide, and acetonitrile.

Table S6: Steady-state absorption and emission data for BODIPY dyads **5a-f** as obtained in toluene, chloroform, acetone, dimethyl sulfoxide, and acetonitrile solution.

BODIPY	Solvent[a]	λ_{abs} (nm)[b]	λ_{em} (nm)[c]	Φ_f[d]
5a	Toluene	636	649	0.69
	Chloroform	633	645	0.63
	Acetone	627	638, 681	<0.01
	DMSO	636	647, 694	<0.01
	Acetonitrile	626	636, 691	<0.01
5b	Toluene	638	663	0.47
	Chloroform	634	653	<0.01
	Acetone	628	638	<0.01
	DMSO	636	653, 702	<0.01
	Acetonitrile	-[e]	-[e]	-[e]
5c	Toluene	636	680	0.53
	Chloroform	633	683	0.05
	Acetone	627	635, 684	0.01
	DMSO	636	646, 705	0.01
	Acetonitrile	626	631, 691	<0.01
5d	Toluene	691	712	0.47
	Chloroform	687	716	0.43
	Acetone	679	716	0.36
	DMSO	695	737	0.20
	Acetonitrile	679	723	0.25
5e	Toluene	647	661	0.73
	Chloroform	642	658	0.75
	Acetone	636	653	0.80
	DMSO	647	664	0.65
	Acetonitrile	634	653	0.83
5f	Toluene	653	669	0.71
	Chloroform	648	667	0.70
	Acetone	641	662	0.72
	DMSO	653	674	0.43
	Acetonitrile	640	661	0.52

[a] Spectrograde solvents were used for all measurements [b] Absorption maximum. [c] Fluorescence emission maxima. [d] Fluorescence quantum yield determined *vs* nile blue (Φ_f = 0.27, λ_{exc} = 605 nm in spectrograde ethanol). [e] Not soluble.

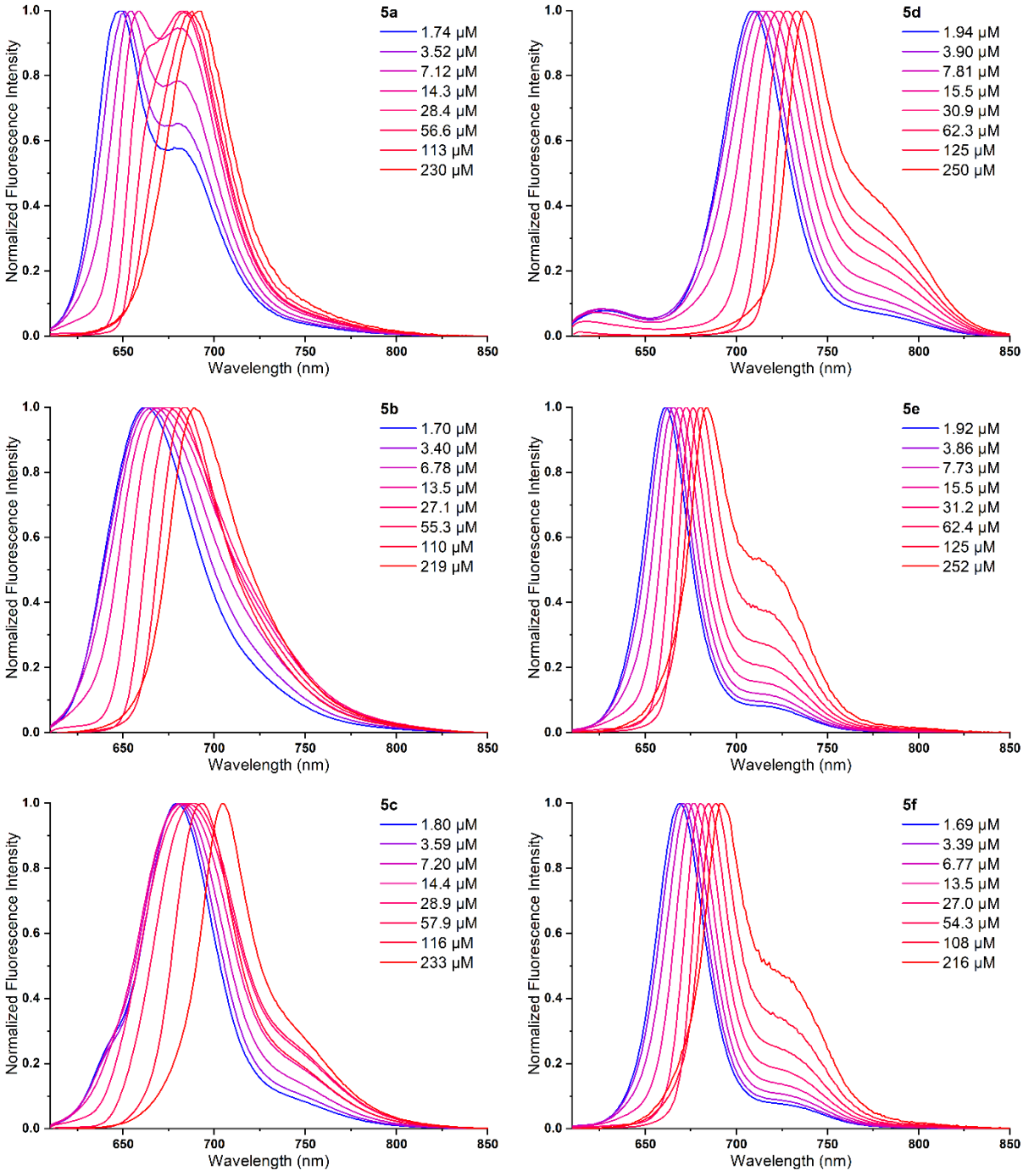

Figure S15: Normalized fluorescence emission spectra for a dilution series of BODIPYs **5a-f** in toluene (λ_{exc} = 605 nm).

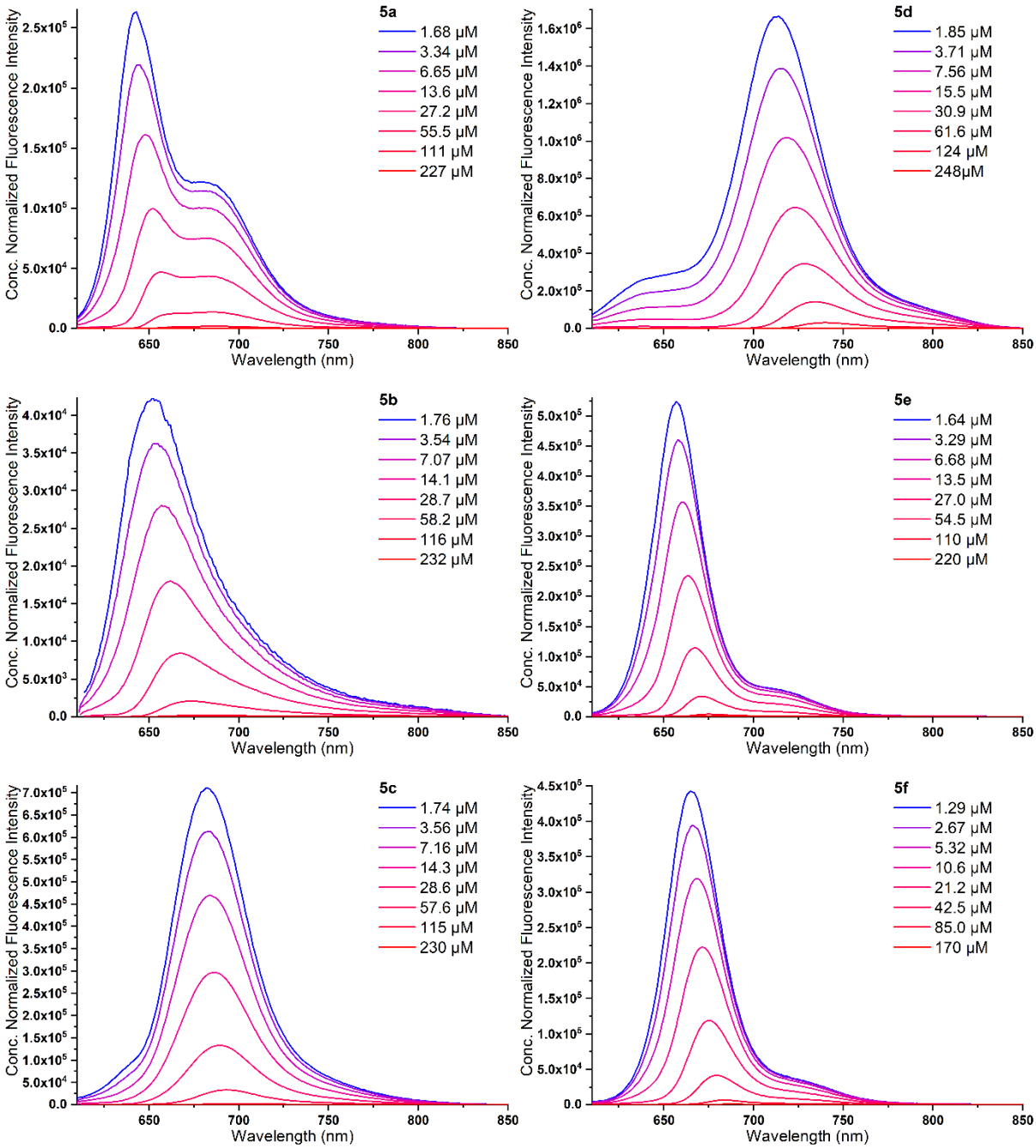

Figure S16: Fluorescence emission spectra, normalized to concentration, for the dilution series of BODIPYs **5a-f** in chloroform (λ_{exc} = 605 nm).

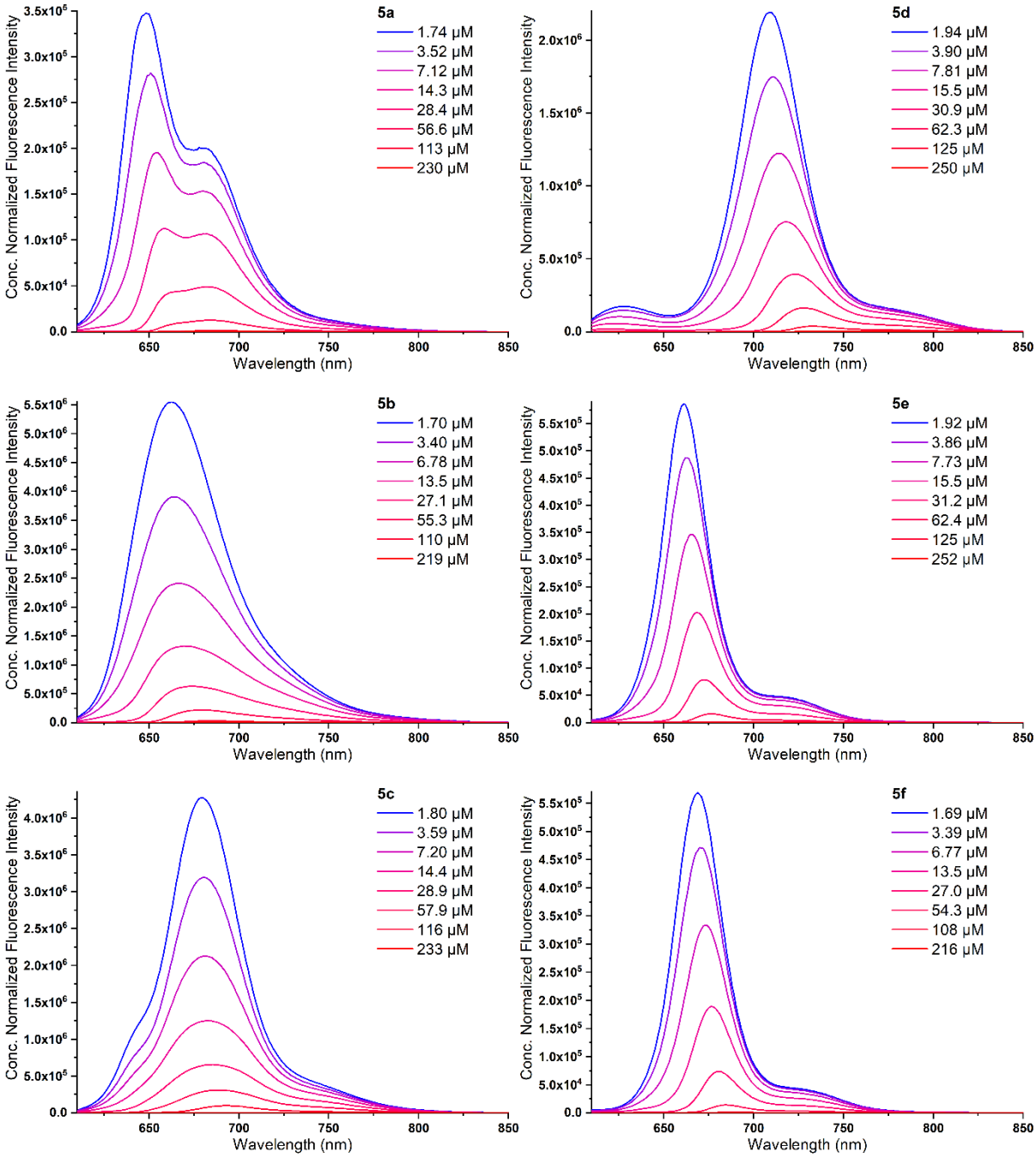

Figure S17: Fluorescence emission spectra, normalized to concentration, for the dilution series of BODIPYs **5a-f** in toluene (λ_{exc} = 605 nm).

10. Additional femtosecond transient absorption spectra and data

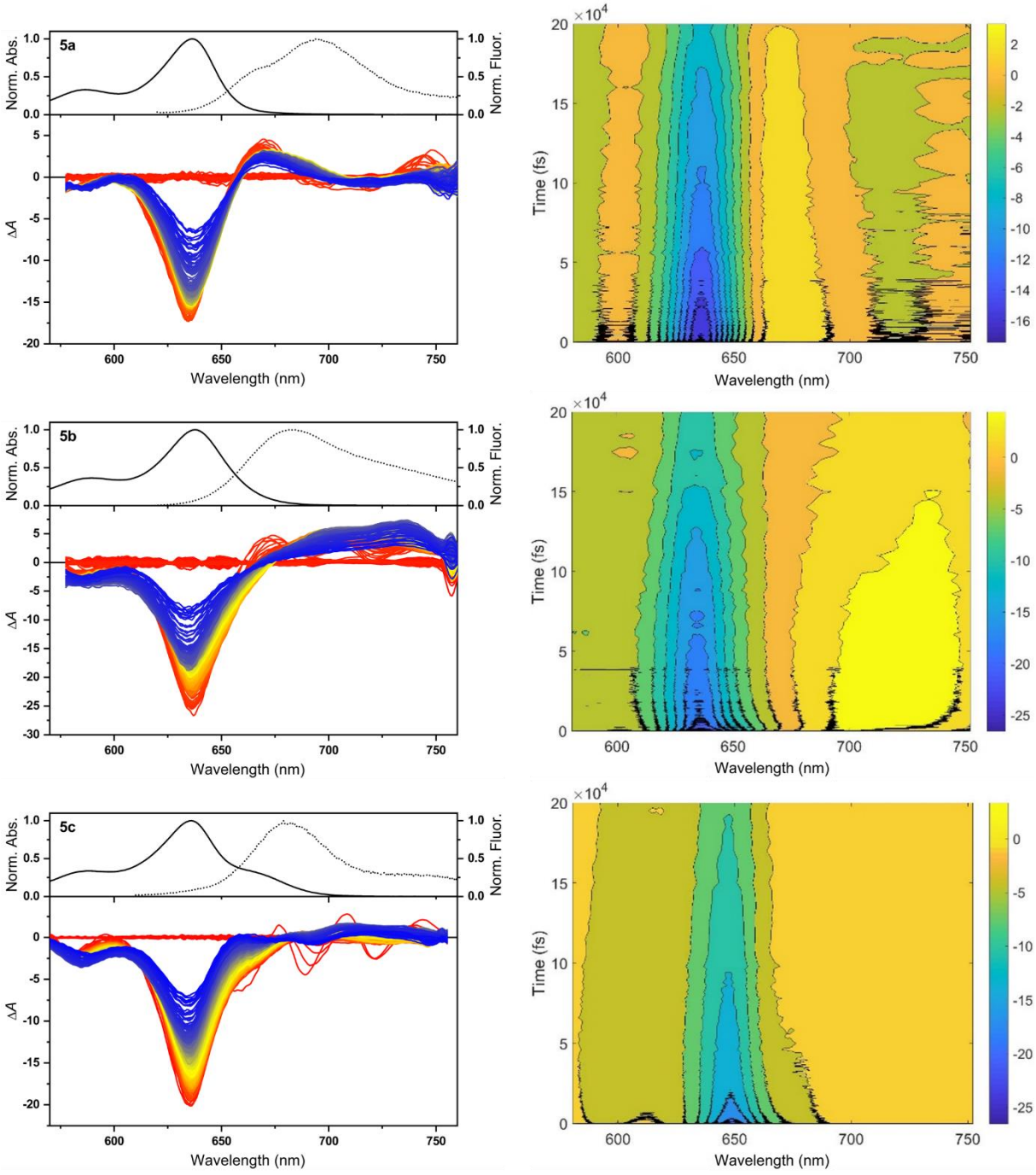

Figure S18: Raw transient absorption spectra of BODIPYs **5a-c** in toluene solution (left). For reference, the absorption and emission spectra of each compound are depicted on top. The corresponding time/frequency maps are shown on the right panels.

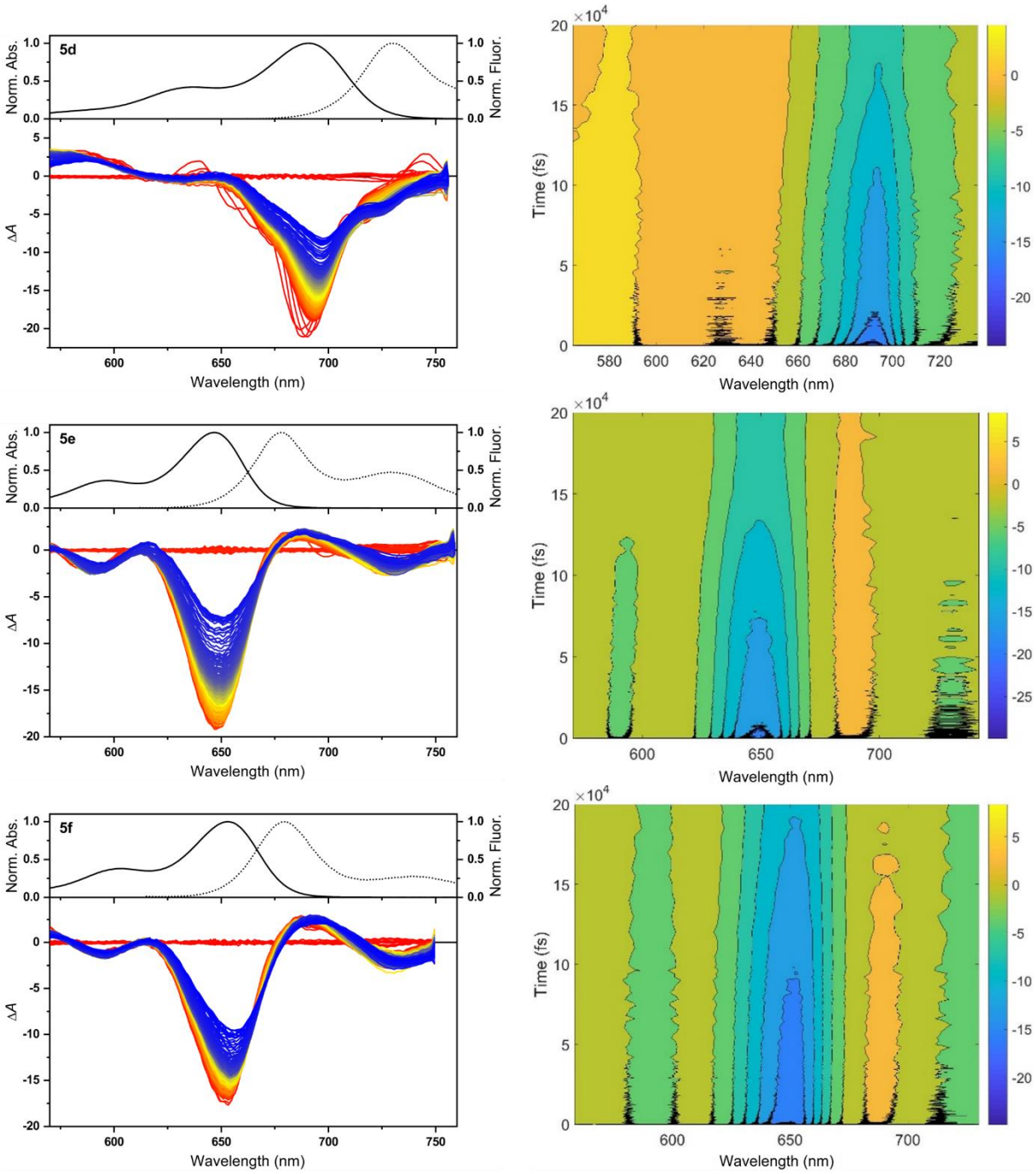

Figure S19: Raw transient absorption spectra of BODIPYs **5d-f** in toluene solution (left). For reference, the absorption and emission spectra of each compound are depicted on top. The corresponding time/frequency maps are shown on the right panels.

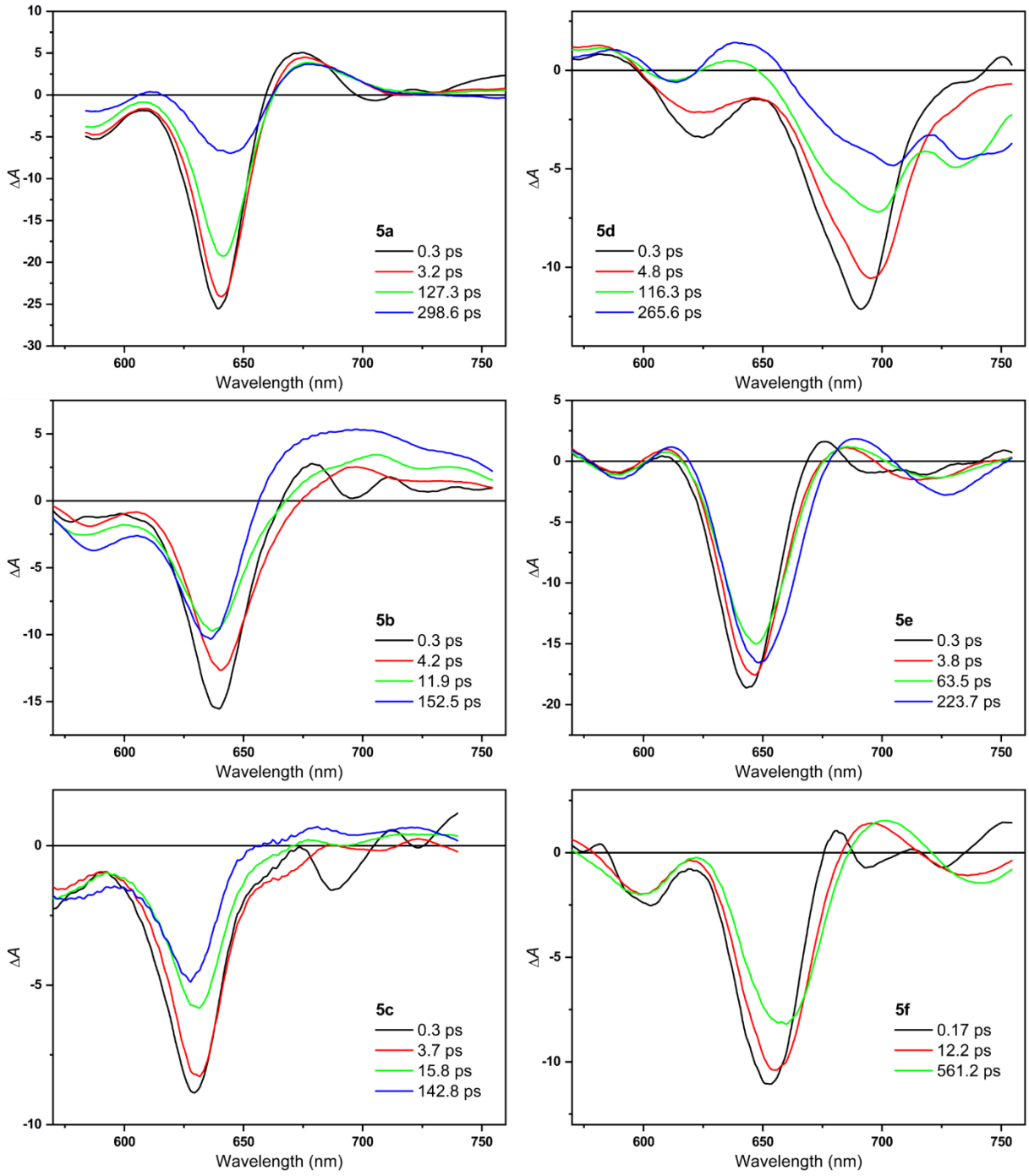

Figure S20: Evolution-associated difference spectra for BODIPYs **5a-f** in chloroform solution as obtained by singular value decomposition and global fitting of the transient data (target analysis).

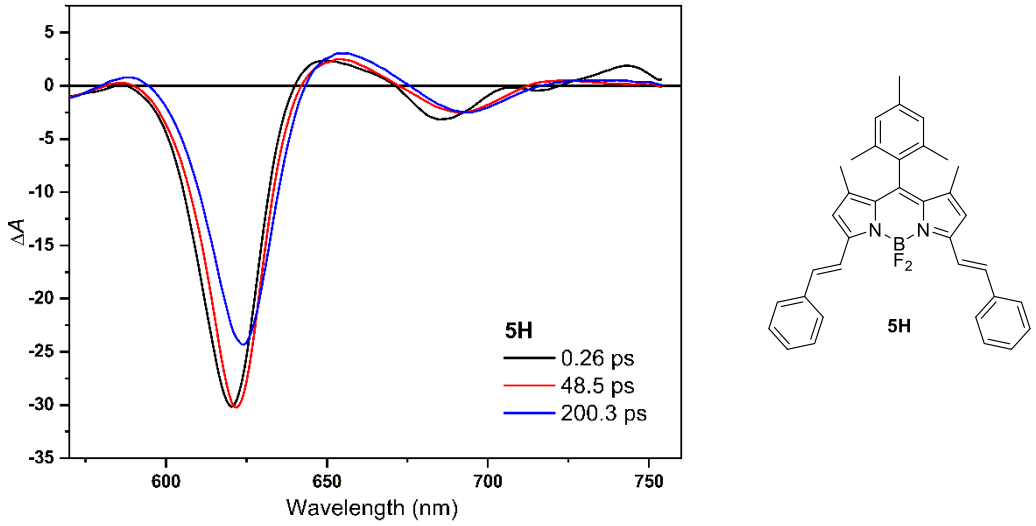

Figure S21: Evolution-associated difference spectra for distyryl-BODIPY reference compound **5H** in toluene solution as obtained by singular value decomposition and global fitting of the transient data.

The initial evolution-associated difference spectra (EADS) of the reference compound **5H** present an intense negative band peaked at 620 nm, assigned to ground-state bleaching (GSB). Furthermore, a low-intensity excited-state absorption (ESA) and a stimulated emission (SE) band, respectively peaked at 648 and 684 nm, are also observed. This spectral component evolves toward the second EADS in 260 fs. The spectral difference among the two initial EADS is very small, and this transition can be interpreted as a fast electronic relaxation of the excited state. The second component further evolves in 48.5 ps toward the final EADS. During this evolution, the intensity of the bleaching signal decreases and its maximum red-shifts slightly. At the same time, the ESA and SE bands also red-shift, although their intensity remains almost unvaried. Considering the timescale of this evolution, the most likely interpretation for the observed spectral changes is a structural relaxation occurring in the excited state, possibly involving a partial rotation of the phenyl substituents. The lifetime of the final spectral component is estimated by the analysis as 200 ps. This value is affected by a significant error, as the longest time delay accessed within the measurements is also 200 ps. Because of its strong fluorescence (Φ_f = 0.98 in toluene), it is expected that the effective lifetime of S_1 would be in the order of a few nanoseconds.

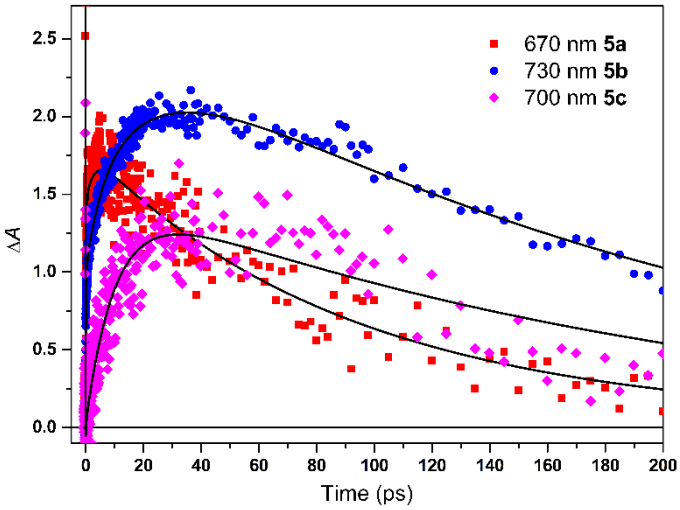

Figure S22: Comparison of the kinetic traces registered in the red part of the spectrum for BODIPYs **5a-c** in toluene solution.

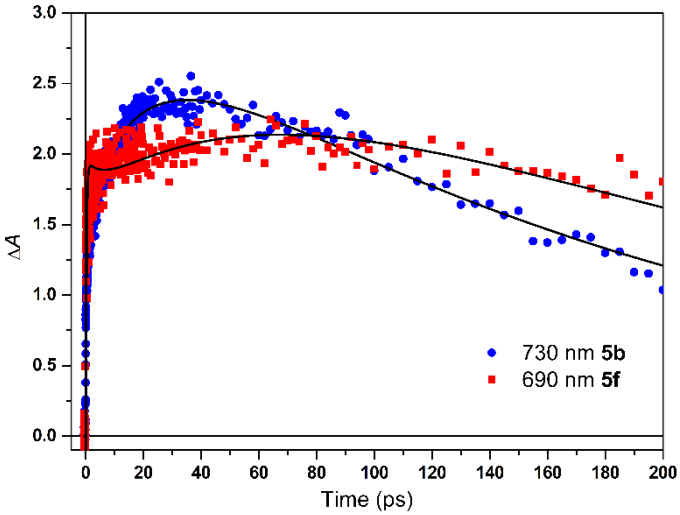

Figure S23: Comparison of the kinetic traces registered in the red part of the spectrum for BODIPYs **5b** and **5f** in toluene solution.

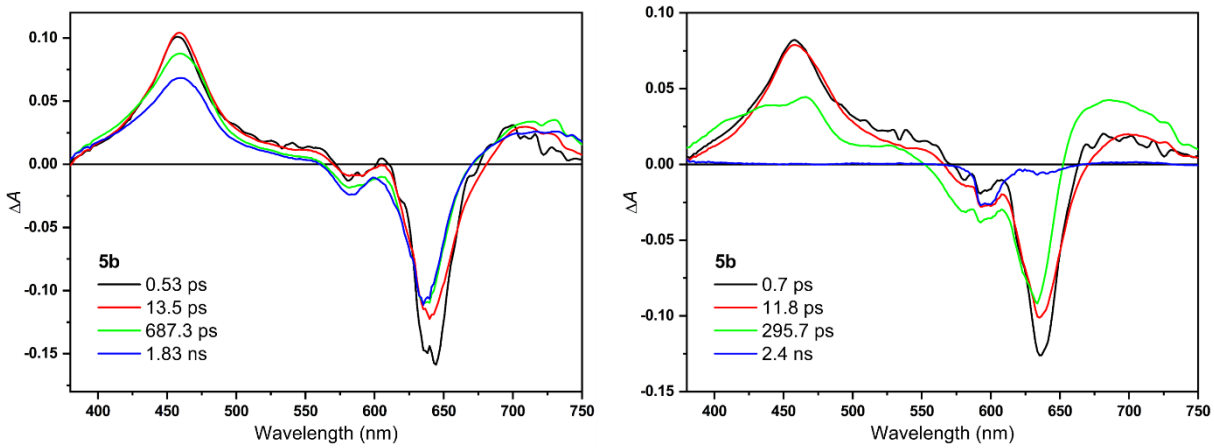

Figure S24: Evolution-associated difference spectra for sample **5b** in toluene (left) and chloroform (right) solution as obtained by singular value decomposition and global fitting of the transient data, measured on a timescale spanning up to 1.5 ns.

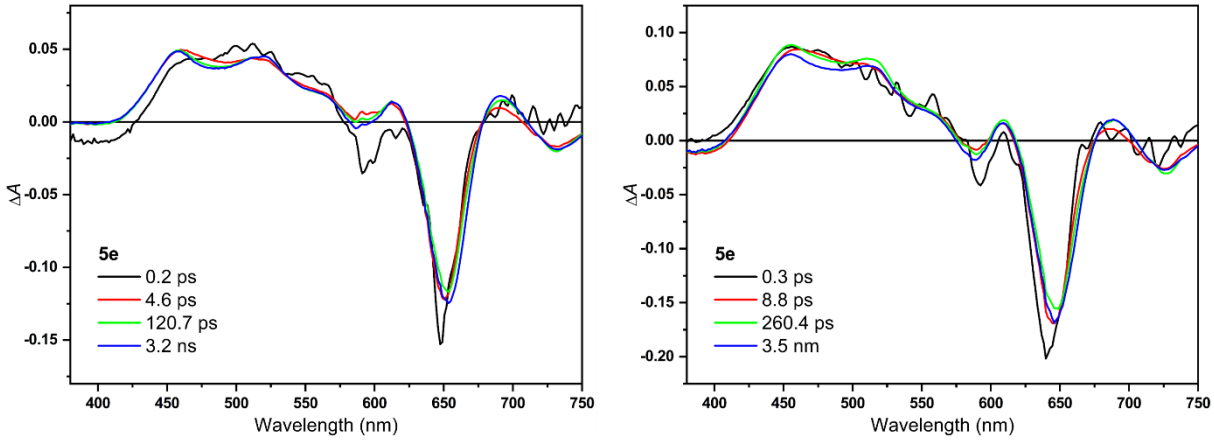

Figure S25: Evolution-associated difference spectra for sample **5e** in toluene (left) and chloroform (right) solution as obtained by singular value decomposition and global fitting of the transient data, measured on a timescale spanning up to 1.5 ns.

The excited state dynamics of samples **5b** and **5e** were probed up to a pump probe delay of 1.5 ns and over a wider spectral range covering the 380–750 nm interval. In case of sample **5b**, substantial differences are observed in the excited state evolution depending on the solvent polarity, with the transient signal recovering to a large extent in chloroform. This behavior further supports the idea that charge separation among the styryl-BODIPY and the phenoxazine units is occurring upon excitation. In contrast, minor differences among the data recorded in toluene and chloroform were observed in case of dyad **5e**, where charge separated states are not involved. The early lifetimes obtained from global analysis of these data show some differences as compared with those obtained from broadband pump-probe measurements reported in previous figures. These differences can be attributed to the lower time resolution of the experiment performed using a white light continuum probe (*ca.* 150 fs) and to the different excitation conditions. Measurements reported in Figure S24-S25 were performed using a narrowband pump pulse centered at 600 nm, while for the previously shown transient spectra a broadband pump pulse spanning the 560–780 nm region was used.

11. Excited state geometry optimizations

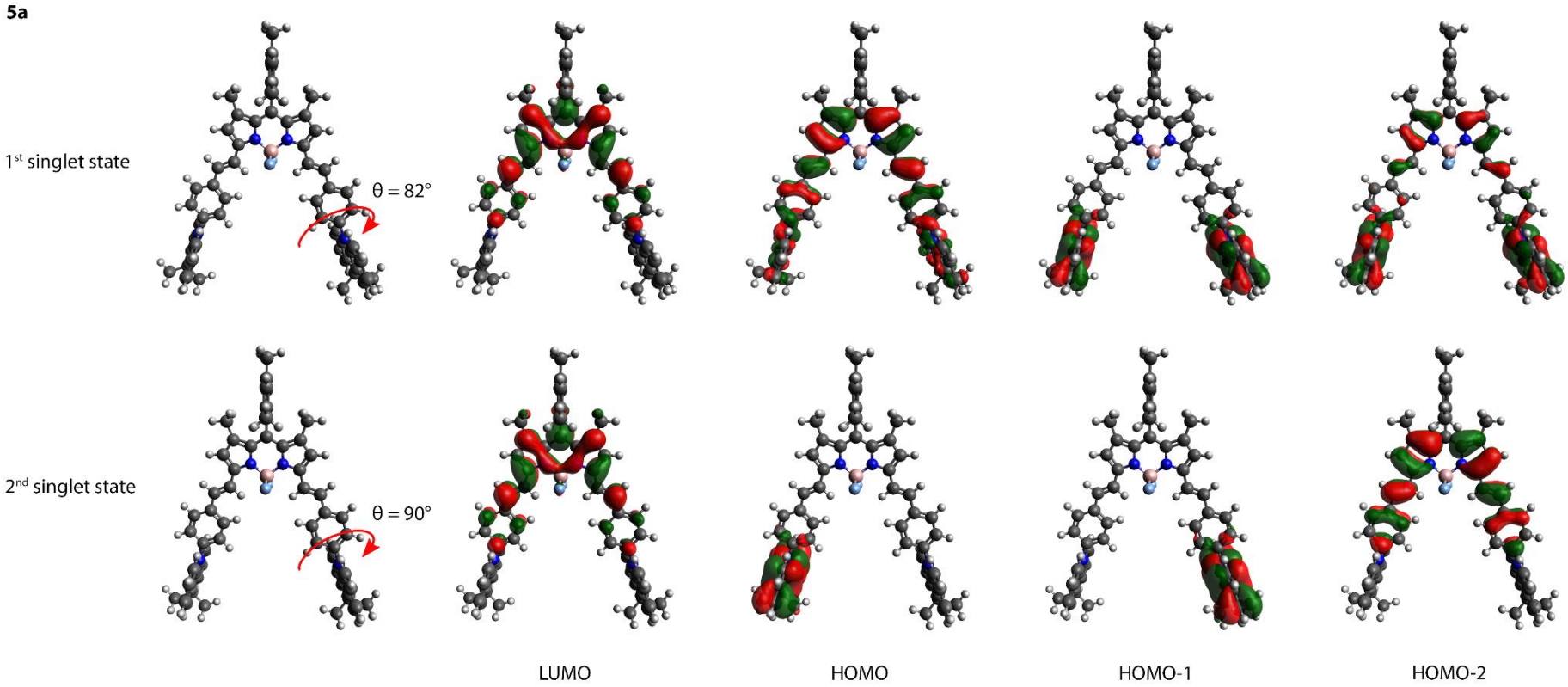

Figure S26: Orbital topologies for the optimized first and second singlet excited states for BODIPY **5a** in the gas phase as obtained using time-dependent density functional theory calculations with M06-2X/6-311G(d). Isosurface values of 0.02 (a.u.) were used for all orbitals.

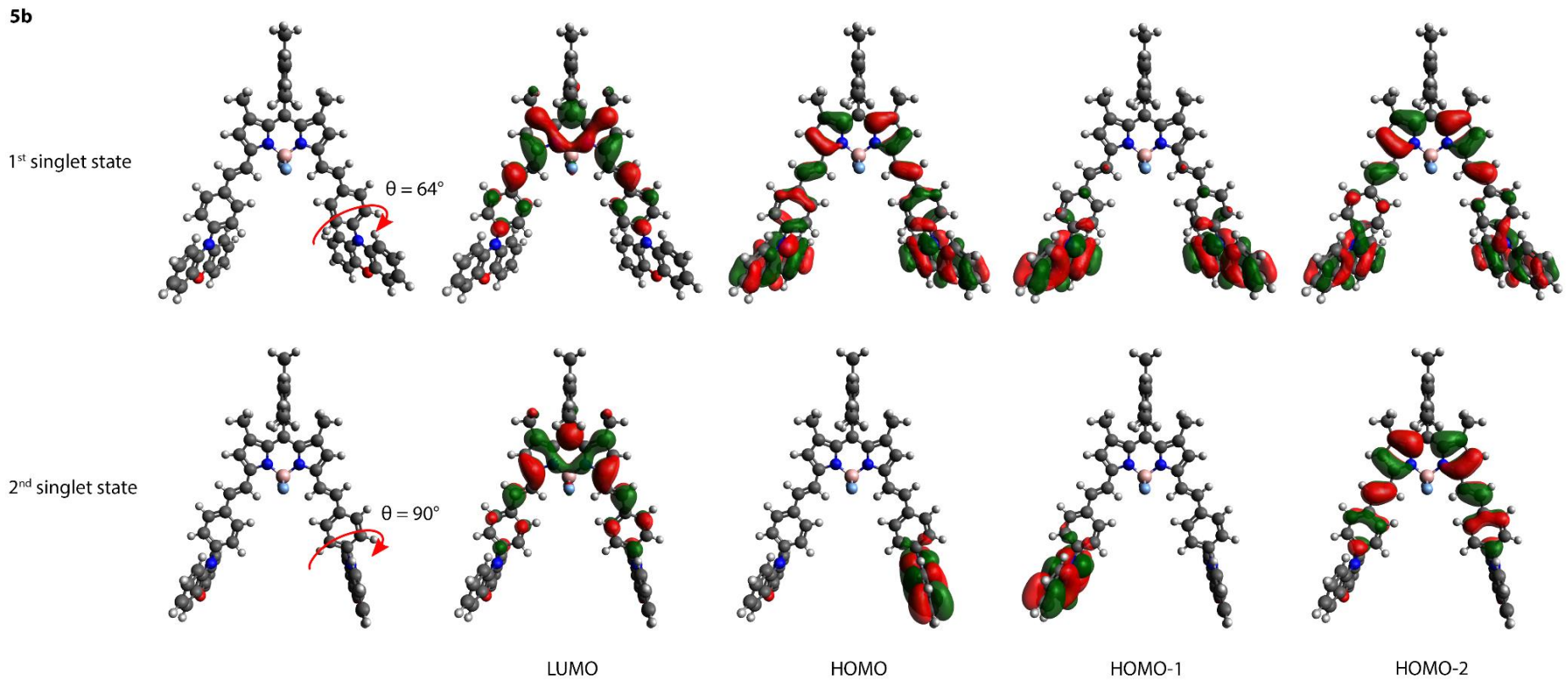

Figure S27: Orbital topologies for the optimized first and second singlet excited states for BODIPY **5b** in the gas phase as obtained using time-dependent density functional theory calculations with M06-2X/6-311G(d). Isosurface values of 0.02 (a.u.) were used for all orbitals.

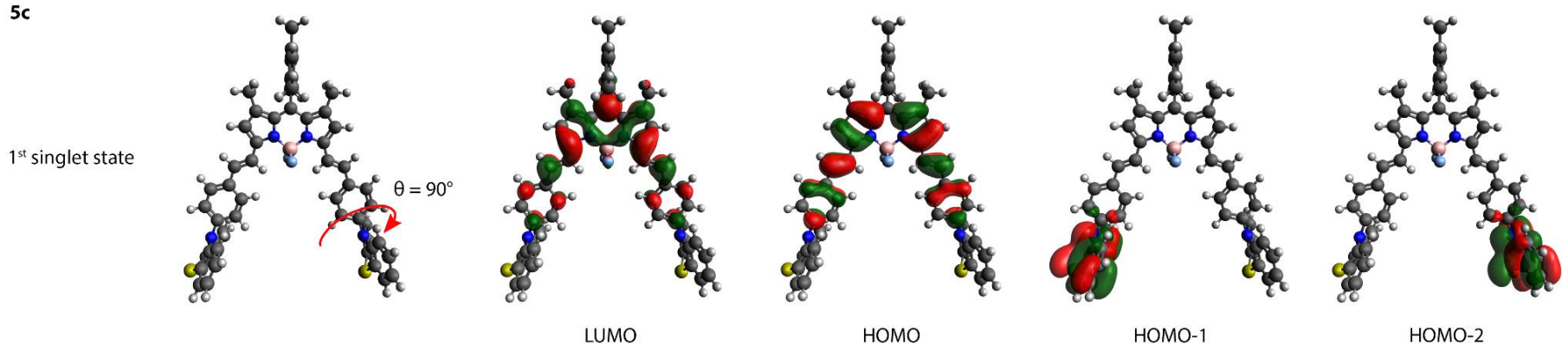

Figure S28: Orbital topologies for the optimized first singlet excited state for BODIPY **5c** in the gas phase as obtained using time-dependent density functional theory calculations with M06-2X/6-311G(d). Isosurface values of 0.02 (a.u.) were used for all orbitals. We were unable to optimize the second singlet excited state due to state rearrangements during the optimization procedure.

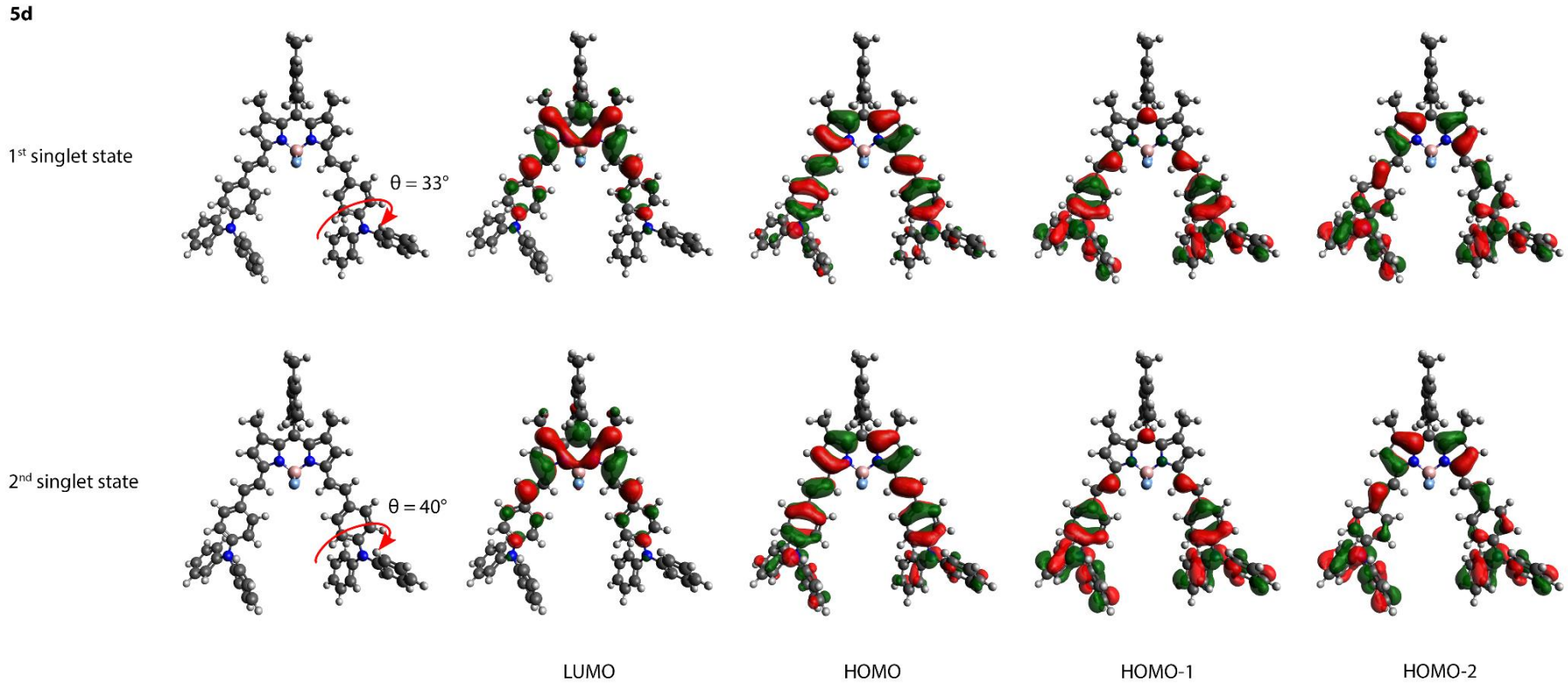

Figure S29: Orbital topologies for the optimized first and second singlet excited states for BODIPY **5d** in the gas phase as obtained using time-dependent density functional theory calculations with M06-2X/6-311G(d). Isosurface values of 0.02 (a.u.) were used for all orbitals.

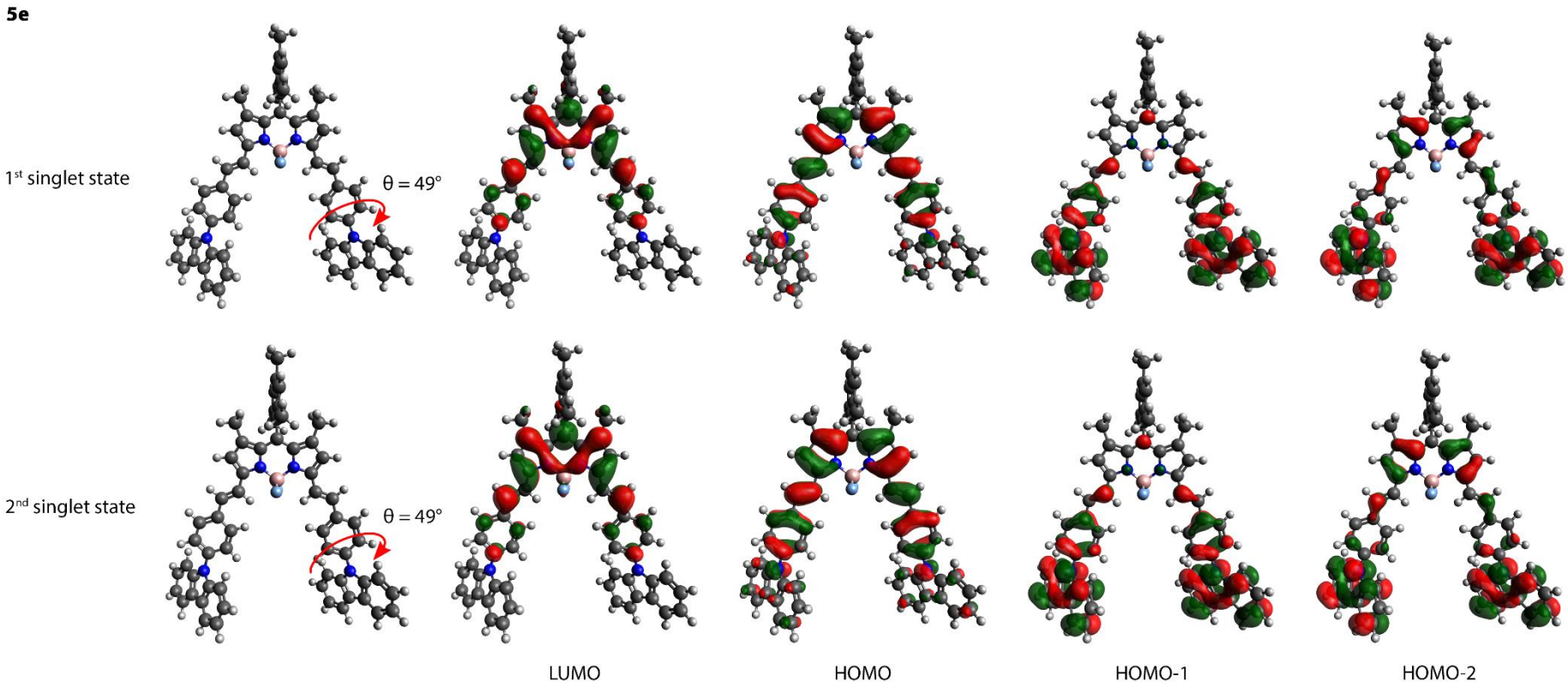

Figure S30: Orbital topologies for the optimized first and second singlet excited states for BODIPY **5e** in the gas phase as obtained using time-dependent density functional theory calculations with M06-2X/6-311G(d). Isosurface values of 0.02 (a.u.) were used for all orbitals.

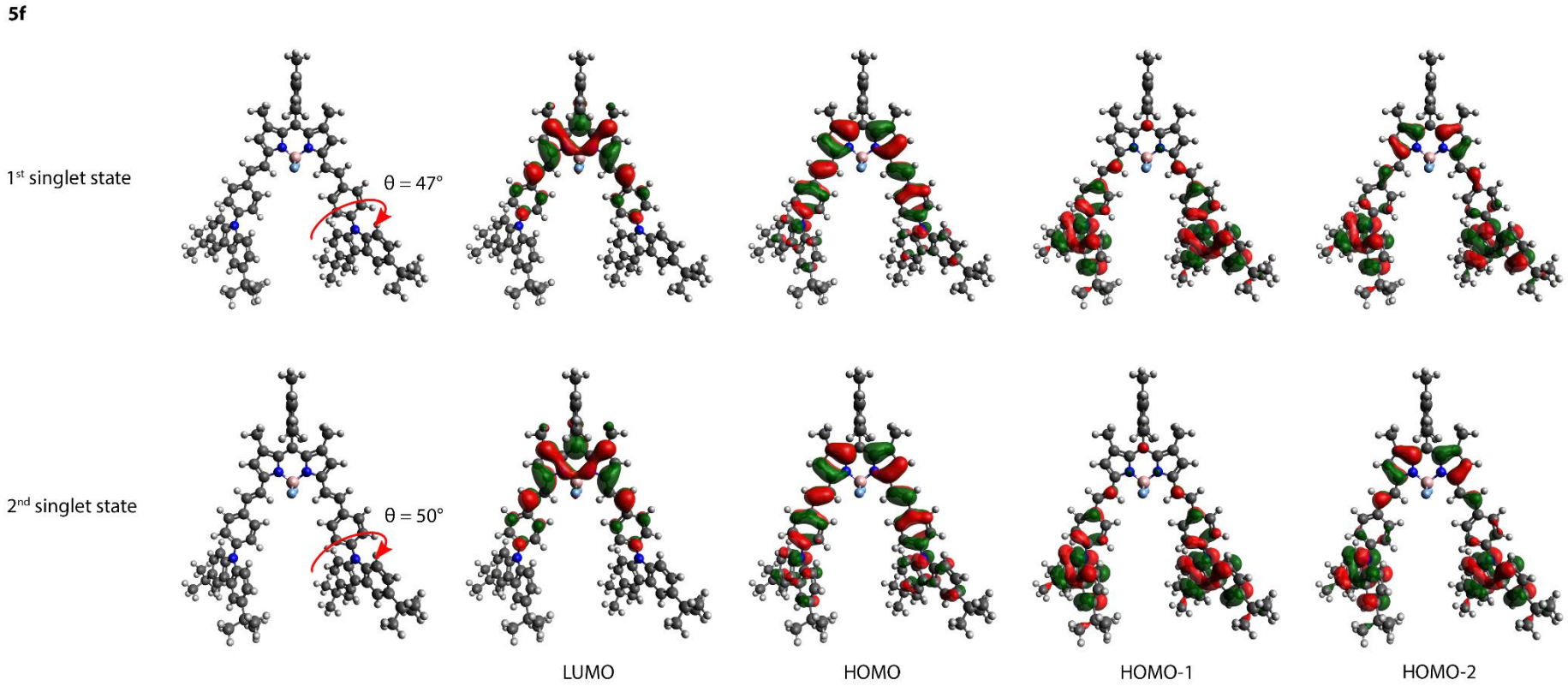

Figure S31: Orbital topologies for the optimized first and second singlet excited states for BODIPY **5f** in the gas phase as obtained using time-dependent density functional theory calculations with M06-2X/6-311G(d). Isosurface values of 0.02 (a.u.) were used for all orbitals.

Table S7: Time-dependent density functional theory results for the vertical first and second singlet excitation energies and corresponding oscillator strengths determined from the 1st excited optimized singlet state. The dominant nature of the one-particle excitations is also given.

BODIPY	$S_0 \rightarrow S_1$			$S_0 \rightarrow S_2$			$\Delta E_{S1\text{-}S2}$ (eV)
	ΔE (eV)[a]	Osc. Str.[b]	Nature[c]	ΔE (eV)[a]	Osc. Str.[b]	Nature[c]	
5a	2.19	1.02	H→L (86%)	2.84	0.05	H-1→L (91%)	0.65
5b	2.10	0.96	H→L (73%)	2.62	0.29	H-1→L (91%)	0.52
5c	2.20	1.02	H→L (98%)	2.97	0.00	H-1→L (92%)	0.77
5d	2.02	1.03	H→L (95%)	2.98	1.11	H-1→L (93%)	0.96
5e	2.12	1.02	H→L (96%)	3.18	0.90	H-1→L (88%)	1.06
5f	2.10	1.04	H→L (95%)	3.07	0.93	H-1→L (89%)	0.97

[a] Vertical excitation energy. [b] Oscillator strength. [c] H = HOMO, L = LUMO.

Table S8: Time-dependent density functional theory results for the vertical first and second singlet excitation energies and corresponding oscillator strengths determined from the 2nd excited optimized singlet state. The dominant nature of the one-particle excitations is also given.

BODIPY	$S_0 \rightarrow S_1$			$S_0 \rightarrow S_2$			$\Delta E_{S1\text{-}S2}$ (eV)
	ΔE (eV)[a]	Osc. Str.[b]	Nature[c]	ΔE (eV)[a]	Osc. Str.[b]	Nature[c]	
5a	2.24	0.97	H-2→L (97%)	2.61	0.00	H→L (92%)	0.37
5b	2.24	0.97	H-2→L (98%)	2.25	0.00	H→L (93%)	0.01
5c[d]	-	-	-	-	-	-	-
5d	2.07	0.98	H→L (93%)	2.91	1.00	H-1→L (92%)	0.84
5e	2.15	0.95	H→L (94%)	3.11	0.88	H-1→L (88%)	0.96
5f	2.15	0.95	H→L (91%)	3.01	0.80	H-1→L (90%)	0.86

[a] Vertical excitation energy. [b] Oscillator strength. [c] H = HOMO, L = LUMO. [d] We were unable to optimize the second singlet excited state for BODIPY **5c** due to state rearrangements occurring during the optimization procedure.

12. ^{1}H and ^{13}C NMR spectra

4-(9,9-Dimethyl-9,10-dihydroacridin-10-yl)benzaldehyde (**4a**)

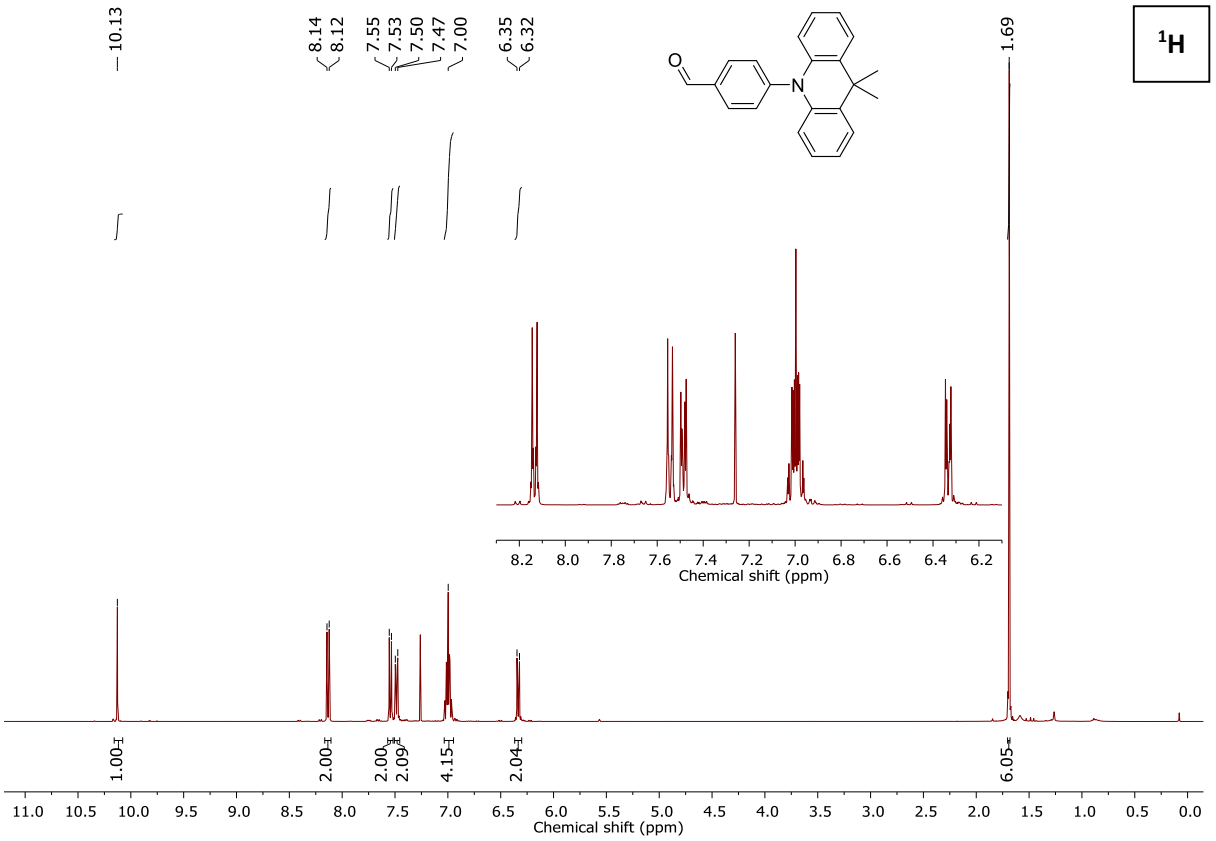

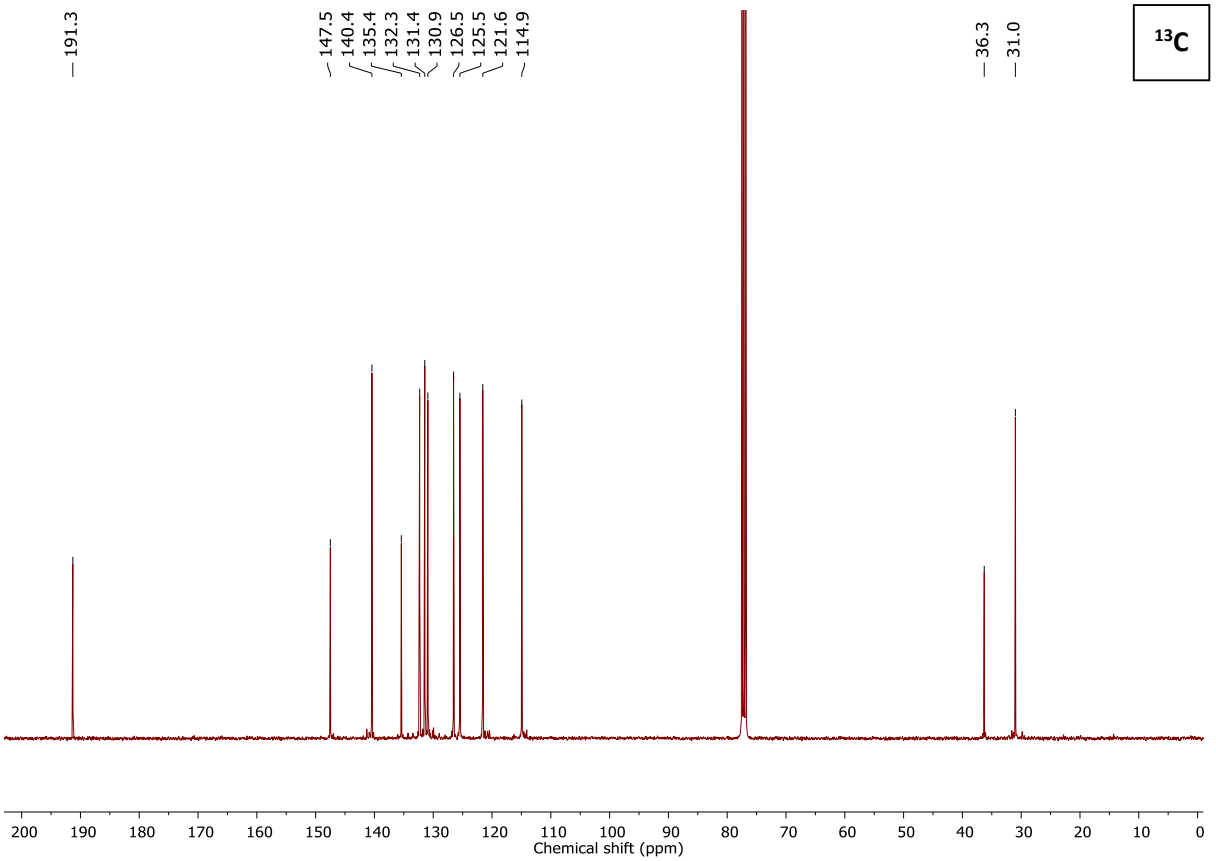

4-(Phenoxazin-10-yl)benzaldehyde (**4b**)

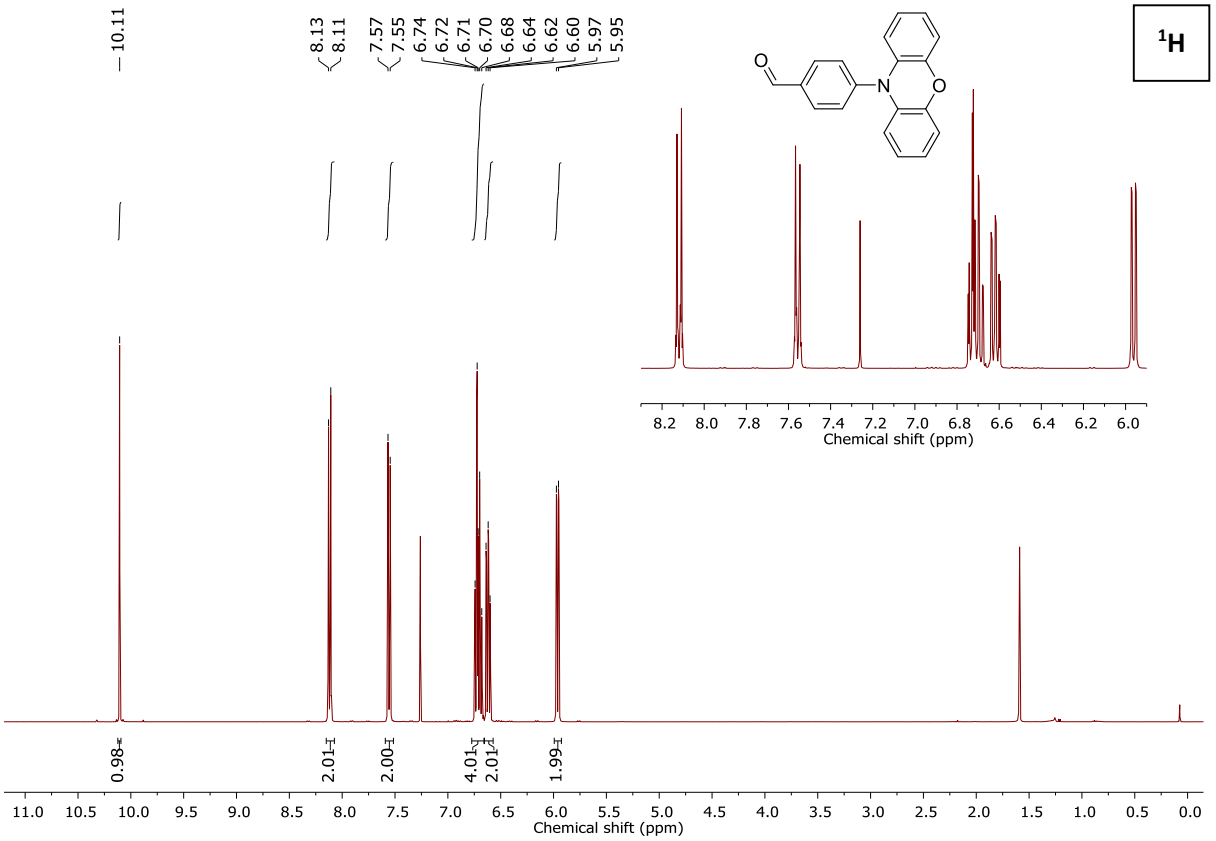

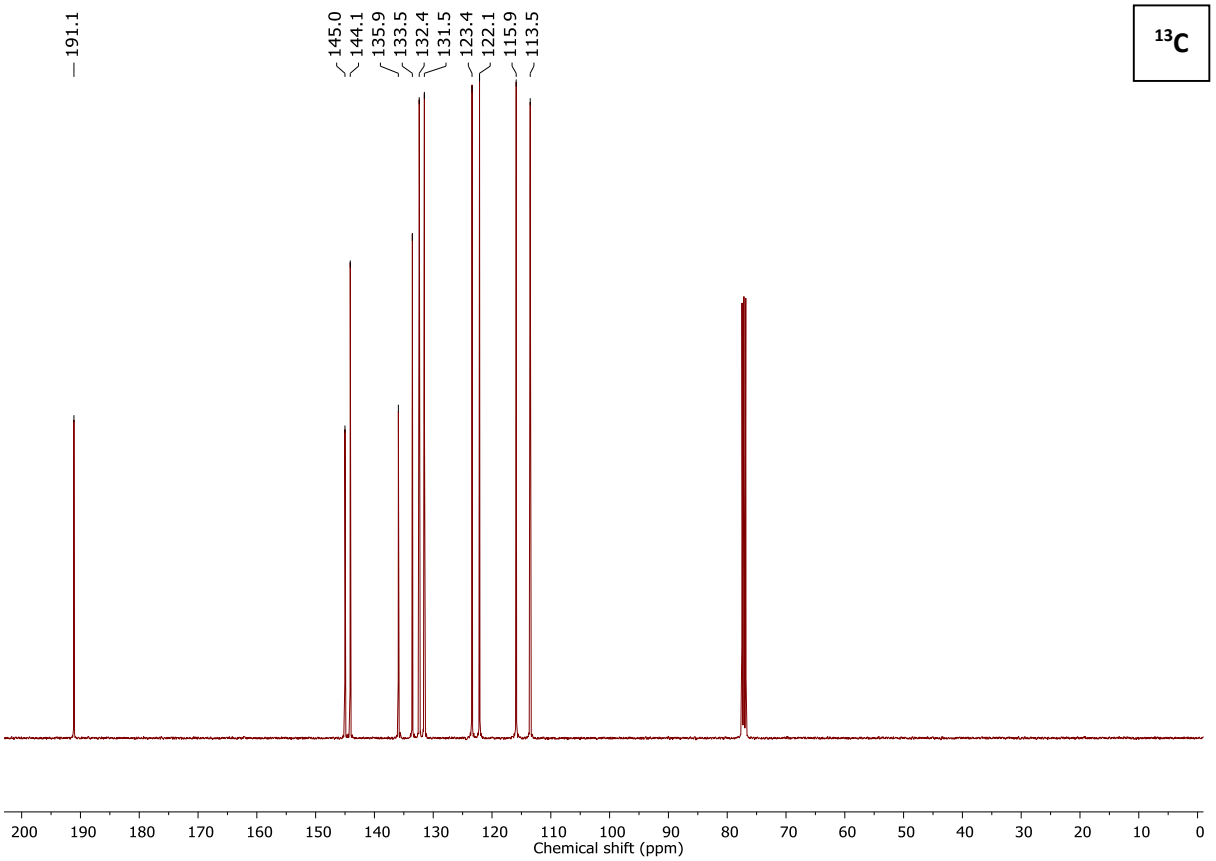

4-(Phenothiazin-10-yl)benzaldehyde (**4c**)

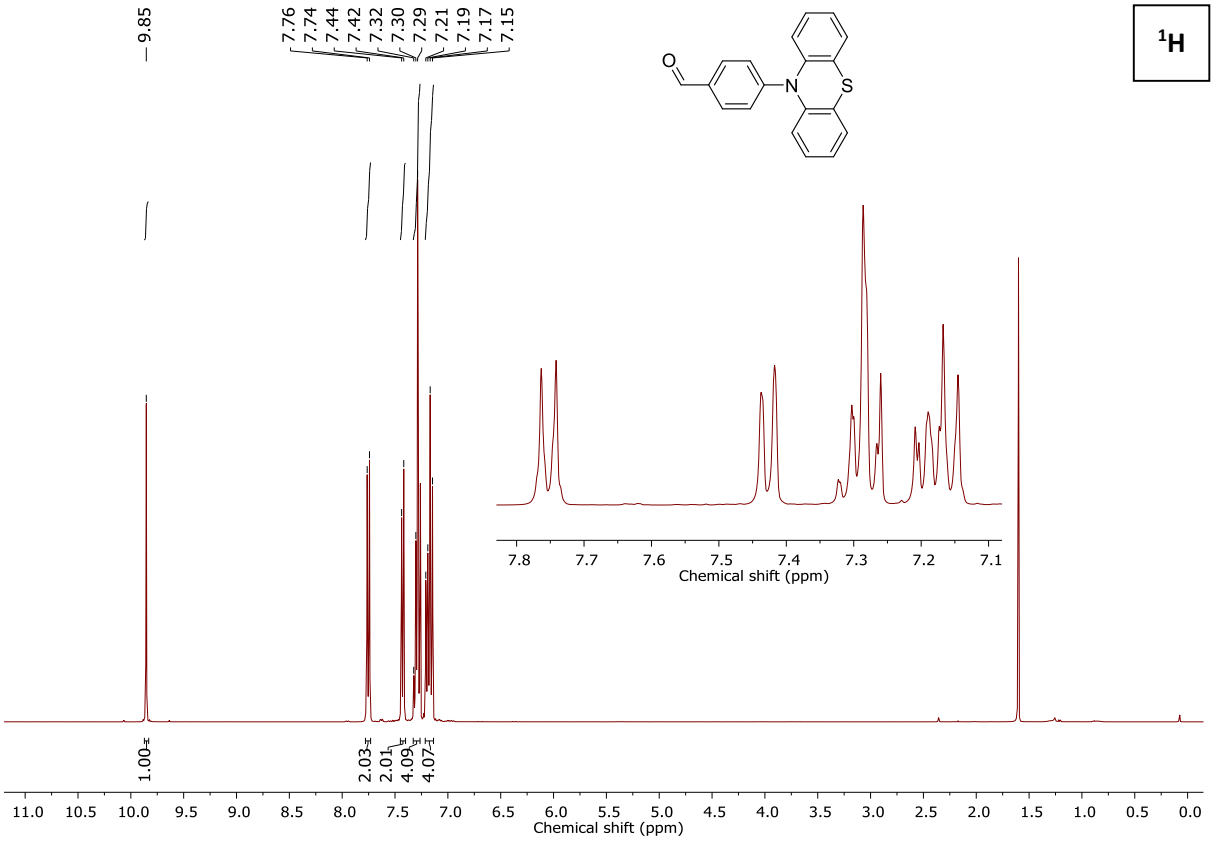

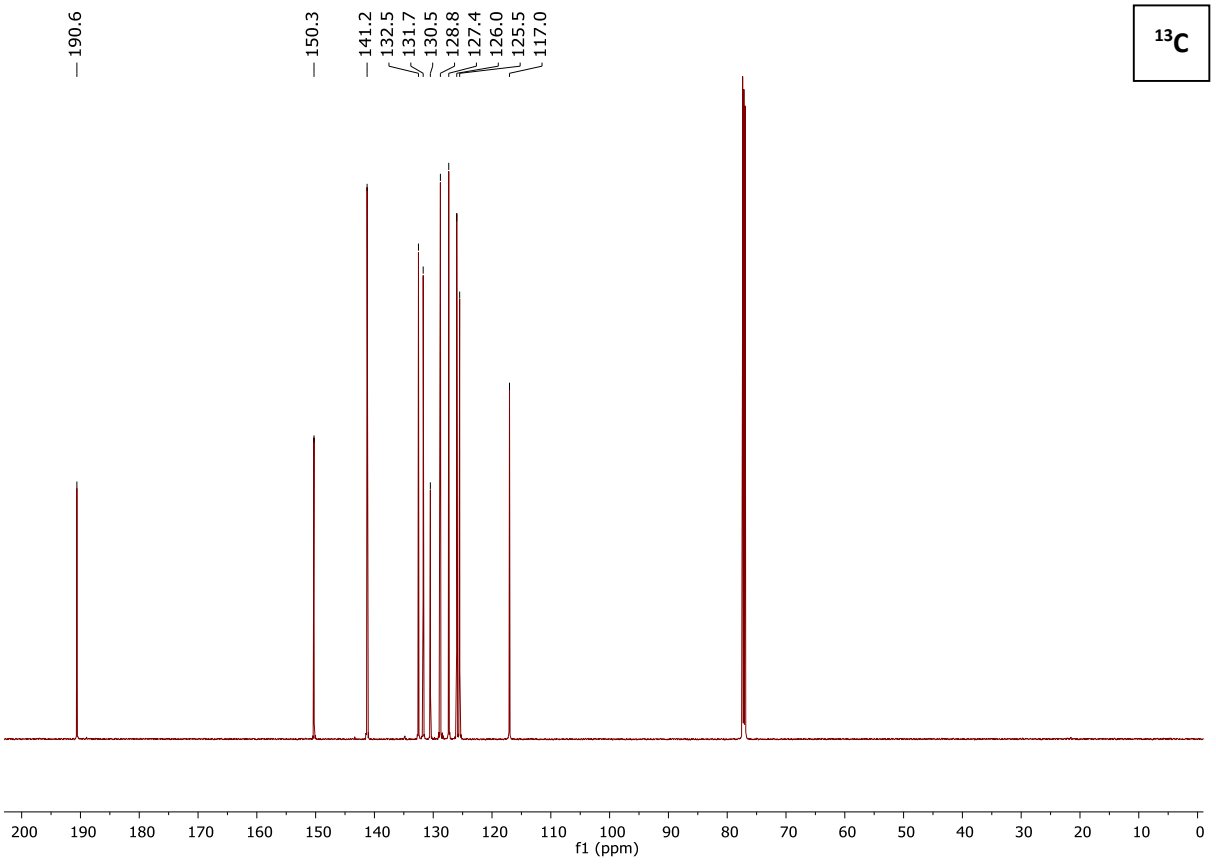

4-(Diphenylamino)benzaldehyde (**4d**)

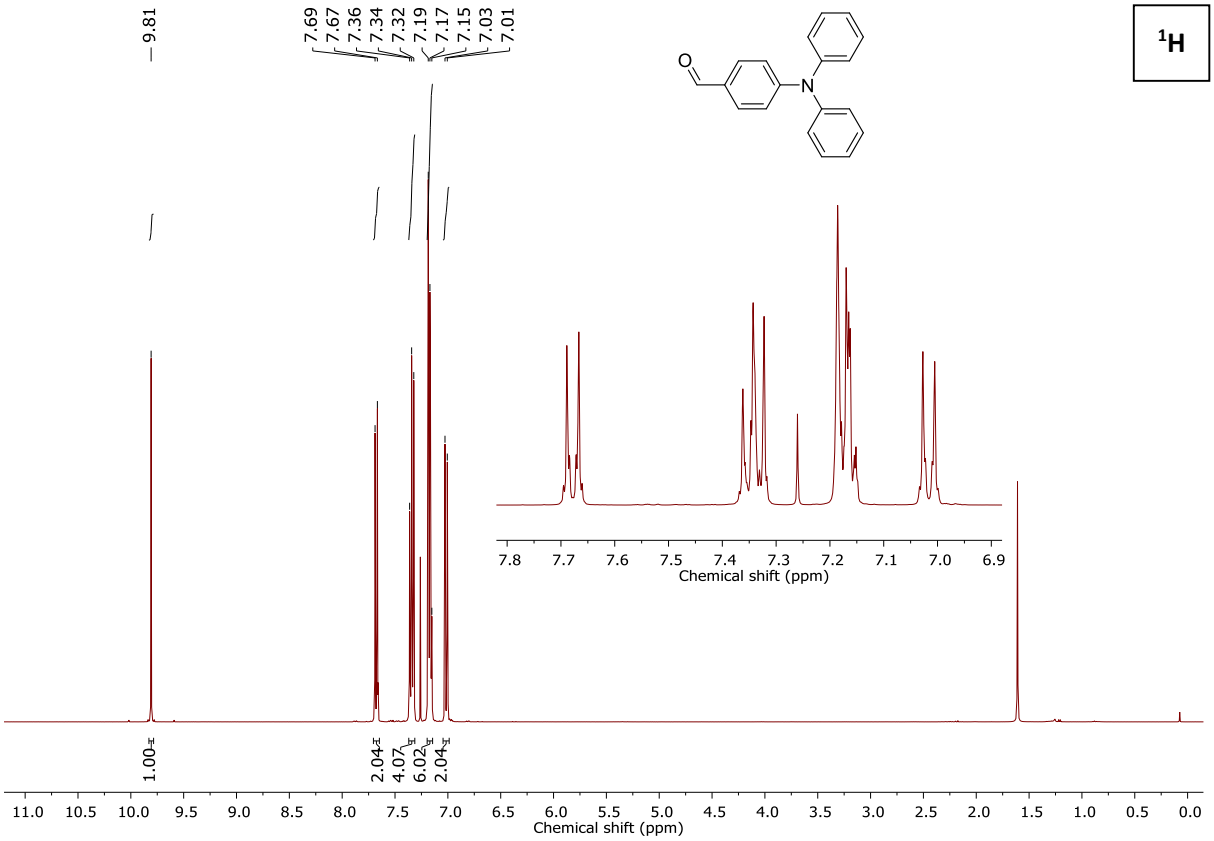

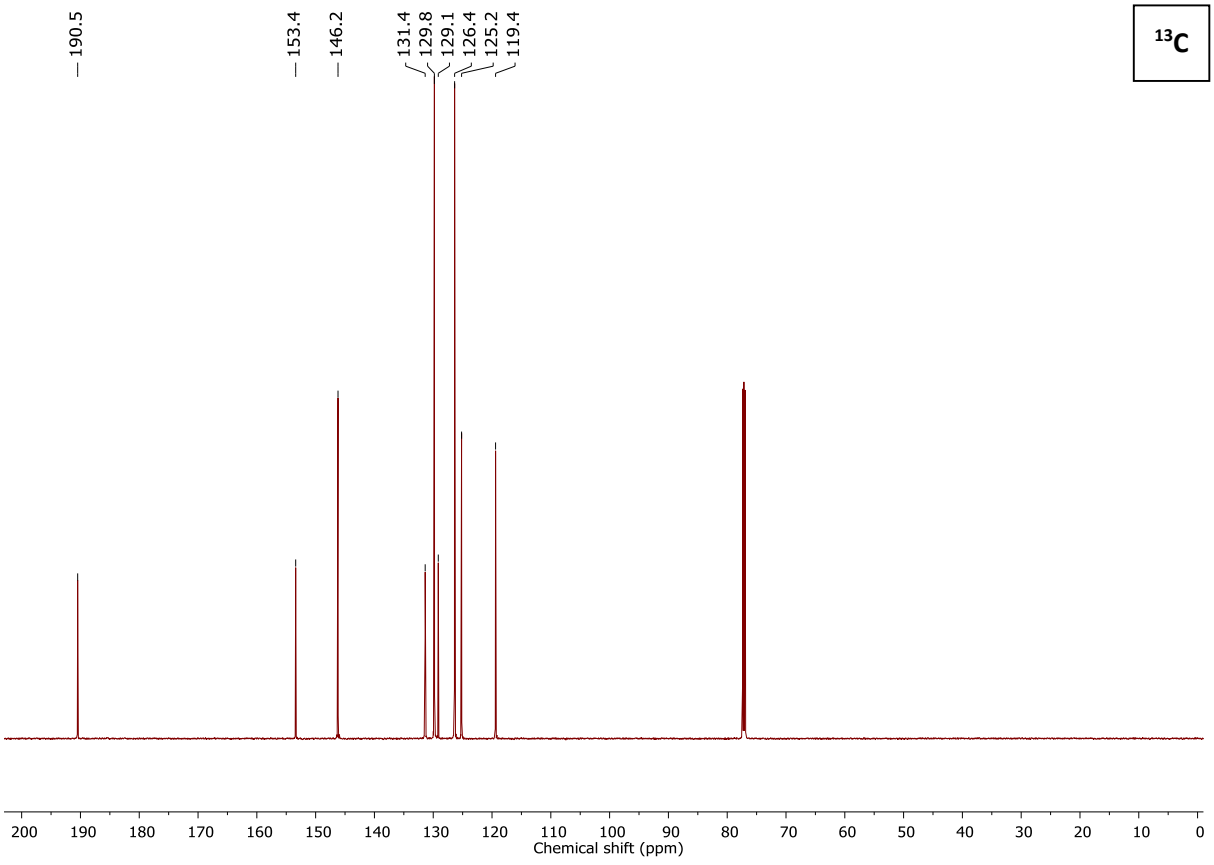

4-(Carbazol-9-yl)benzaldehyde (**4e**)

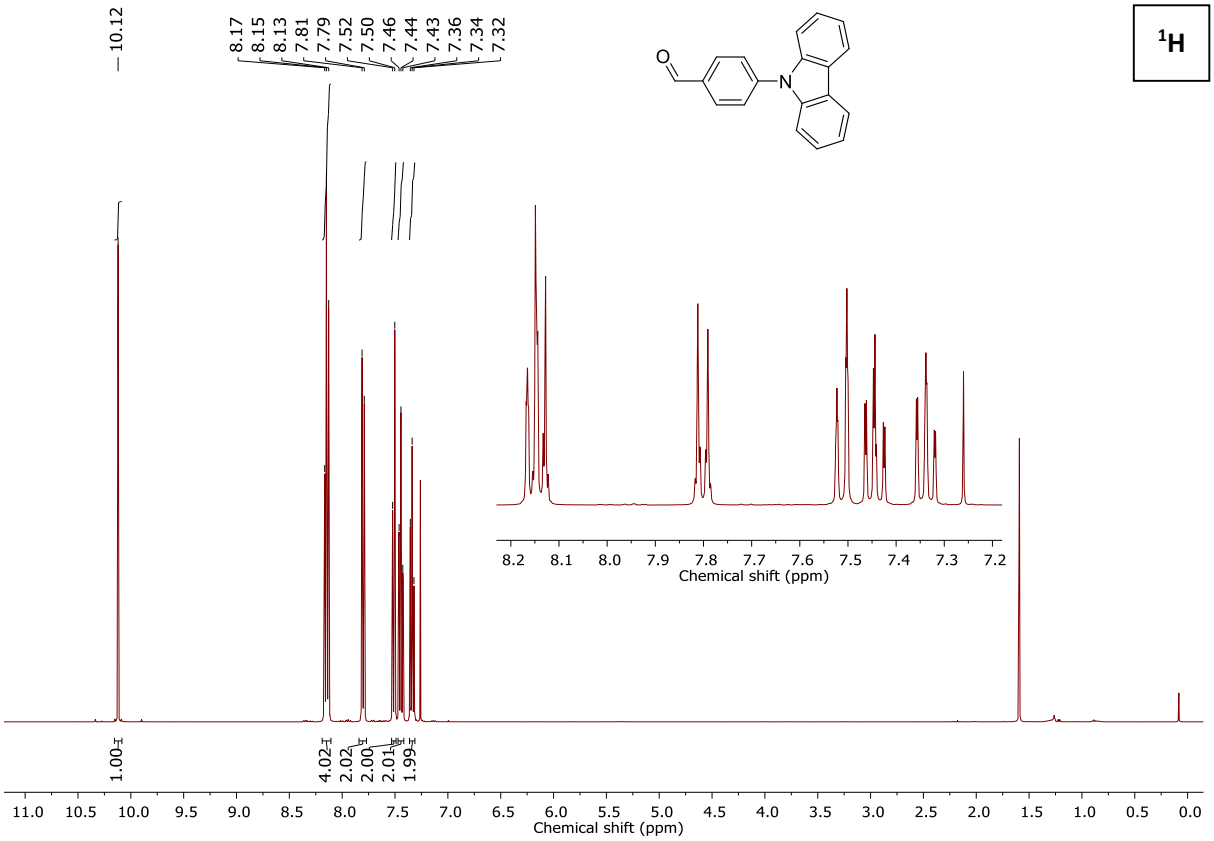

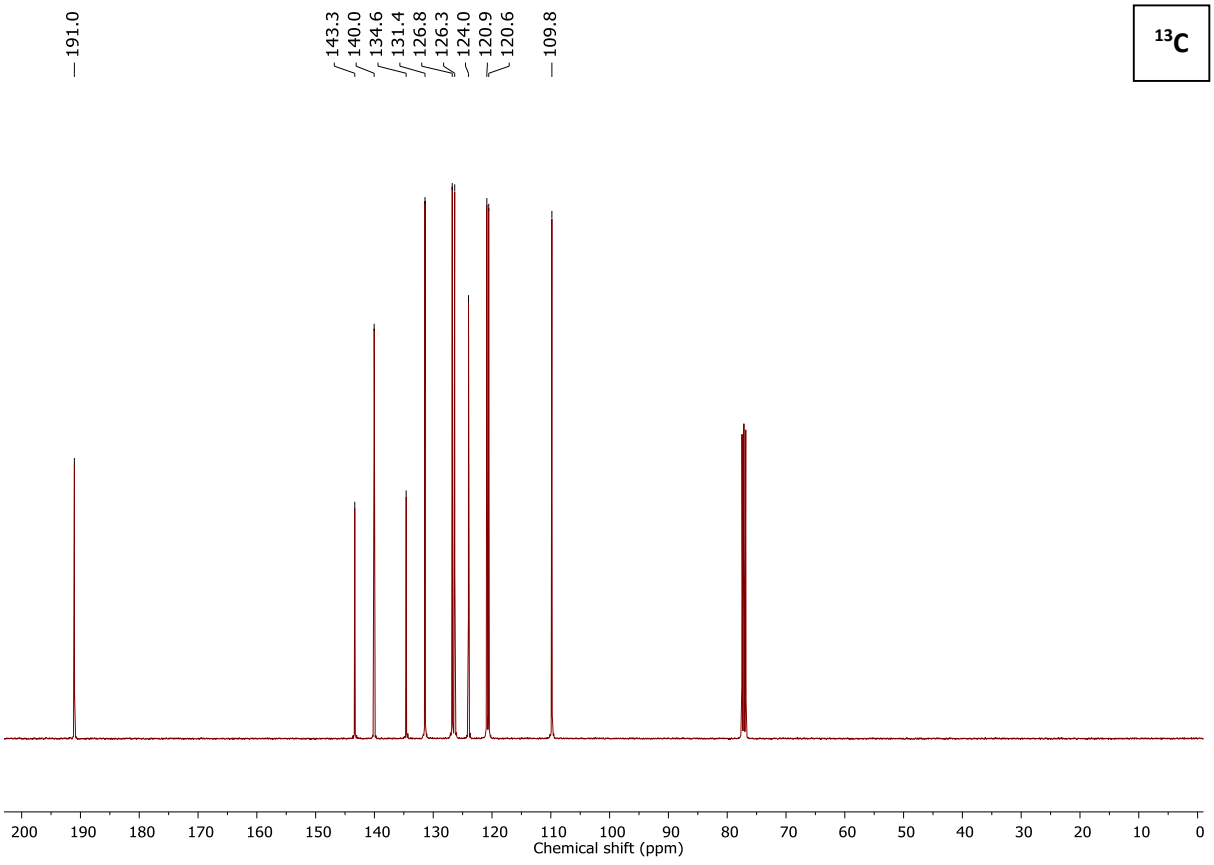

4-(3,6-Di-*tert*-butylcarbazol-9-yl)benzaldehyde (**4f**)

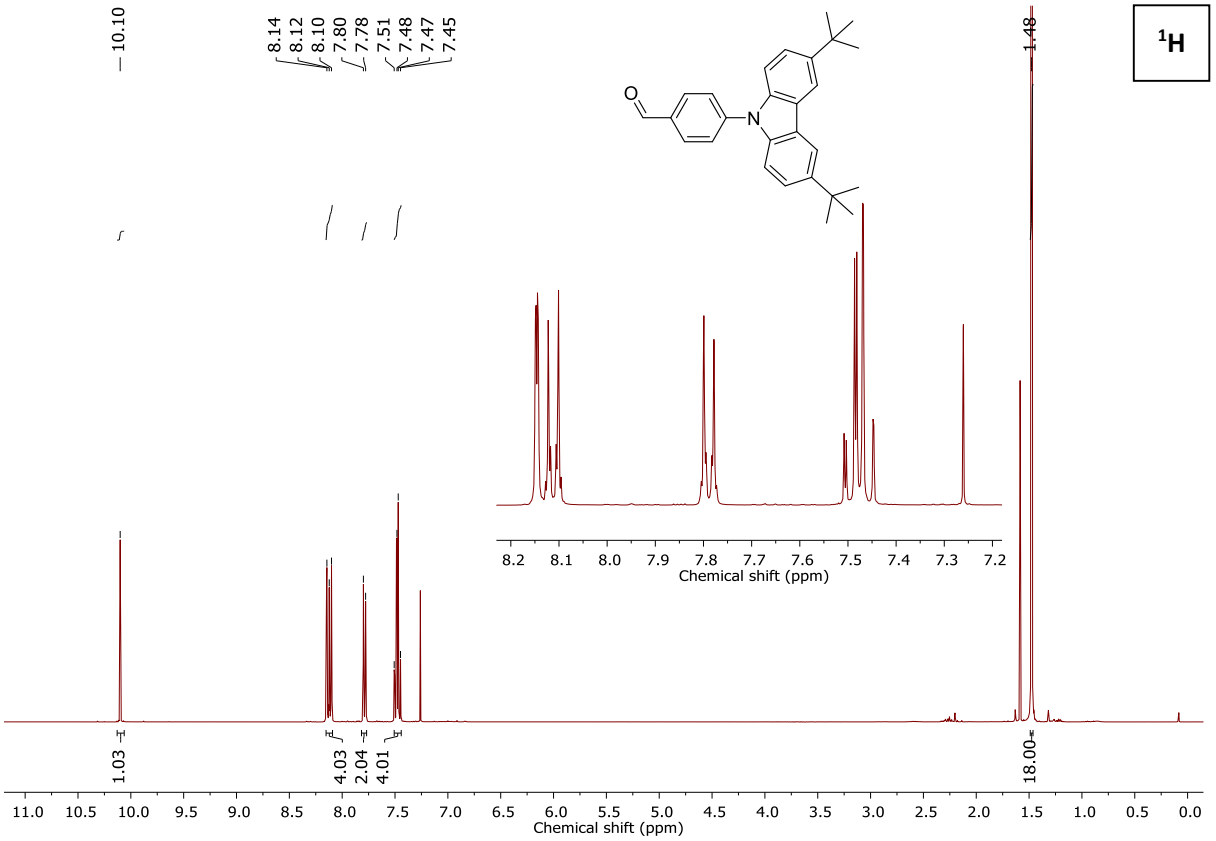

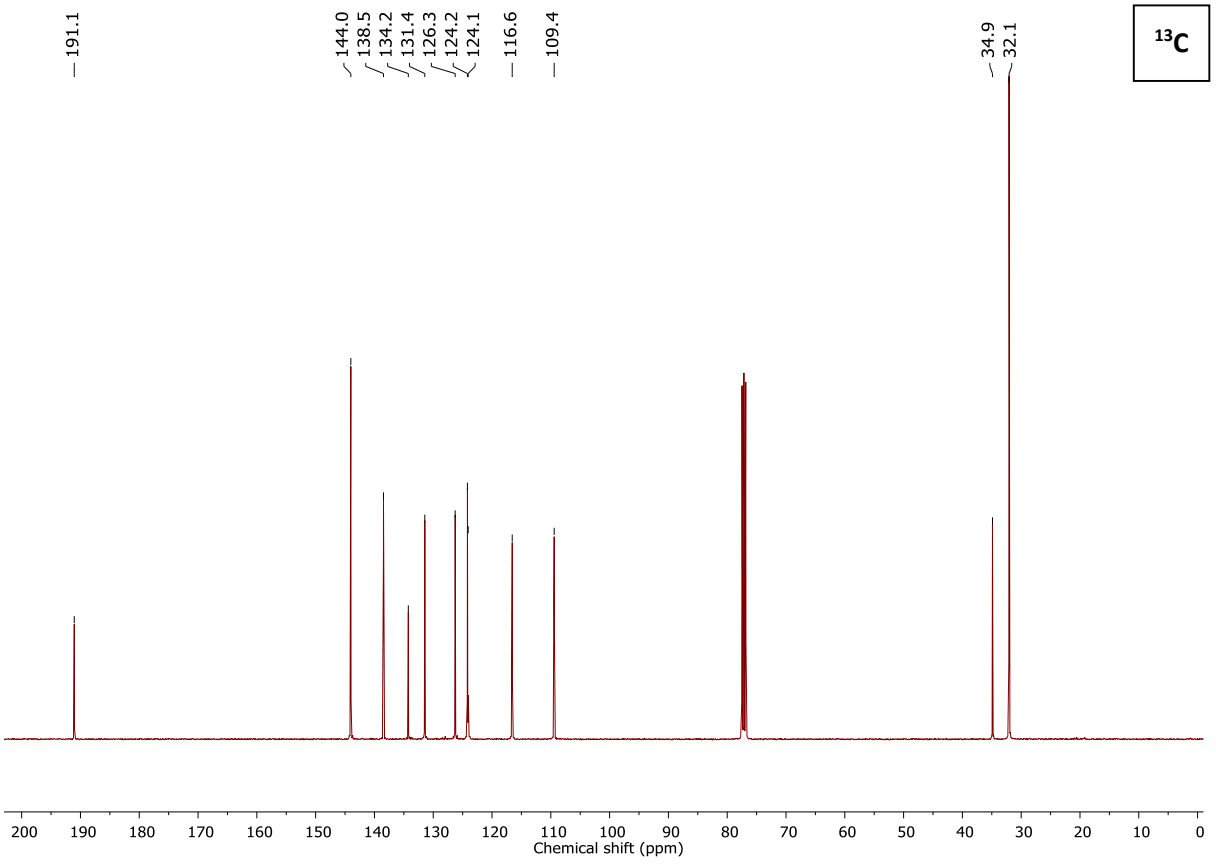

1,7-Dimethyl-3,5-di(4-(9,9-dimethyl-9,10-dihydroacridin-10-yl)styryl)-8-mesityl-4,4-difluoro-4-bora-3a,4a-diaza-*s*-indacene (**5a**)

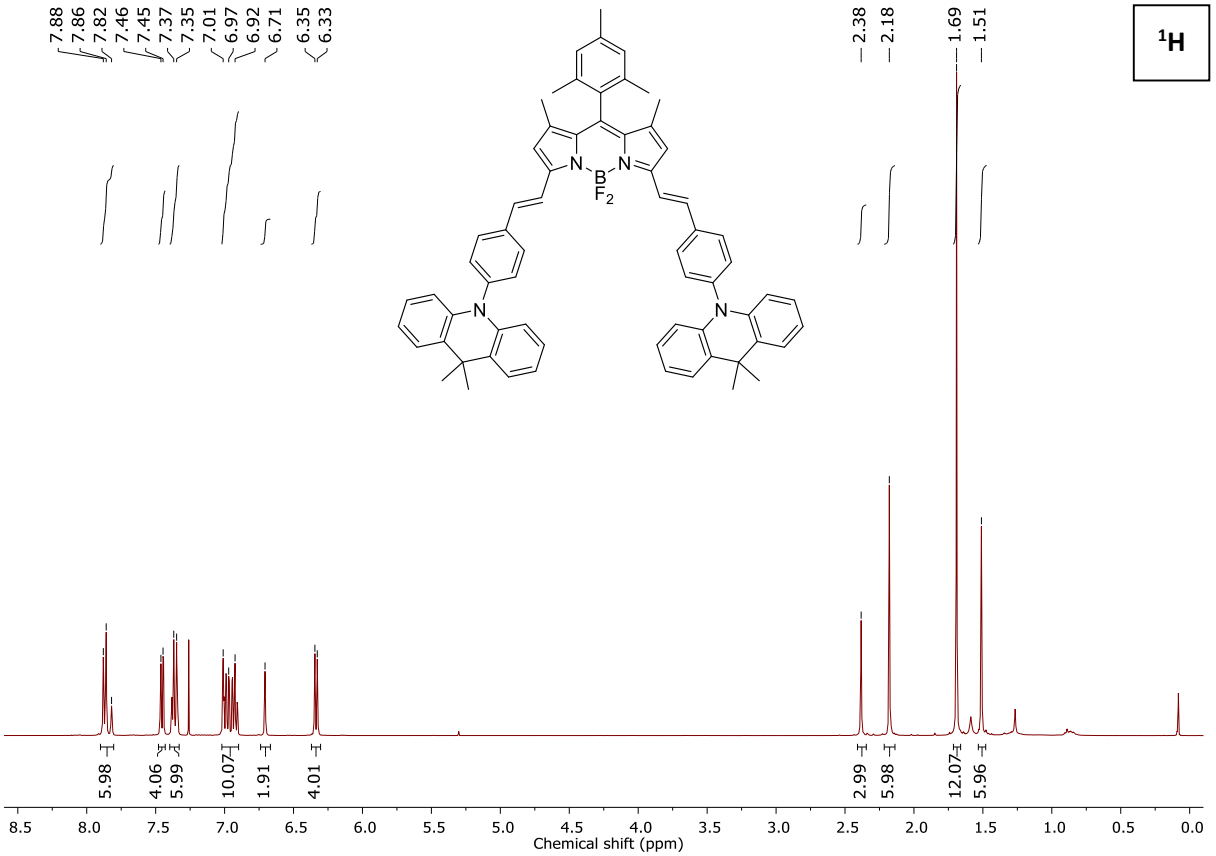

^{1}H

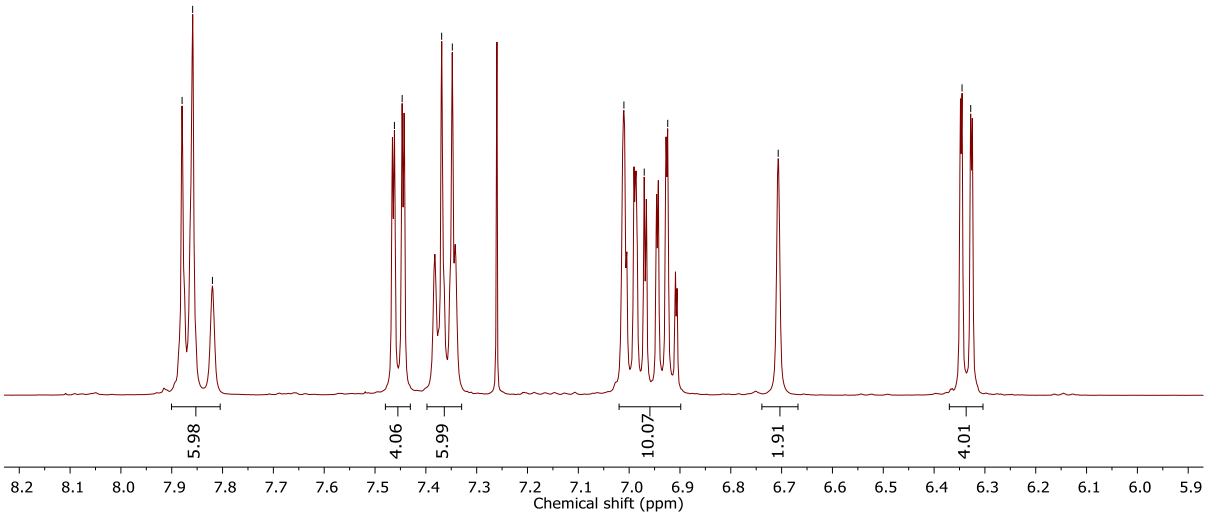

^{1}H
zoom-in
5.9-8.2 ppm

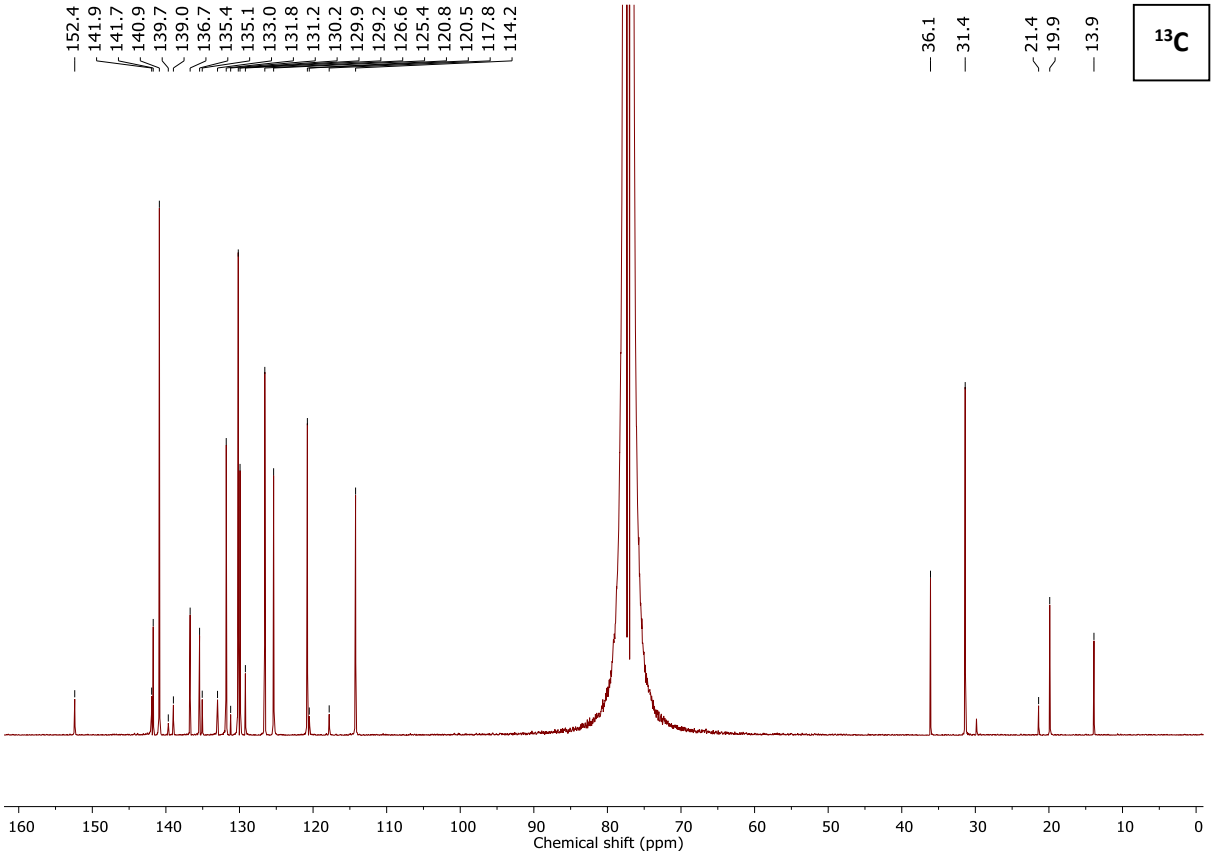
152.4
141.9
141.7
140.9
139.7
139.0
136.7
135.4
135.1
133.0
131.8
131.2
130.2
129.9
129.2
126.6
125.4
120.8
120.5
117.8
114.2
36.1
31.4
21.4
19.9
13.9
13C
160
150
140
130
120
110
100
90
80
70
60
50
40
30
20
10
0
Chemical shift (ppm)

1,7-Dimethyl-3,5-di(4-(phenoxazin-10-yl)styryl)-8-mesityl-4,4-difluoro-4-bora-3a,4a-diaza-*s*-indacene (**5b**)

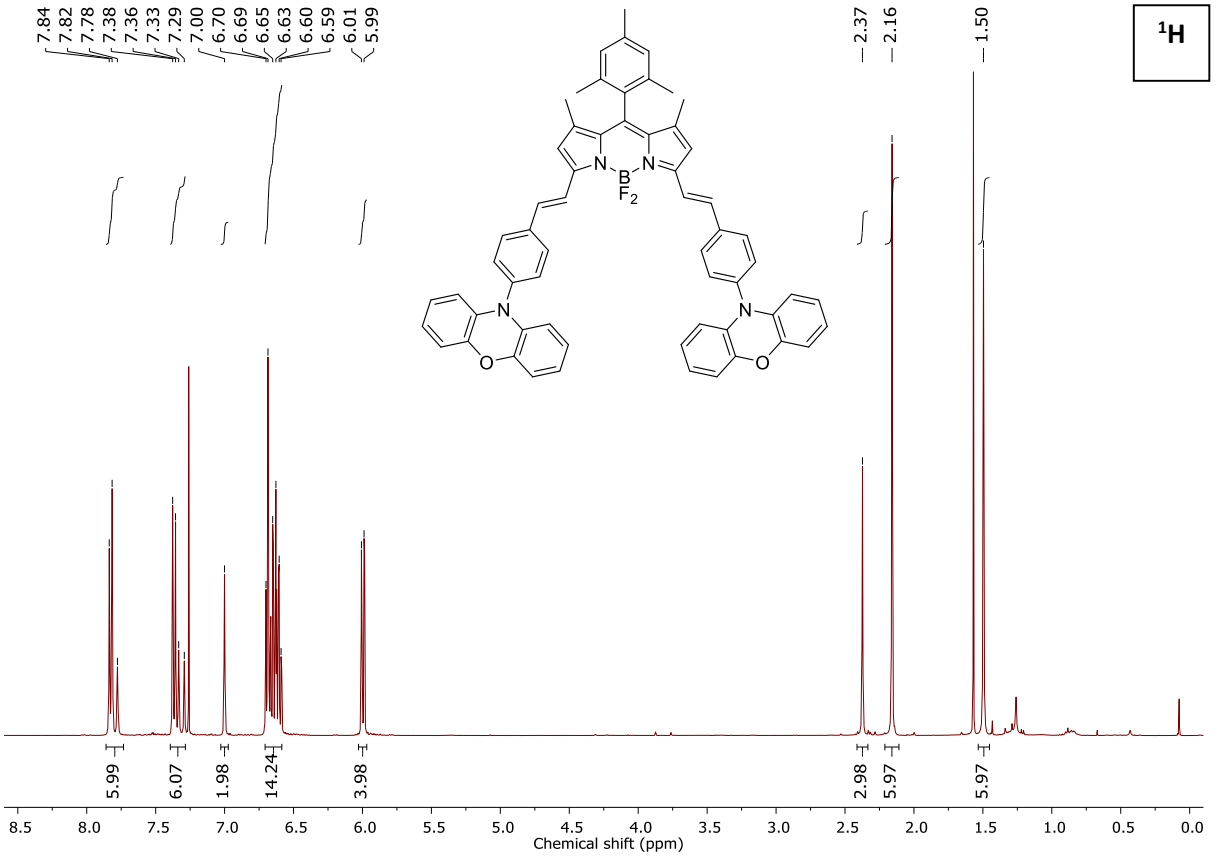

^{1}H

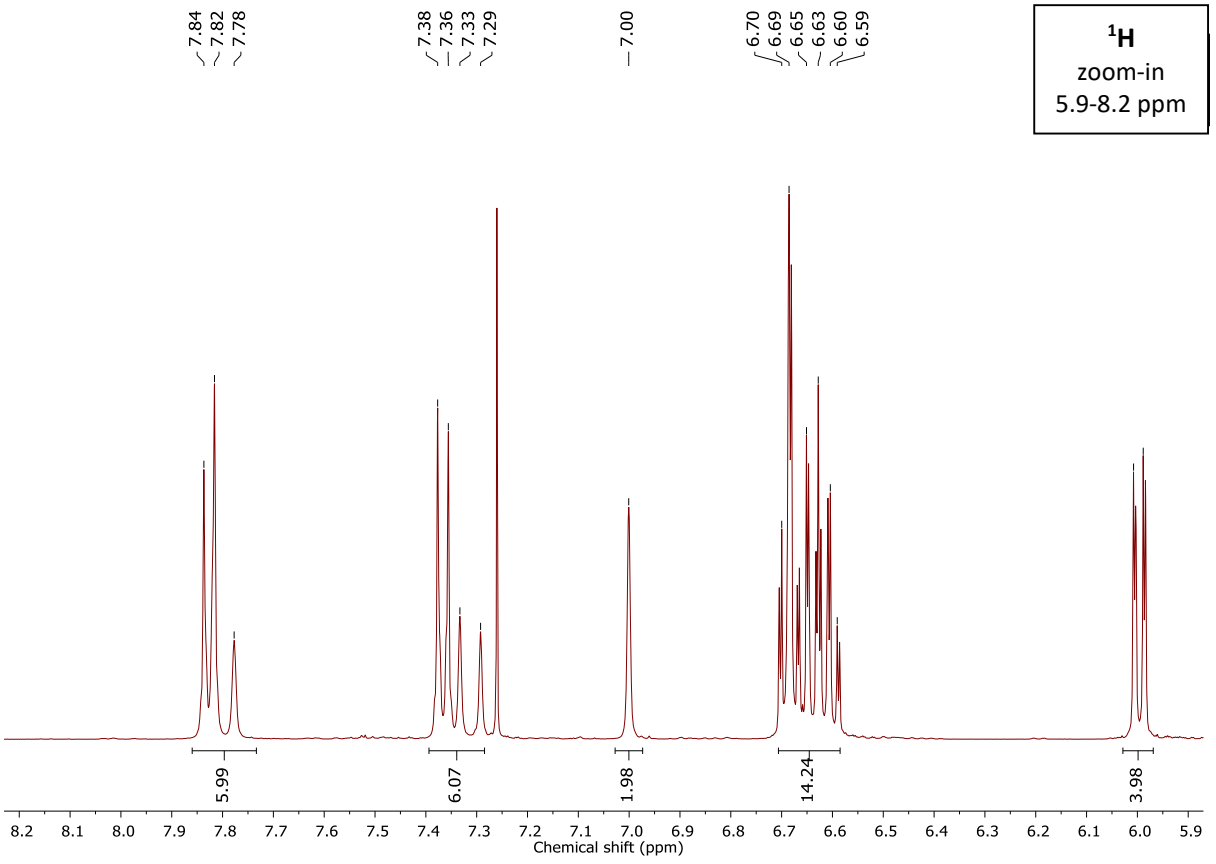

^{1}H
zoom-in
5.9-8.2 ppm

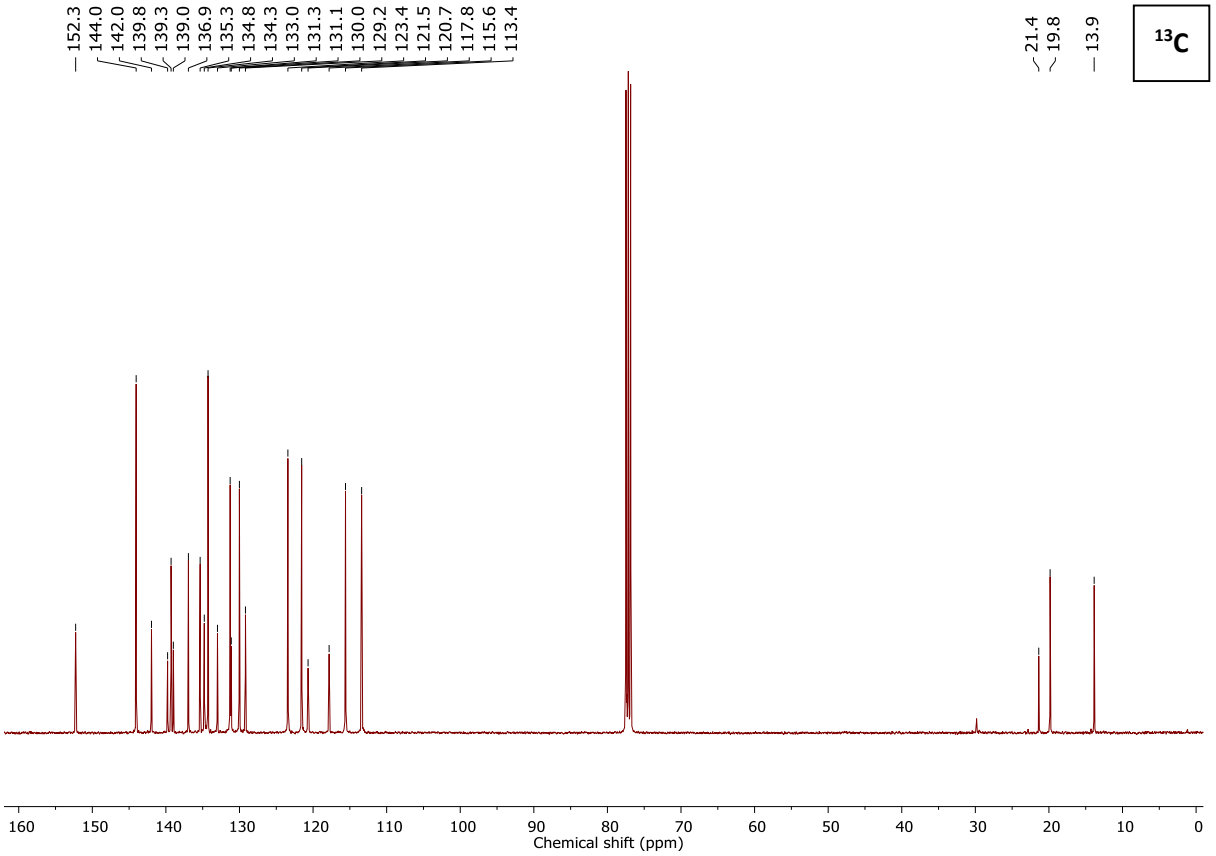
152.3
144.0
142.0
139.8
139.3
139.0
136.9
135.3
134.8
134.3
133.0
131.3
131.1
130.0
129.2
123.4
121.5
120.7
117.8
115.6
113.4
21.4
19.8
13.9
13C
160
150
140
130
120
110
100
90
80
70
60
50
40
30
20
10
0
Chemical shift (ppm)

1,7-Dimethyl-3,5-di(4-(phenothiazin-10-yl)styryl)-8-mesityl-4,4-difluoro-4-bora-3a,4a-diaza-*s*-indacene (**5c**)

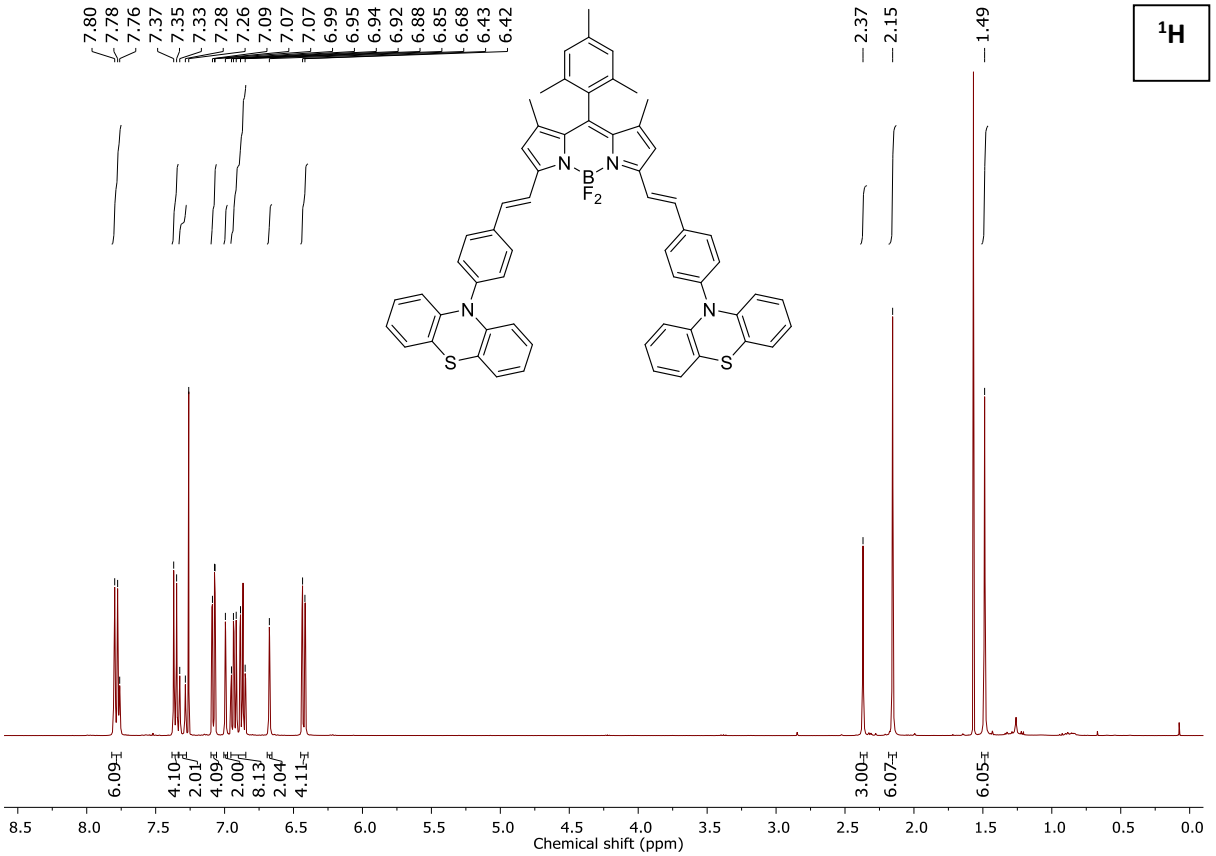

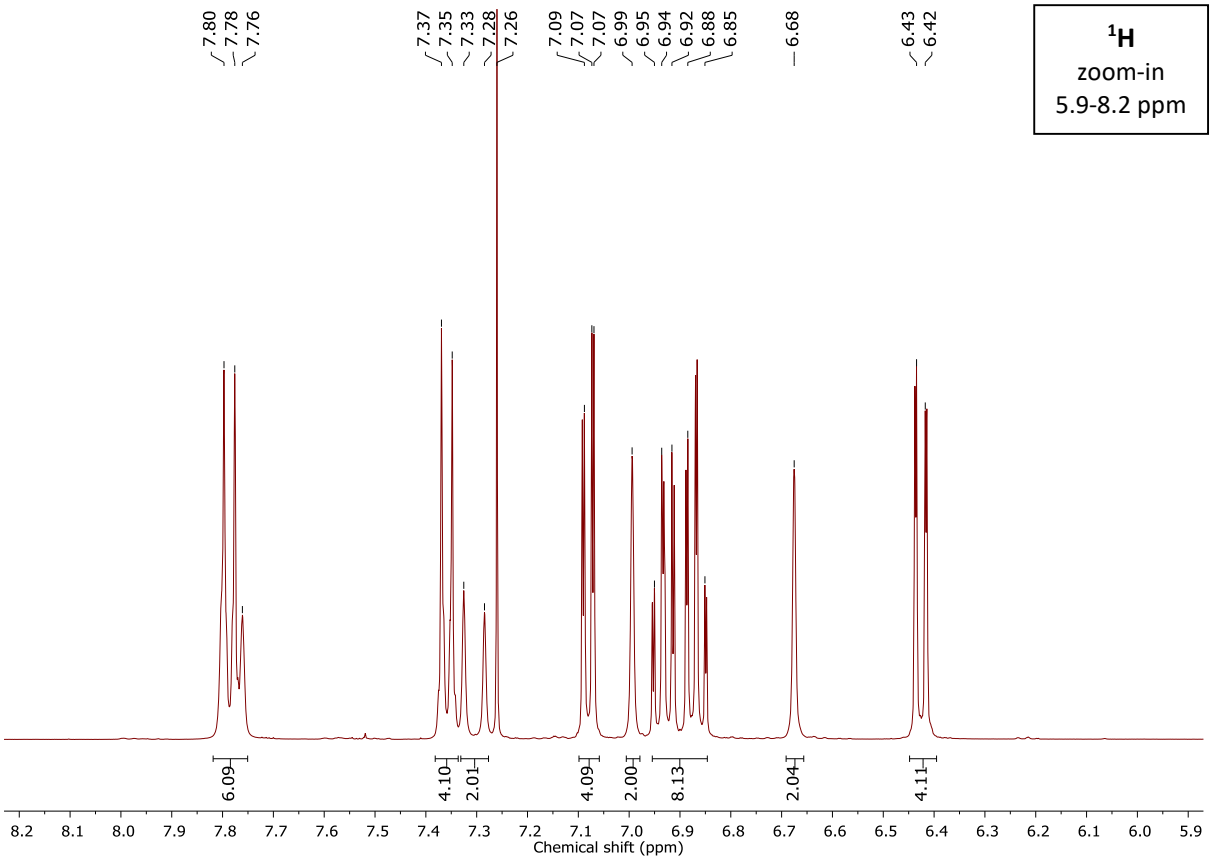

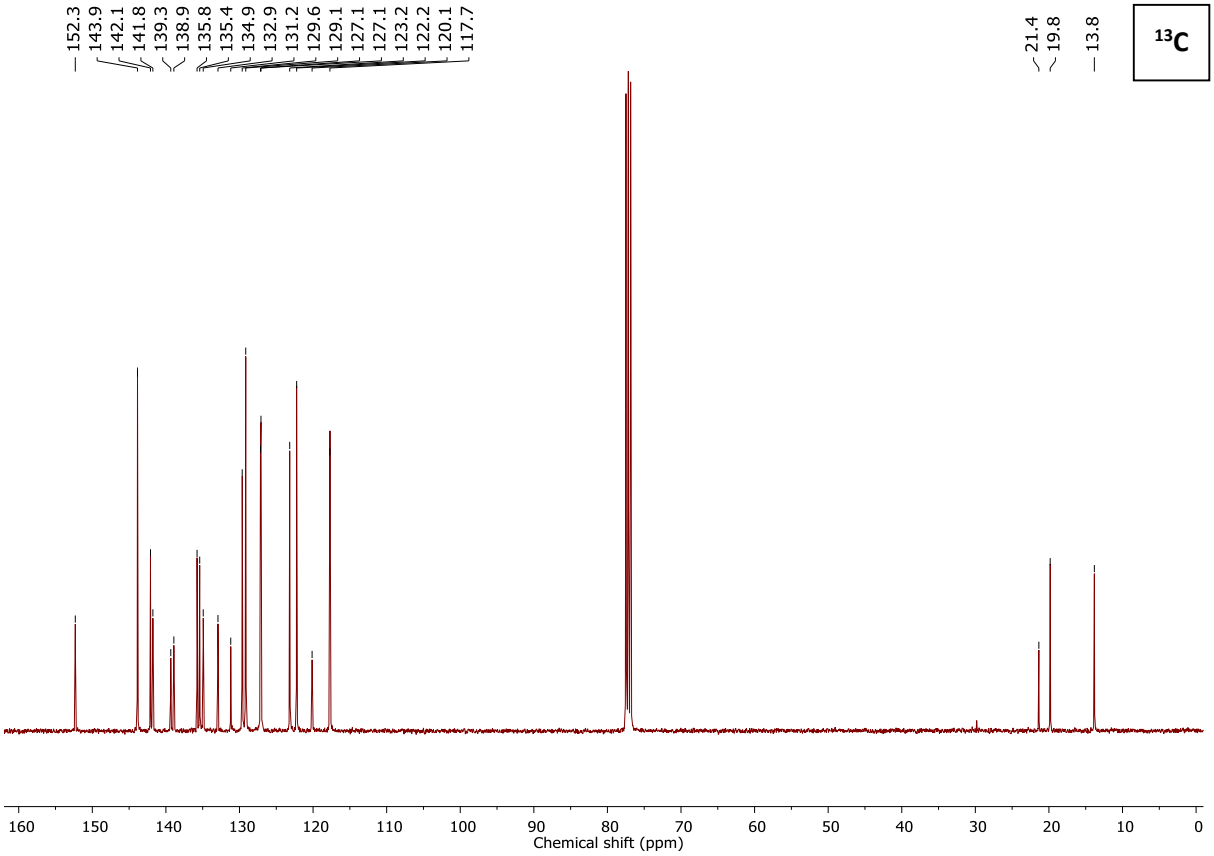
152.3
143.9
142.1
141.8
139.3
138.9
135.8
135.4
134.9
132.9
131.2
129.6
129.1
127.1
127.1
123.2
122.2
120.1
117.7
21.4
19.8
13.8
13C
160
150
140
130
120
110
100
90
80
70
60
50
40
30
20
10
0
Chemical shift (ppm)

1,7-Dimethyl-3,5-di(4-(diphenylamino)styryl)-8-mesityl-4,4-difluoro-4-bora-3a,4a-diaza-*s*-indacene (**5d**)

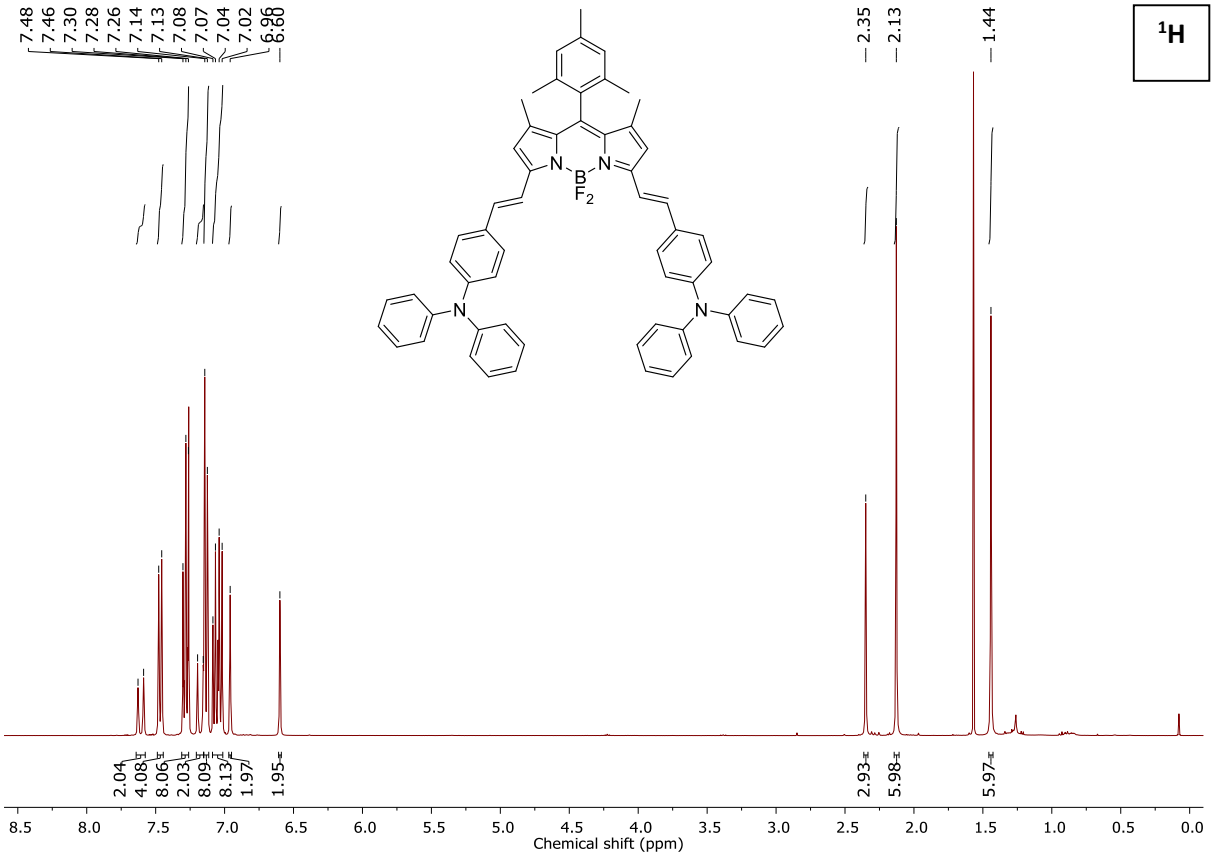

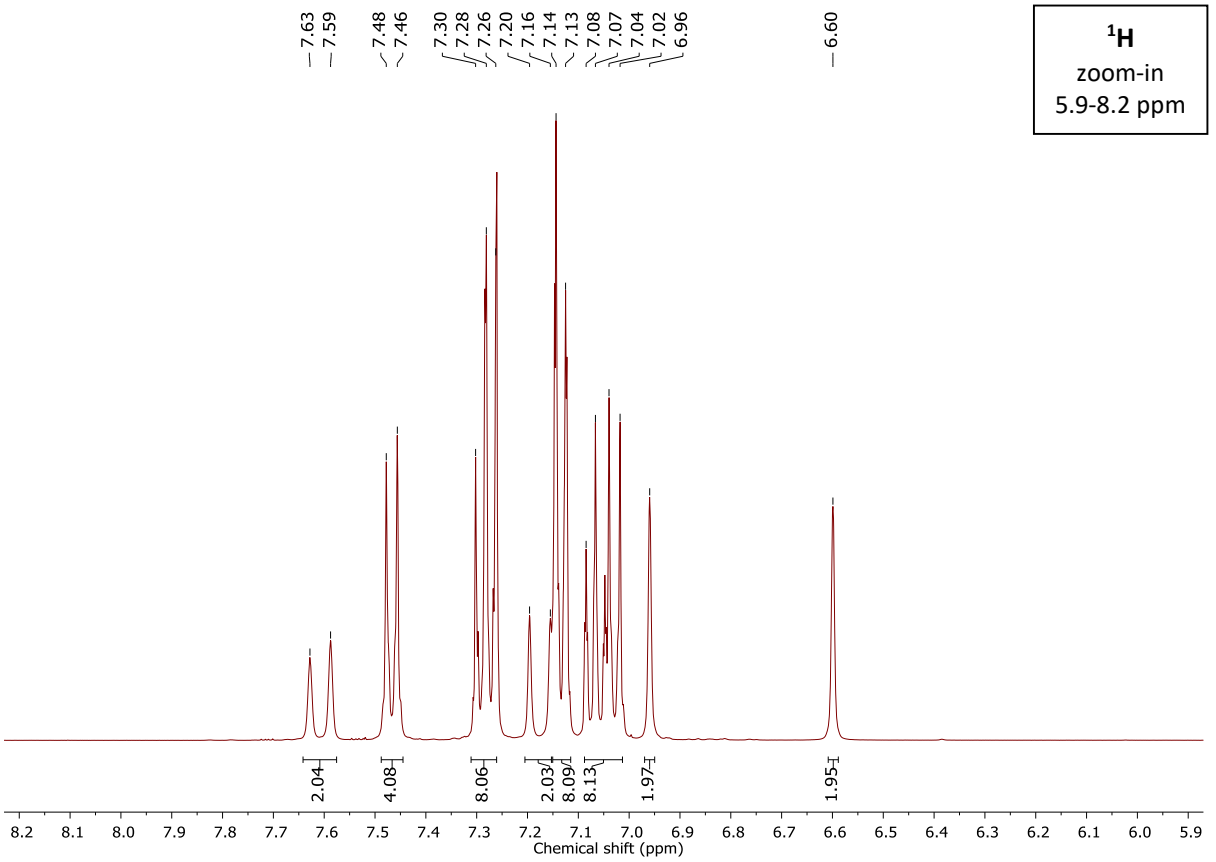

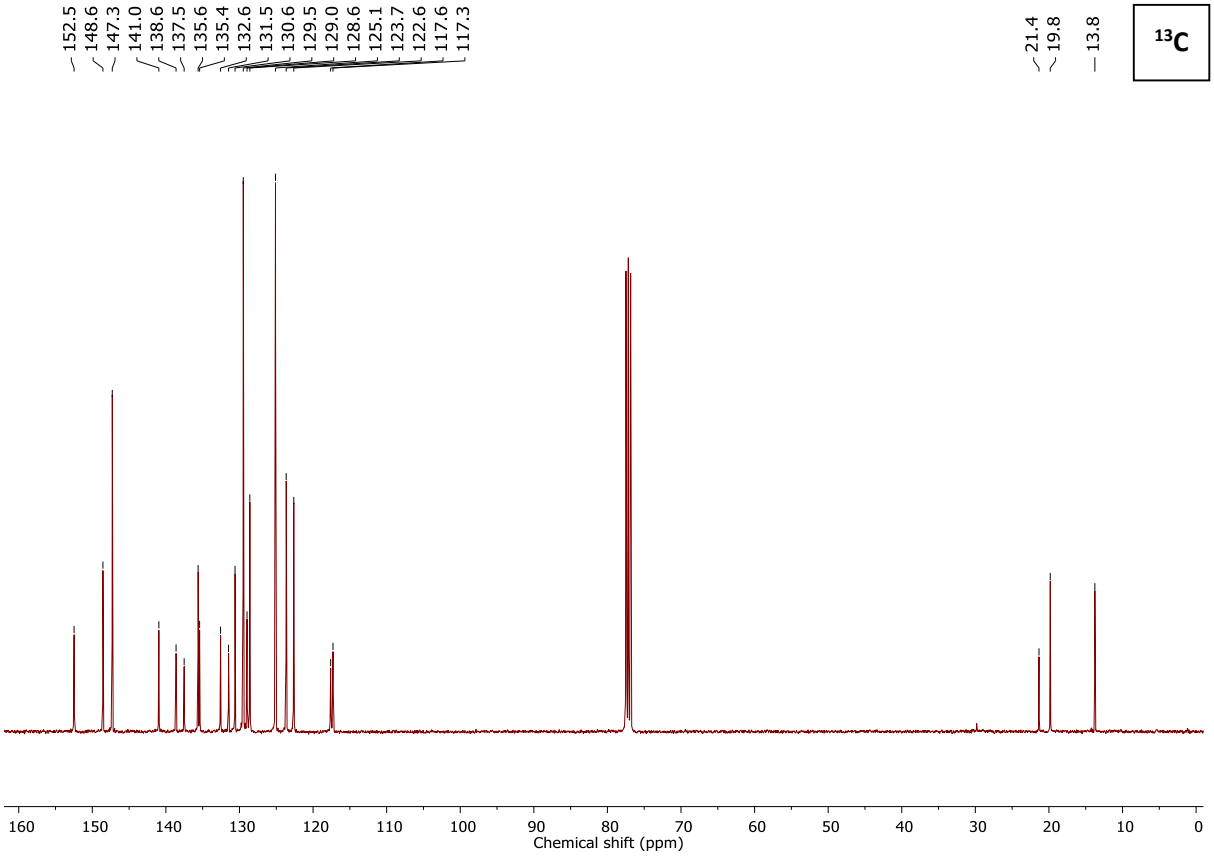
152.5
148.6
147.3
141.0
138.6
137.5
135.6
135.4
132.6
131.5
130.6
129.5
129.0
128.6
125.1
123.7
122.6
117.6
117.3
21.4
19.8
13.8
^{13}C
160
150
140
130
120
110
100
90
80
70
60
50
40
30
20
10
0
Chemical shift (ppm)

1,7-Dimethyl-3,5-di(4-(carbazol-9-yl)styryl)-8-mesityl-4,4-difluoro-4-bora-3a,4a-diaza-*s*-indacene (**5e**)

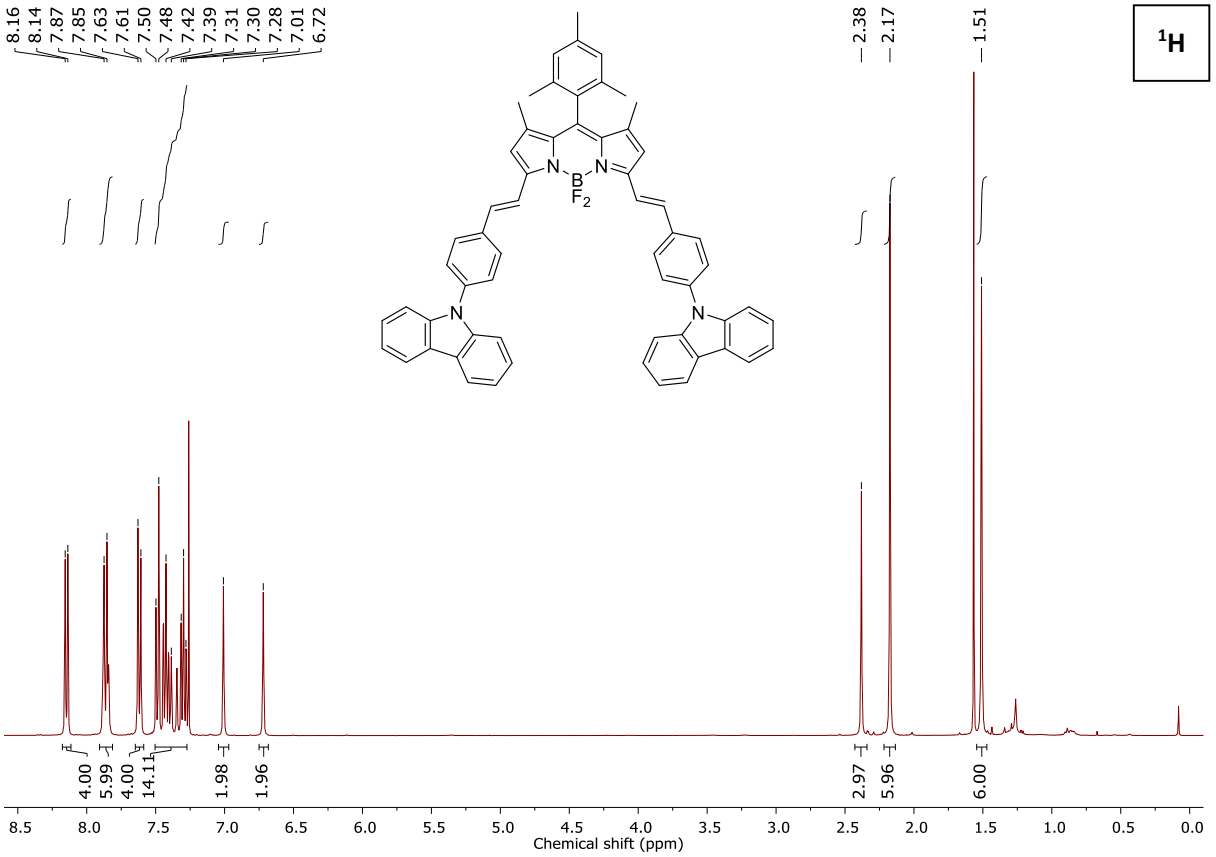

^{1}H

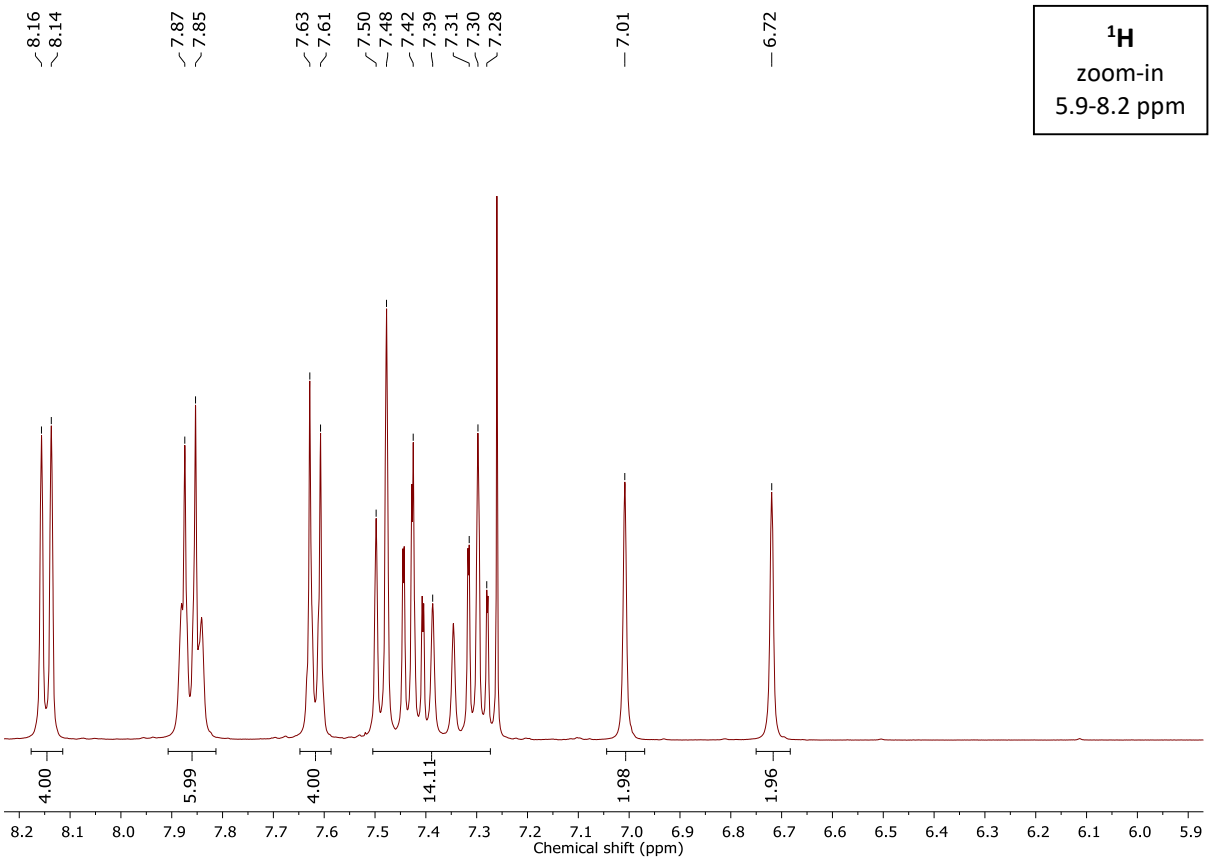

^{1}H
zoom-in
5.9-8.2 ppm

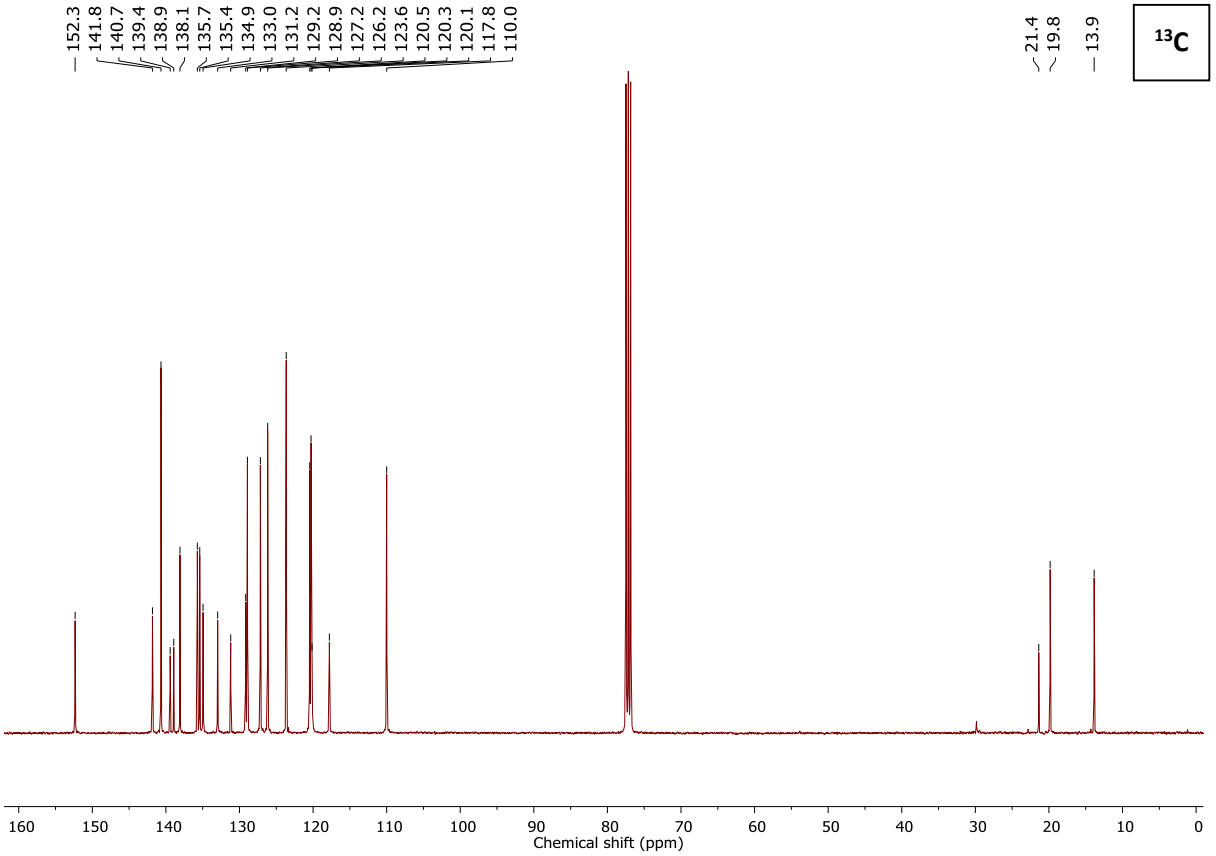
152.3
141.8
140.7
139.4
138.9
138.1
135.7
135.4
134.9
133.0
131.2
129.2
128.9
127.2
126.2
123.6
120.5
120.3
120.1
117.8
110.0
21.4
19.8
13.9
13C
160
150
140
130
120
110
100
90
80
70
60
50
40
30
20
10
0
Chemical shift (ppm)

1,7-Dimethyl-3,5-di(4-(3,6-di-*tert*-butylcarbazol-9-yl)styryl)-8-mesityl-4,4-difluoro-4-bora-3a,4a-diaza-*s*-indacene (**5f**)

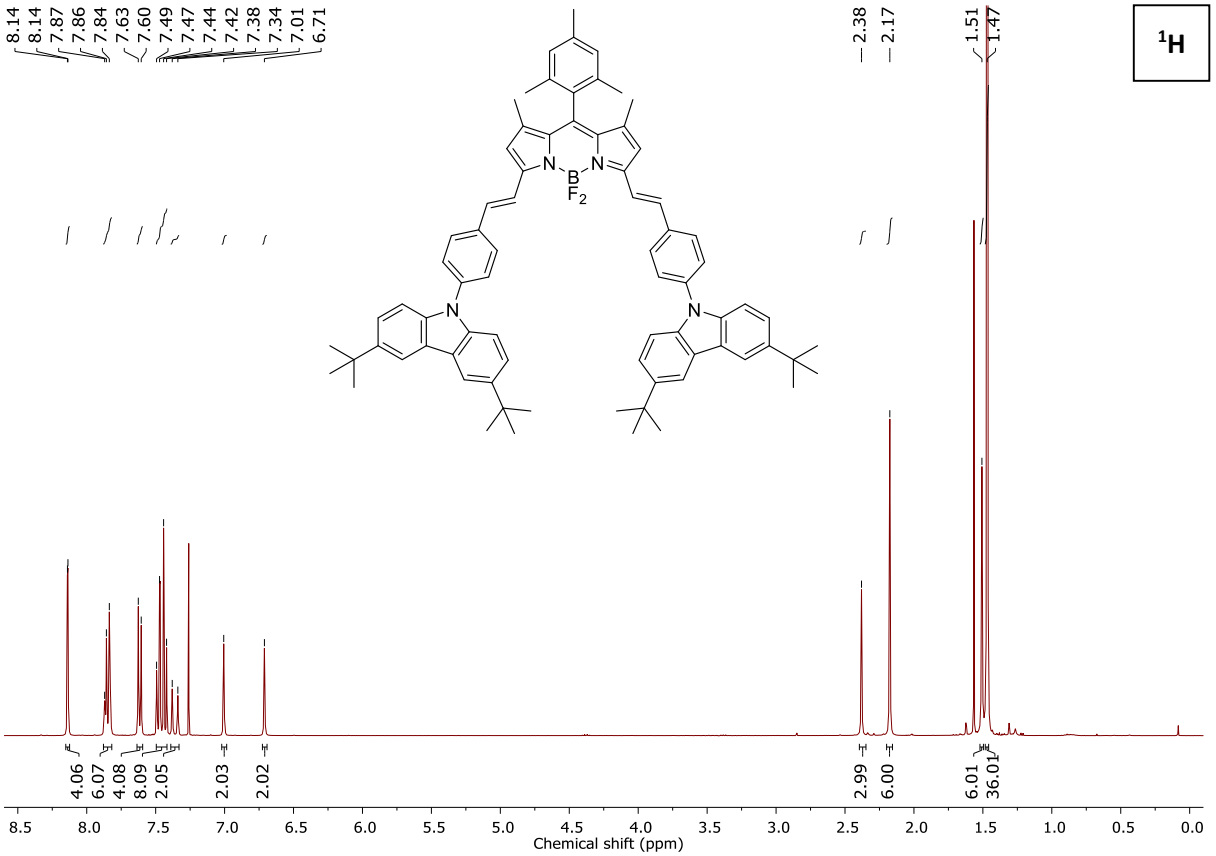

^{1}H

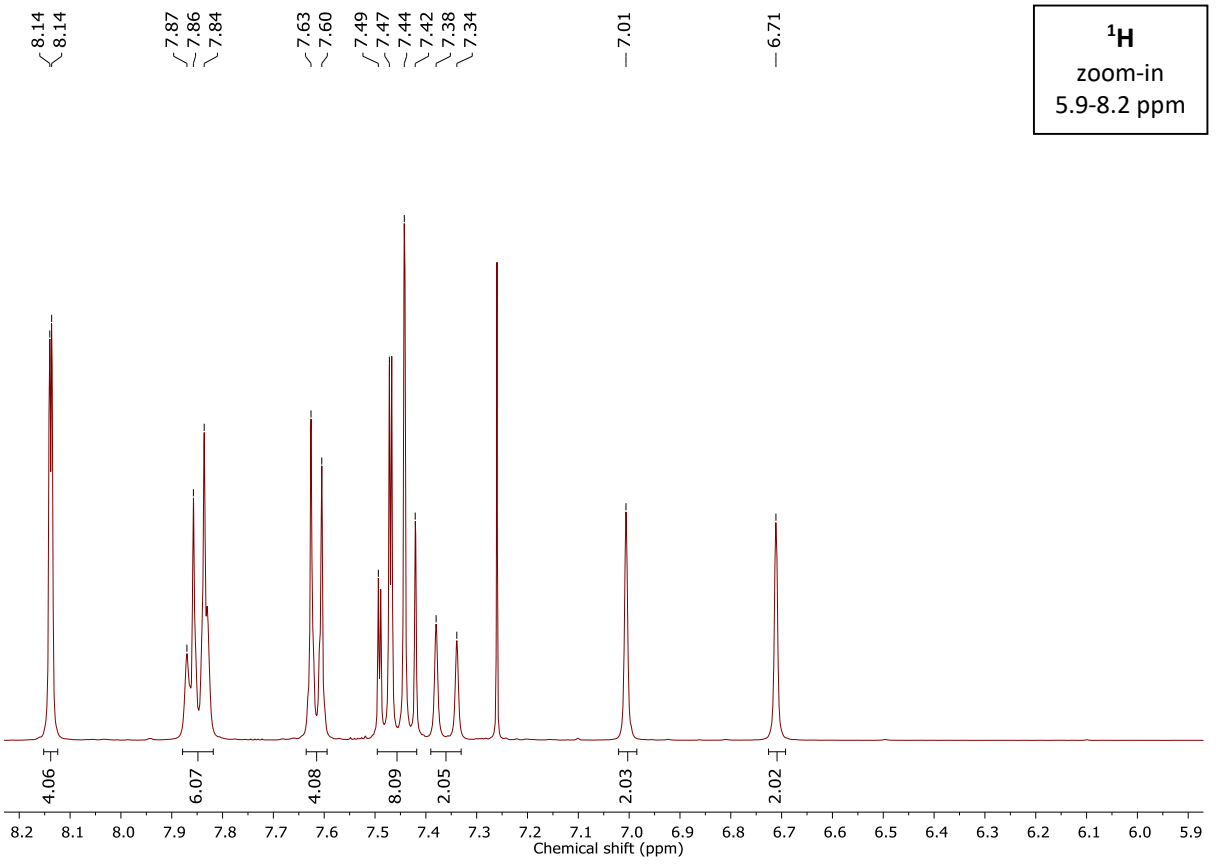

^{1}H
zoom-in
5.9-8.2 ppm

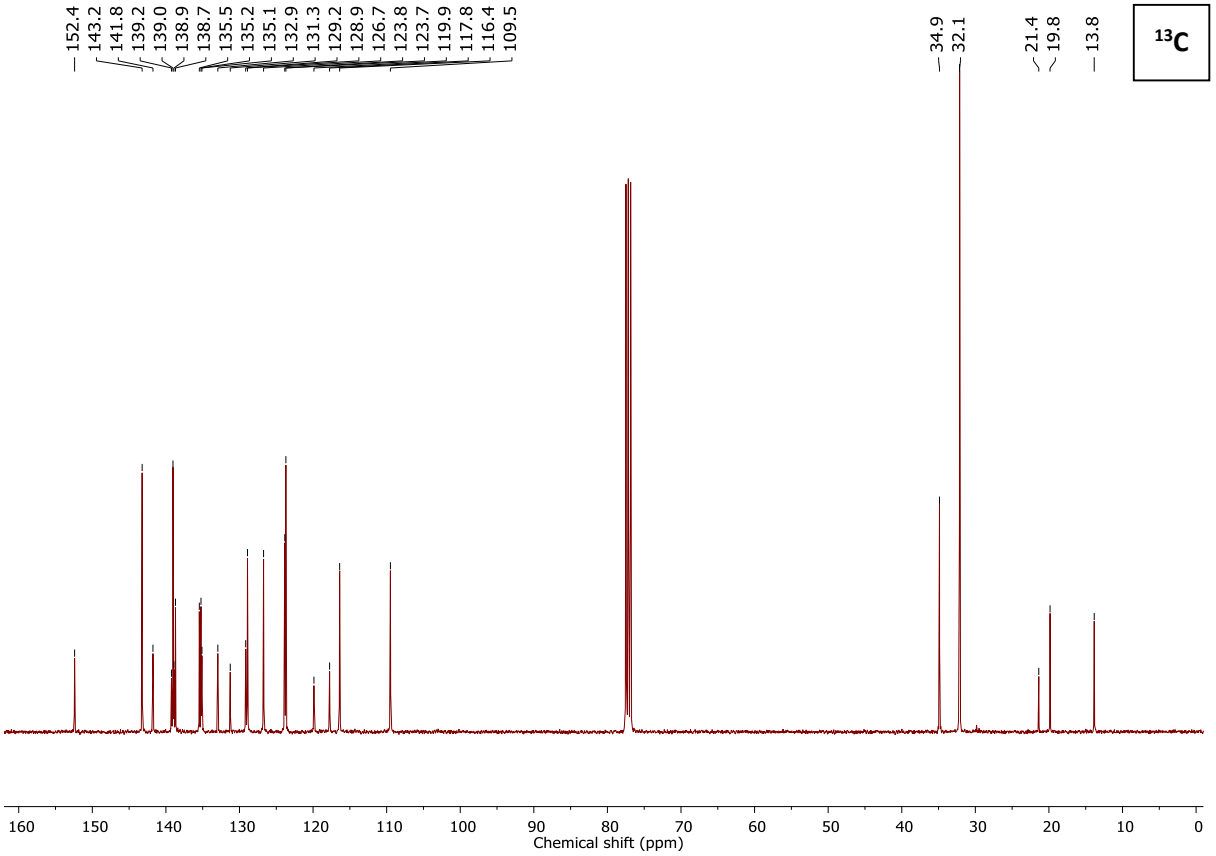
152.4
143.2
141.8
139.2
139.0
138.9
138.7
135.5
135.2
135.1
132.9
131.3
129.2
128.9
126.7
123.8
123.7
119.9
117.8
116.4
109.5
34.9
32.1
21.4
19.8
13.8
13C
160
150
140
130
120
110
100
90
80
70
60
50
40
30
20
10
0
Chemical shift (ppm)

1,7-Dimethyl-3,5-distyryl-8-mesityl-4,4-difluoro-4-bora-3a,4a-diaza-*s*-indacene (**5H**)

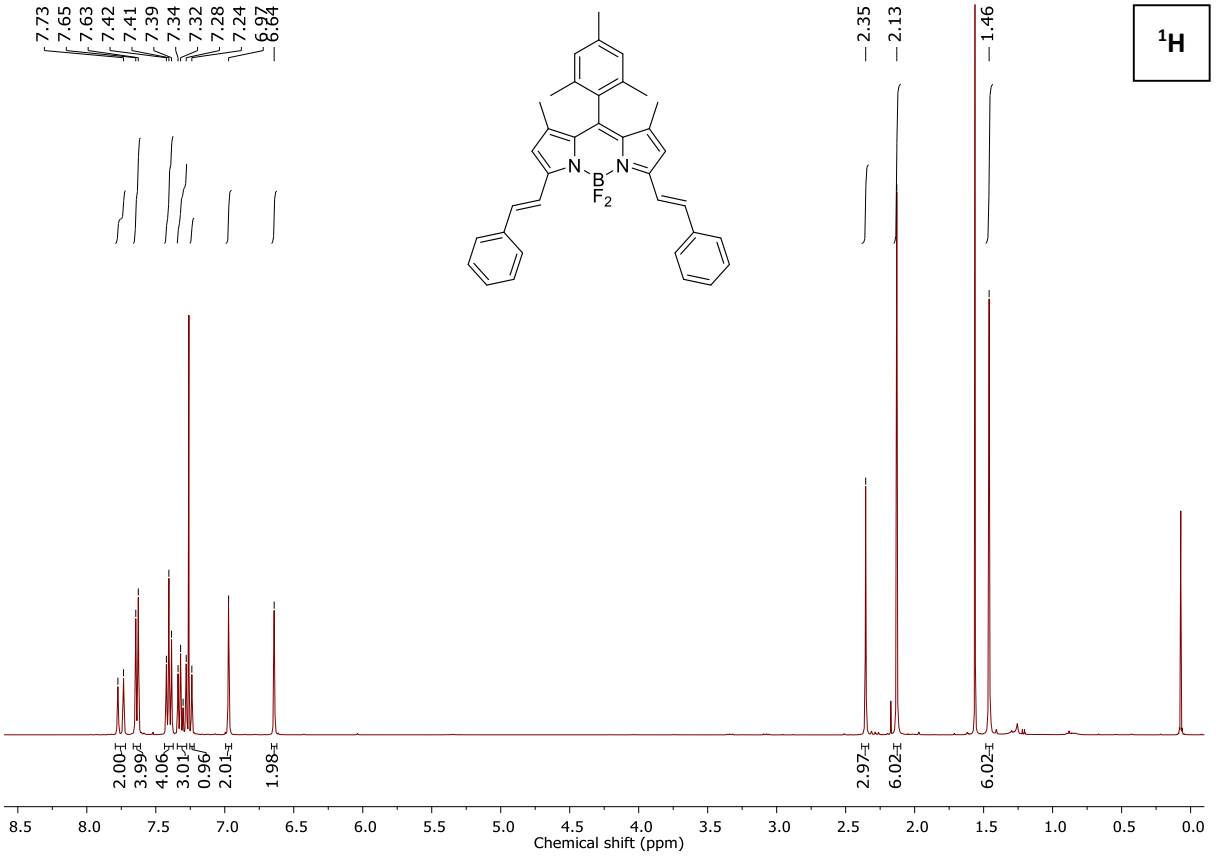

^{1}H

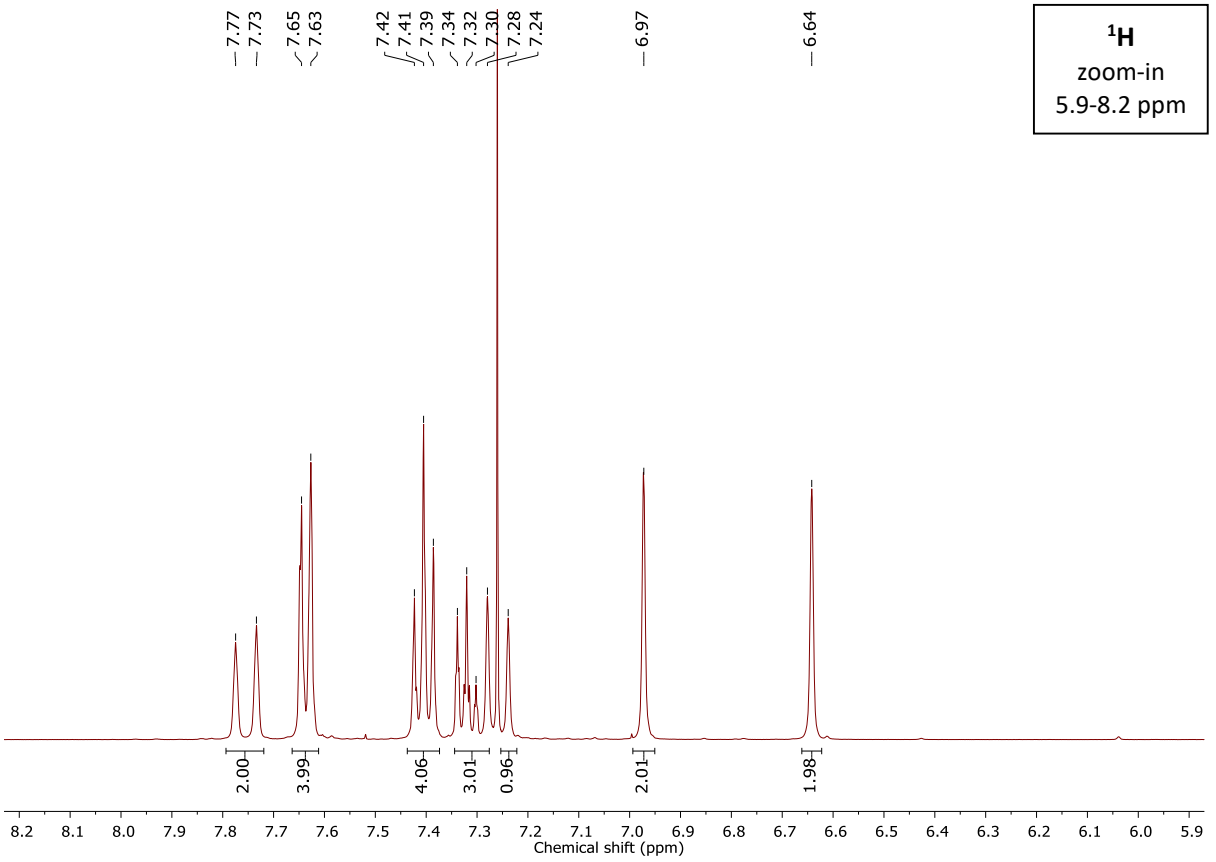

^{1}H
zoom-in
5.9-8.2 ppm

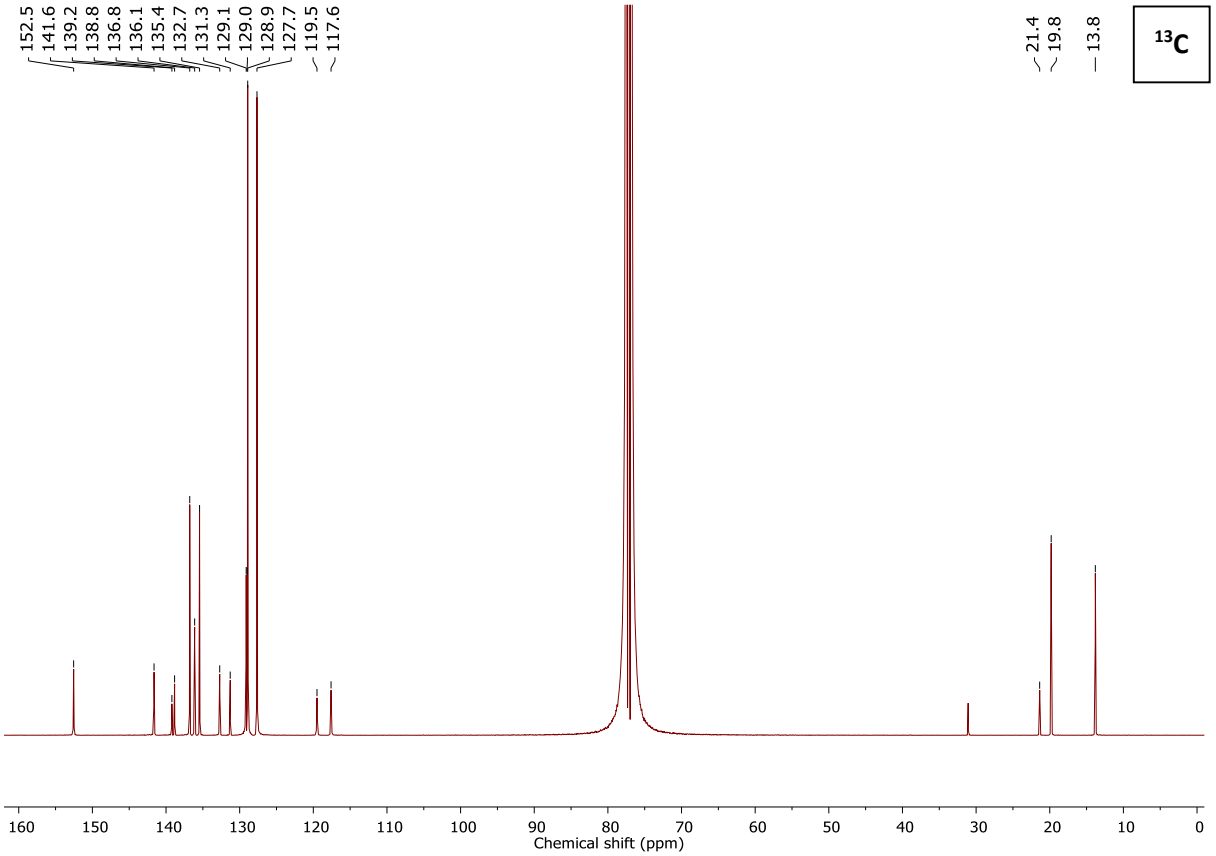
152.5
141.6
139.2
138.8
136.8
136.1
135.4
132.7
131.3
129.1
129.0
128.9
127.7
119.5
117.6
21.4
19.8
13.8
^{13}C
160
150
140
130
120
110
100
90
80
70
60
50
40
30
20
10
0
Chemical shift (ppm)

13. References

1. M. J. Frisch, G. W. Truck, H. B. Schlegel, G. E. Scuseria, M. A. Robb, J. R. Cheeseman, G. Scalmani, V. Barone, G. A. Petersson, H. Nakatsuji, X. Li, M. Caricato, A. V. Marenich, J. Bloino, B. G. Janesko, R. Gomperts, B. Mennucci, H. P. Hratchian, J. V. Ortiz, A. F. Izmaylov, J. L. Sonnenberg, D. Williams-Young, F. Ding, F. Lipparini, F. Egidi, J. Goings, B. Peng, A. Petrone, T. Henderson, D. Ranasinghe, V. G. Zakrzewski, J. Gao, N. Rega, G. Zheng, W. Liang, M. Hada, M. Ehara, K. Toyota, R. Fukuda, J. Hasegawa, M. Ishida, T. Nakajima, Y. Honda, O. Kitao, H. Nakai, T. Vreven, K. Throssell, J. A. Montgomery, J. E. Peralta, F. Ogliaro, M. Bearpark, J. J. Heyd, E. N. Brothers, K. N. Kudin, V. N. Staroverov, T. A. Keith, R. Kobayashi, J. Normand, K. Raghavachari, A. P. Rendell, J. C. Burant, S. S. Iyengar, J. Tomasi, M. Cossi, J. M. Millam, M. Klene, C. Adamo, R. Cammi, J. W. Ochterski, R. L. Martin, K. Morokuma, O. Farkas, J. B. Foresman and D. J. Fox, *Gaussian, Inc., Wallingford CT*, 2016.
2. T. Le Bahers, C. Adamo and I. Ciofini, *J. Chem. Theory Comput.*, 2011, **7**, 2498-2506.
3. A. M. Brouwer, *Pure Appl. Chem.*, 2011, **83**, 2213-2228.
4. J. A. Bonacin, F. M. Engelmann, D. Severino, H. E. Toma and M. S. Baptista, *J. Brazil. Chem. Soc.*, 2009, **20**, 31-36.
5. F. Wilkinson, W. P. Helman and A. B. Ross, *J. Phys. Chem. Ref. Data*, 1993, **22**, 113-262.
6. R. W. Redmond and J. N. Gamlin, *Photochem. Photobiol.*, 1999, **70**, 391-475.
7. J. J. Snellenburg, S. P. Laptenok, R. Seger, K. M. Mullen and I. H. M. v. Stokkum, *J. Stat. Soft.*, 2012, **49**, 1-22.
8. Y. Rong, C. Wu, J. Yu, X. Zhang, F. Ye, M. Zeigler, M. E. Gallina, I. C. Wu, Y. Zhang, Y. H. Chan, W. Sun, K. Uvdal and D. T. Chiu, *ACS Nano*, 2013, **7**, 376-384.
9. E. Jürgens, K. N. Buys, A.-T. Schmidt, S. K. Furfari, M. L. Cole, M. Moser, F. Rominger and D. Kunz, *New J. Chem.*, 2016, **40**, 9160-9169.
10. J. Deckers, T. Cardeynaels, H. Penxten, A. Ethirajan, M. Ameloot, M. Kruk, B. Champagne and W. Maes, *Chem. Eur. J.*, 2020, **26**, 15212-15225.
11. Rigaku Oxford Diffraction, CrysAlisPro Software system, Rigaku Corporation, Wrocław, Poland, **2020**.
12. O. V. Dolomanov, L. J. Bourhis, R. J. Gildea, J. A. K. Howard and H. Puschmann, *J. Appl. Cryst.*, 2009, **42**, 339-341.
13. C. B. Hübschle, G. M. Sheldrick and B. Dittrich, *J. Appl. Cryst.*, 2011, **44**, 1281-1284.
14. G. M. Sheldrick, *Acta Cryst. A Found. Adv.*, 2015, **71**, 3-8.
15. G. M. Sheldrick, *Acta Cryst. C Struct. Chem.*, 2015, **71**, 3-8.
16. A. L. Spek, *Acta Cryst. C Struct. Chem.*, 2015, **71**, 9-18.